ISTANBUL TECHNICAL UNIVERSITY ★ GRADUATE SCHOOL OF SCIENCE ENGINEERING AND TECHNOLOGY

MEMBRANE PROTEIN-BASED IN VITRO METHODS

Ph.D. THESIS

Fatih İNCİ

Department of Advanced Technologies

Molecular Biology-Genetics and Biotechnology Programme

FEBRUARY 2013

ISTANBUL TECHNICAL UNIVERSITY ★ GRADUATE SCHOOL OF SCIENCE ENGINEERING AND TECHNOLOGY

MEMBRANE PROTEIN-BASED IN VITRO METHODS

Ph. D. THESIS

Fatih İNCİ
(521072033)

Department of Advanced Technologies

Molecular Biology-Genetics and Biotechnology Programme

Thesis Advisor: Assoc. Prof. Dr. Fatma Neşe KÖK

FEBRUARY 2013

İSTANBUL TEKNİK ÜNİVERSİTESİ ★ FEN BİLİMLERİ ENSTİTÜSÜ

ZAR PROTEİN-TABANLI İN VİTRO METOTLAR

DOKTORA TEZİ

Fatih İNCİ
(521072033)

İleri Teknolojiler Anabilim Dalı

Moleküler Biyoloji-Genetik ve Biyoteknoloji Programı

Tez Danışmanı: Doç. Dr. Fatma Neşe KÖK

ŞUBAT 2013

Fatih İnci, a **Ph.D.** student of ITU **Graduate School of Science Engineering and Technology** student ID **521072033**, successfully defended the **thesis** entitled "**MEMBRANE PROTEIN-BASED IN VITRO METHODS**", which he prepared after fulfilling the requirements specified in the associated legislations, before the jury whose signatures are below.

Thesis Advisor :	**Assoc. Prof. Dr. Fatma Neşe KÖK** İstanbul Technical University	.....
Jury Members :	**Assoc. Prof. Dr. Ayten Yazgan KARATAŞ** İstanbul Technical University	.....
	Prof. Dr. Gamze Torun KÖSE Yeditepe University	.....
	Assoc. Prof. Dr. Hakan Özgür ÖZER İstanbul Technical University	.....
	Assoc. Prof. Dr. Melek ÖZKAN Gebze Institute of High Technology	.....

Date of Submission : 27 December 2012
Date of Defense : 13 February 2013

To my family,

FOREWORD

I would like to express my sincere gratitude to my supervisor Assoc. Prof. Dr. Fatma Neşe Kök for her encouragement, guidance and support throughout all period of my Ph.D. studies. I am indebted her for giving me the chance in her research group, and she has truly helped me to have scientific point of view in interdisciplinary concepts during my studies. Her invaluable help and encouragement have allowed me to work in several scientific fields, and I actually believe that she has given me a chance to meet the fascinating world of science.

I would also like to thank thesis committee, Assoc. Prof. Dr. Ayten Yazgan Karataş, Prof. Dr. Gamze Torun Köse, Assoc. Prof. Dr. Hakan Özgür Özer, and Assoc. Prof. Dr. Melek Özkan, for their guidance and support in my thesis.

I was very lucky by having friends, and would like to acknowledge Evren Taştan, Sakip Önder, Başak Türken, Abdülhalim Kılıç, Deniz Karasu, Selcan Güngör Özkerim, Perihan Merve Buldur, and new labmates in KökBioLab. They always asisted me and shared all their knowledge and opinion in my studies. I would also like to thank Oğuzhan Latif Kılınç, Garbis Atam Akçeoğlu, Aziz Kaan Korkmaz, Bahtiyar Yılmaz, Ali Altıntaş, Necla Sena Alikişioğlu, Ceren Alkım, and Deniz Şahin for their friendship and support. Additionally, I would like to thank Ümit Çelik for their insight and help on my experiments.

I would like to give my special thanks to Merve Tokaç for her enduring support and encouragement. She always gave me morale support and helped at my stressful times.

I would like to express my special thanks to Gülşah and Batuhan F. İnci for their invaluable support, encouragement and love. I always feel their help and guidance throughout my life.

I owe my deepest gratitude to my family, Gülizar Bedir and Şahzade Çiftci, and all my relatives for their endless love, patience, and support throughout my life and my stressful times. Lastly and more importantly, I wish to thank my mother Sultan İnci and my father Selahattin İnci, for their patience, support and love, and they are my real friends throughout my life. Here, I would like to express my sincere to my grandfathers, Şamil İnci and Neşet Çiftci, who I lost during my thesis process, and also dedicate this thesis to them.

This study was supported by TUBITAK under Grant No.TBAG-108T933, and ITU-BAP under Grant No. 33620. TUBITAK also provided me an invaluable scholarship during my Ph.D. studies.

February 2013

Fatih İNCİ
Molecular Biology and Genetics

TABLE OF CONTENTS

Page

ABBREVIATIONS

PBS	**:** Phosphate Buffered Saline
NaCl	**:** Sodium Hydroxide
KCl	**:** Potassium Chloride
Na_2HPO_4	**:** Disodium Hydrogen Phosphate
H_2O	**:** Water
KH_2PO_4	**:** Monopotassium Phosphate
DMSO	**:** Dimethylsulfoxide
DTSP	**:** 3,3′-Dithiodipropionic acid di(N-hydroxysuccinimide)
DSPE-PEG	**:** 1,2-distearoyl-sn-glycero-3-phosphoethanolamine -N-[amino (polyethylene glycol)-2000] (ammonium salt)
PC	**:** Phosphatidylcholine
SM	**:** Sphingomyelin
PS	**:** Phosphatidylserine
PE	**:** Phosphatidylethanolamine
MDR1	**:** Multi Drug Resistance 1 Protein
P-gp	**:** P-glycoprotein
SPR	**:** Surface Plasmon Resonance
QCM-D	**:** Quartz Crystal Microbalance-Dissipation
AFM	**:** Atomic Force Microscopy
D	**:** Dissipation
F	**:** Frequency
TEM	**:** Transmission Electron Microscopy
TIRF	**:** Total Internal Reflection Fluorescence Microscopy
EIS	**:** Electrochemical Impedance Spectroscopy
CV	**:** Cyclic Voltammetry
FRAP	**:** Fluorescence Recovery After Photobleaching
FTIR	**:** Fourier Transform Infrared Spectroscopy

LIST OF TABLES

Page

LIST OF FIGURES

Page

MEMBRANE PROTEIN-BASED IN VITRO METHODS

SUMMARY

Biological membranes, which consist of lipids, carbohydrates and proteins, are only a few nanometers thick and highly complex structures. Membrane proteins have several crucial roles in cell structure and functionality such as molecule transportation, biological energy conversion, cellular behavior, communication, and recognition. Thus, problems in the membrane protein structure and function result in deficiencies in cell processes and dysfunctions in product formation, and these problematic cases cause a number of diseases from diabetes to cancer. These proteins are therefore targets of many drugs. To investigate membrane protein structure and function, design of cell membrane mimicking systems are essential. Model membrane systems offer a great opportunity to form *in vitro* membrane protein research platforms. Tethered lipid bilayer membrane platform, which is one of the most important model membrane systems, generates an extra space for the integration of large integral proteins into lipid bilayers. The aim of the thesis is to construct an artificial lipid bilayer system, which could be used in the functional integration of membrane proteins with large domains such as multi-drug resistance protein 1 (MDR1). For this, the constructed lipid bilayer system was characterized and its performance in the drug-membrane protein interactions *in vitro* conditions was evaluated using statin-based drugs.

For constructing an artificial membrane system, gold-coated glass and quartz crystal surfaces were used as support materials. The surfaces were first activated using 3,3′-Dithiodipropionic acid di(N-hydroxysuccinimide) (DTSP) molecule, which breaks its disulphide bond to covalently bind to gold-coated surfaces, and presents an active succinimide group at the other end for further modifications. To generate a reservoir between lipid membranes and gold-coated support surfaces for the insertion of large membrane proteins, a modified lipid (*i.e.*, 1,2-distearoyl-sn-glycero-3-phosphoethanolamine-N-[amino (polyethylene glycol)-2000] (ammonium salt) (DSPE-PEG)) was used as a spacer molecule. Phosphatidylcholine molecule was used to prepare liposome solution due to its high abundance in animal and plant cells, and liposomes with 100 nm diameters were produced using an extruder system. To evaluate each binding events and lipid bilayer formation of protein-free and protein-loaded liposomes, Surface Plasmon Resonance (SPR) and Quartz Crystal Microbalance-Dissipation (QCM-D) methods were used. The artificial lipid membrane platform was further characterized using liquid-Atomic Force Microscopy system, and thus, the topology of the lipid layer was evaluated. Additionally, drug-protein interactions were investigated on the constructed tethered lipid bilayer platform.

To attach the spacer layer, a broad range of DSPE-PEG concentrations (0.01 to 0.06 mg/mL) were tried, and the binding of DSPE-PEG molecule was found to increase

with the increased concentrations according to the characterization experiments (*i.e.*, SPR and QCM-D). The molecular arrangement of spacer varies in different PEG surface coverages. For instance, low surface coverages demonstrated higher intramolecular interactions (mushroom-like regime) whereas in high coverages, they interact with other PEG chains, and generate intermolecular interactions (brush-like regime). Characterization methods demonstrated that this conformational transition likely to occur between 0.01 and 0.02 mg/mL concentrations. A significant lipid layer formation was not observed when high (0.05 and 0.06 mg/mL) and low (0.02 and 0.03 mg/mL) concentrations of DSPE-PEG molecule were tested. Both SPR and QCM-D experiments implied that 0.03 mg/mL of DSPE-PEG concentration provided optimum conditions to form lipid bilayer structure. The structural conformation of spacer molecule was visually evaluated using liquid-AFM system. Condensed structure and directional behavior of spacer molecule was observed under aqeous conditions. To evaluate the rewettability of spacer molecule, DSPE-PEG coated layer was first dried, and then re-hydrated. Drying procedure caused the spacer molecule to be in collapse structure, and it increased the roughness parameters of the constructed layer. By re-hydration, uniform coating of the spacer molecule on support surface was observed again, and thus, the constructed layer assumed its previous shape. This presented an advantage for the designed platform since it allows the dry storage of the first layer till the construction of the whole platform for further experiments. In addition, the dimension of the constructed spacer layer was investigated, and spacer molecules presented more condensed and directional behavior in aqueous condition. The directional behaviors of spacer molecule possibly aided to not only lift the lipid layer from the surface, and also, deform the liposomes to form a lipid bilayer structure on the surface. Moreover, the viscoelastic features of PEG residues in spacer molecule significantly decreased the roughness parameters of the unmodified gold-coated surfaces, and presented more flat surface for lipid bilayer construction steps.

To determine liposome binding/spreading and lipid bilayer formation, the effect of DSPE-PEG concentration was evaluated with a fixed volume and concentration of liposomes. Spacer concentration significantly affected the construction of lipid layer platform. QCM-D analysis indicated liposome deformation and the formation of flattened structure at optimum DSPE-PEG concentration (0.03 mg/mL). Non-deformation or partially deformation of liposomes was observed when the other spacer concentrations were tested, and the construction of lipid bilayer platform was continued using 0.03 mg/mL of DSPE-PEG concentration. To visualize the lipid bilayer structure, liquid-AFM system was performed, and it was observed that the overall roughness parameters decreased, and more flat surface (0.452 nm as compared to 0.683 nm) were visualized after the liposome spreading. Thus, AFM analysis of the constructed layer supported the results obtained by QCM-D experiments, and indicated lipid bilayer formation.

To evaluate the integration of membrane proteins into lipid bilayer, MDR1 protein was used as a model protein, and a broad range of MDR1 amounts (0.7 to 5.0 μL) was analyzed using both SPR and QCM-D methods. Optical thickness measurements demonstrated that 1 μL of MDR1-loaded liposomes resulted in the highest binding/spreading. Further, dissipation analysis supported the results obtained by SPR, and it indicated that 1 μL of MDR1 protein amount provided optimum conditions for lipid layer formation. Further observations on QCM-D analysis demonstrated that lipid layer fluidity decreased when MDR1 protein was used, since

the mobility of phospholipids was restricted in the presence of a large protein, as in natural cellular membranes. To visualize MDR1 protein-incorporated lipid bilayers, liquid-AFM analysis was used, and several jut-outs with ca. 1.2 – 2.8 nm in height were observed on the constructed layer. Theoretical dimensions of the exoplasmic regions of MDR1 protein in lipid bilayers are reported as ca. 2 nm in literature. Therefore, the experimental and theoretical results for the exoplasmic section of the membrane protein were observed to be comparable, and AFM analysis supported the results obtained by both SPR and QCM-D. Moreover, anti-MDR1 and anti-Pin8 mouse monoclonal antibody binding studies were performed to evaluate the integration and orientation of MDR1 protein in the constructed lipid bilayer platform. Upon the light of the antibody studies, the integration and correct orientation of MDR1 protein was observed, and thus, MDR1 protein was successfully and efficiently inserted into the lipid bilayers without any observable damage on the native structure of protein.

To investigate drug-membrane protein interactions, statin-based drugs were used. Due to its solubility in water, pravastatin molecule was selected for the experiments, and the other statin-based drugs (*e.g.,* simvastatin and lovastatin) were eliminated because of their lipophilic and non-polar properties, which interfere with the stability of lipid bilayers. As the result of pravastatin-MDR1 protein interaction, it was observed that the optical thickness parameter increased with increased pravastatin concentrations in a concentration dependent manner (*i.e.,* 0.01 and 0.05 mg/mL).

In this thesis, an artificial lipid bilayer platform was successfully constructed for MDR1 protein, which has extra- or intracellular domains, and the interactions between statin-based drugs and MDR1 protein were investigated. Until now, there is no other study to investigate the interactions between statin-based drugs and MDR1 protein on model membrane systems in literature, and thus, artificial lipid membrane platform offers a novelty to investigate these interactions *in vitro* conditions. Further, the presented lipid bilayer platform holds a great promise to be used in membrane protein characteristics and drug-membrane protein interactions without any alteration on the native protein structure. Therefore, the constructed platform is an alternative system to address the challenges in membrane protein research for large membrane-spanning proteins. Further, this platform could be tailored to be integrated with microfluidics and biosensor systems, and it could provide multipurpose platforms to investigate with different membrane proteins and drugs *in vitro* conditions.

ZAR PROTEİN-TABANLI İN VİTRO METOTLAR

ÖZET

Lipitleri, karbohidratları ve proteinleri içeren biyolojik zarlar yalnızca birkaç nanometre kalınlığında ve yüksek karmaşıklıkta yapılardır. Zar proteinleri, molekül taşınması, biyolojik enerji dönüşümü, hücresel davranış, iletişim ve tanıma gibi hücre yapı ve fonksiyonlarında birçok önemli göreve sahiptir. Bu yüzden, zar protein yapı ve fonksiyonundaki sorunlar hücre işlevlerinde problemlere yolaçar ve bu durum diyabetten kansere kadar birçok hastalığa neden olur. Zar proteinleri bu nedenle birçok ilacın hedefi konumundadır. Zar protein yapı ve fonksiyonunu araştırmak için hücre zarını taklit eden sistemler gereklidir. Model zar sistemleri, *in vitro* zar protein araştırma platformaları oluşturmak için önemli bir olanak sunar. En önemli model zar platformlarından biri olan yüzeye bağlı lipit çift-katman zar sistemi geniş integral proteinlerin lipit çift-katman içerisine yerleştirilebilmesi için gerekli bir aralık içerir.

Bu tezin amacı, çoklu-ilaç direnci proteini (MDR1) gibi geniş hücre dışı ve içi bölümleri olan zar proteinlerinin fonksiyonel entegrasyonunda kullanılabilecek bir yapay lipit çift-katman sistemi kurmaktır. Bunun için kurulan lipit çift-katman sistemi karakterize edildi ve ilaç-zar protein etkileşimlerinin incelenmesindeki performansı *in vitro* koşullarda statin-tabanlı ilaçlar kullanılarak belirlendi.

Yapay zar sistemi kurmak için, altın-kaplı cam ve kuvars kristal yüzeyler destek materyal olarak kullanıldı. Yapısında bulunan disülfit bağını koparıp kovalent olarak altın-kaplı yüzeylere bağlanan ve sonraki modifikasyonlar için diğer uçta aktif bir süksinimid sunan 3,3′-ditiyobis(N-süksinimid propionat) (DTSP) molekülü kullanılarak yüzeyler ilk önce aktive edildi. Geniş zar proteinlerinin lipit zarlara entegrasyonunda zar ile altın-kaplı destek arasında boşluk oluşturmak için modifiye edilmiş lipid molekülü (1,2-distearoil-sn-glisero-3-fosfoetanolamin-N-[amino(polietilenglikol)-2000] (DSPE-PEG)) aracı molekül olarak kullanıldı. Hayvan ve bitki hücrelerinde yüksek miktarda bulunduğundan fosfatidilkolin molekülü lipozom solüsyonun hazırlanması için kullanıldı ve 100 nm çaplı lipozomlar ekstrüder sistem ile oluşturuldu. Her bağlanma olayını ve proteinli ve proteinsiz lipozomların lipit çift-katman oluşturmalarını gerçek zamanlı izlemek için Yüzey Plazmon Rezonans (SPR) ve Kuvars Kristal Mikroterazi-Disipasyon (QCM-D) karakterizasyon metotları kullanıldı. Ayrıca, yapay lipit zar platformu sıvı-Atomik Güç Mikroskopi (AFM) sistemi uygulanılarak görüntülendi ve böylelikle, lipit katman topografisi incelendi. Ek olarak, ilaç-protein etkileşimleri kurulan yüzeye bağlı lipit çift-katman platformunda araştırıldı.

Aracı molekülü yüzeye bağlamak için çeşitli DSPE-PEG derişimleri (0.01 – 0.06 mg/mL) denendi ve karakterizasyon deneylerinde (SPR ve QCM-D) yüzeye bağlanan DSPE-PEG miktarının yüksek başlangıç derişimi ile arttığı bulundu. Aracı moleküllerin yüzeyde aldığı konformasyonlar farklı DSPE-PEG yüzey kaplaması durumlarında çeşitlilik gösterdi. Örneğin, yüzeyin düşük miktarda kaplanması

molekül içi etkileşimleri (mantar tipi yapı oluşumu) avantajlı hale getirirken, yüzeyin yüksek oranda kaplanması, ile DSPE-PEG moleküllerinin moleküller arası etkileşimlere (fırça tipi yapı oluşumu) girdiği görüldü. Karakterizasyon metotlarında bu şekilde bir konformasyonel geçişin varlığı 0.01 ve 0.02 mg/mL derişimleriyle oluşturulan yüzeylerde tespit edildi. Yüksek (0.05 ve 0.06 mg/mL) ve düşük (0.02 ve 0.03 mg/mL) DSPE-PEG derişimleri test edildiğinde kayda değer bir lipit katman oluşumu gözlenmedi. SPR ve QCM-D çalışmalarının her ikisinde de 0.03 mg/mL DSPE-PEG derişimi lipit çift-katman oluşumu için optimum koşulları sağladı. Sıvı-AFM sistemi kullanılarak aracı molekülün yapısal konformasyonu karakterize edildi. Aracı molekülün konformasyonel davranışını farklı koşullarda incelemek için DSPE-PEG kaplı katman öncelikle kurutuldu ve sonra tekrar ıslatıldı. Kurutma işlemi sonucunda yüzeyde küresel yapılar gözlendi. Bu durum, kurulan katmanın pürüzlülük parametresini arttırdı. Bu katman tekrar sulu ortama konulduğunda aracı molekülün önceki şeklini aldığı tespit edildi ve böylelikle, DSPE-PEG katmanının sonraki aşamalar için hazırlanıp kuru saklanabileceği tespit edildi. Ek olarak, oluşturulan aracı molekül katmanın boyutu incelenerek sıvı koşullarda bu katmanın daha yoğun ve yönlenmiş bir davranış ortaya koyduğu gözlemlendi. Aracı molekül katmanının bu yönlenmiş davranışı lipozomların deformasyonunu sağlayarak lipit çift-katmanı oluşturmasını ve bu katmanın yüzeyden yükseltilmesini sağladığı tespit edildi. Ayrıca, modifiye edilmemiş altın-kaplı yüzeylerin pürüzlülük parametreleri aracı molekülün bağlanmasından sonra belirgin bir şekilde azaldı ve daha düz bir yüzey elde edildi. Pürüzlülük parametresindeki bu azalmanın aracı moleküldeki PEG altbirimlerinin vizkoelastik özelliklerinden dolayı olduğu düşünüldü.

DSPE-PEG derişiminin lipozomların bağlanma/yayılma ve lipit çift-katman oluşturması üzerindeki etkisini incelemek için sabit hacim ve derişimdeki lipozom solüsyonları kullanıldı. Aracı molekülün derişimi lipit katman platformunun kurulmasını kayda değer bir biçimde etkiledi. SPR ve QCM-D analizleri ışığında 0.03 mg/mL DSPE-PEG derişiminin kullanıldığında lipozom deformasyonu ve lipit katman oluşumu için optimum koşullar sağlandı. Diğer aracı molekül derişimleri test edildiğinde ya lipozom deformasyonunun olmadığı ya da kısmi deformasyonun gerçekleştiği gözlemlendi. Bu nedenle, lipit çift-katman platformunun kurulması için deneylere 0.03 mg/mL DSPE-PEG derişimi kullanılarak devam edildi. Lipit çift-katman yapısını görüntülemek için sıvı-AFM sisteminden yararlanıldı. AFM çalışmalarında lipozom yayılmasından sonra pürüzlülük parametrelerinin azaldığı (0.683 nm ve 0.776 nm'den 0.452 nm ve 0.555 nm'ye) ve daha düz bir yüzeyin oluştuğu gözlemlendi. Böylelikle, kurulan katmanın destek yüzey üzerinde lipit çift-katman oluştuğu AFM analizi ile de gösterildi.

Zar proteinlerinin lipit çift-katman içerisine entegrasyonunu araştırmak için MDR1 proteini model protein olarak kullanıldı. SPR ve QCM-D metotları kullanılarak çeşitli MDR1 protein miktarlarında (0.7 - 5.0 µL) deneyler yapıldı. Optik kalınlık ölçümleri 1 µL MDR1 protein-yüklü lipozomların yüksek bağlanma/yayılma ile sonuçlandığını gösterdi. Ayrıca, disipasyon analizi SPR'dan elde edilen sonuçları destekledi. QCM-D analizi MDR1 proteini varlığında lipit katmanın akışkanlığının azaldığını gösterdi. Bu durumun doğal hücresel zarlarda olduğu gibi fosfolipitlerin hareketlerinin kısıtlanmasından kaynaklandığı düşünüldü. MDR1-yüklü lipit çift-katmanları görüntülemek için sıvı-AFM analizi yapıldı. Oluşturulan lipit katman üzerinde yaklaşık 1.2 - 2.8 nm yükseklikte birçok belirgin yükselti tespit edildi. Bu sonuçlar MDR1 proteininin sitoplazma dışındaki bölgesi için deneysel ve teorik değerlerin (2 nm) benzer olduğunu ve SPR ve QCM-D'den elde edilen sonuçları

desteklediğini göstermektedir. Ayrıca, oluşturulan lipit katman içerisindeki MDR1 proteininin entegrasyonunu ve oryantasyonunu belirlemek için anti-MDR1 ve anti-Pin8 monoklonal antikor çalışmaları yapıldı. Antikor çalışmaları ışığında, MDR1 proteininin lipit katmanlar içerisine doğal yapısında farkedilebilen herhangi bir bozulma olmadan başarılı ve etkili bir biçimde yerleştirildiği gözlemlendi.

İlaç-zar proteini etkileşimlerini incelemek için statin-tabanlı ilaçlar kullanıldı. Suda çözünebilme özelliğinden dolayı pravastatin molekülü deneyler için seçildi. Lipofilik ve polar olmayan özellikteki diğer statin-tabanlı ilaçlar (örneğin, simvastatin ve lovastatin) lipit çift-katman yapısını etkilediğinden dolayı deneylerde kullanılamadı. Pravastatin-MDR1 protein etkileşiminin araştırıldığı bu deneylerde bağlanma miktarı ilaç derişimine bağlı olarak (0.01 ve 0.05 mg/mL) arttı.

Bu tezde, hücre içi ve dışında geniş bölgeleri olan MDR1 proteini için yüzeye bağlı yapay lipit platformu başarıyla kuruldu. Ayrıca bu platformda statin-tabanlı ilaçlar ve MDR1 proteini arasındaki etkileşimler incelendi. Literatürde statin-tabanlı ilaçlar ve MDR1 proteini arasındaki etkileşimlerin model zar sistemlerinde çalışıldığı herhangi bir ön çalışma bulunmamaktadır. Bu tezde statin-MDR1 proteini etkileşimleri yapay lipit zar platformu kullanılarak yeni bir yöntemle *in vitro* koşullarda incelenerek bu alandaki çalışmalara bir yenilik kattı. Ayrıca, yüzeye bağlı yapay lipit çift-katman sistemi zar proteininin doğal yapısında herhangi bir değişim oluşturmadığından protein karakteristiği ve ilaç-zar protein etkileşimleri çalışmaları için büyük umut vaad etmektedir ve böylelikle, kurulan platform hücre içinde ve dışında geniş bölgeleri olan zar proteinlerinin araştırılmasındaki sorunları çözebilen alternatif bir sistem sunmuştur. Ek olarak, yapay lipit çift-katman platformu ile mikro-akışkan ve biyosensör sistemleri birlikte kullanılarak farklı zar proteinleri ile çeşitli ilaçların *in vitro* koşullarda etkileşimlerinin incelemesini sağlayan çok amaçlı platformlar gelecekte oluşturulabilir.

1. INTRODUCTION

1.1 Purpose of Thesis

The most significant obstacle in the membrane protein research is the purification of membrane proteins with large water-insoluble hydrophobic regions. In aqueous solutions, these proteins cannot conserve their three-dimensional structure, and thus, model membrane systems provide cellular membrane mimicking platforms to preserve their structure and function as in their native environment. In this study, the potential of model membrane systems was studied to evaluate and characterize membrane proteins *in vitro* conditions. For this aim, a tethered lipid bilayer platform was constructed on a solid support surface. Multi-drug resistance (MDR1) protein was used as a model membrane protein, and lipid bilayer was formed using phosphatidylcholine due to its high abundance in mammalian cells. To prevent the potential instability and damages on the membrane protein, a modified lipid molecule (*i.e.,* 1,2-distearoyl-sn-glycero-3-phosphoethanolamine-N-[amino(polyethylene glycol)-2000]) was used as a spacer molecule to elevate the lipid membrane from gold-caoted support surface. To understand the incorporation and orientation of membrane proteins into lipid membranes, anti-MDR1 human monoclonal antibody and anti-Pin-1 mouse monoclonal antibody was used as positive and negative control, respectively. To evaluate the potential interactions between drug/toxin and membrane protein on model membrane systems, statins, cholesterol-lowering drugs, were analyzed on MDR1-incorporated lipid bilayers. All binding events, characterization and optimization studies were performed using Surface Plasmon Resonance and Quartz Crystal Microbalance. The constructed lipid bilayer platform was also visualized using liquid-Atomic Force Microscopy in order to investigate layer-by-layer modification and membrane protein incorporation into lipid bilayer platform.

1.2 Biological Membranes

All living organisms comprise from cells as the structural and functional blocks. All cells are surrounded by plasma membrane, which has several crucial roles in cellular structure and functions such as the control of solute permeability, biological energy conversion, cell division, cell signal trafficking, and recognition (Lodish et al., 2004). Additionally, there are a number of membrane-structured cellular components (*e.g.*, organelles) that have significant characteristic properties including energy production, macromolecule modification and maturation in eukaryotic cells. Further, the plasma membrane defines an external boundary of the cell, and provides a tremendous unity to isolate the cellular components from the exterior environment. This property allows to continuously generate chemical and electrical gradients that work as a bipolar electrode. Additionally, the membrane plays several key roles to support the proteins and other functional components of the cell. The cell membrane is also involved in transportation of molecules into and out of the cell, cellular communication, and adhesion. For instance, at the cell surface, there are several transporters that enable to move specific organic solutes and inorganic ions across the membrane. For cellular communication, there are various receptors that perceive extracellular signals and activate molecular changes in the cell, and there are also adhesion molecules that keep adjacent cells together.

Biological membranes act as a selectively permeable barrier and generate preferential communication regions between intracellular and extracellular space. Membranes are impermeable to most polar or charged solutes, but they are permeable to nonpolar compounds. Their thickness is approximately 4 to 5 nm (40 to 50 Å), and they comprise different laminar structures when their cross section is monitored using an electron microscope. Their permeability is not merely passive, and they include a collection of proteins specialized for encouraging or catalyzing several cellular processes including transportations of molecules. Membranes are also flexible and self-sealing, and their flexibility allows several changes in the cellular shape that assist cell growth and movement. These highly complex and dynamic structures of membranes, only a few nanometers thick, consist of a lipid bilayer where membrane proteins are localized (Figure 1.1). In 1972, Singer and Nicolson presented a cellular membrane model called as fluid mosaic model (Singer

& Nicolson, 1972). According to this model, the cellular membranes display a fluid structure, and membrane-integrated proteins associate with cytoplasm or extracellular side of the membrane (Figure 1.1). This model also demonstrates that lipids and proteins locate randomly through lateral diffusion in lipid bilayer surface with limited rotational mobility.

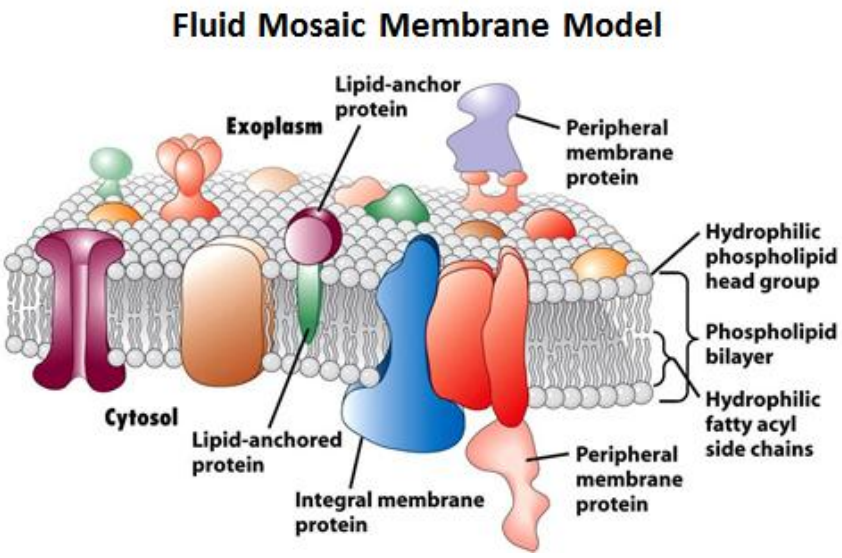

Figure 1.1 : Illustration of highly complex and dynamic structure of biological membrane, adapted from (Lodish, 2008).

1.3 Membrane Composition and Architecture

Researches regarding the composition of plasma membrane hold a vital step to discover and understand cellular membrane function. For instance, common fundamental properties and unique components for specific functions can be realized and discovered by understanding the compositions of plasma membrane components, and thus, the function of cellular membranes was deeply comprehended.

Major compounds of cellular membranes are a variety of lipids, and the rest comprises proteins and carbohydrates. The relative ratio of protein, lipid, and carbohydrates alters in different types of membranes, and the variance in the composition indicates and determines the diversity of biological roles (Nelson & Cox, 2004). For instance, neurons have a myelin sheath, which consists of an extended plasma membrane, and this membrane structure covers around neuron cell several times to generate a passive electrical insulator (Hrdina, 1996). In the membrane composition of the myelin sheath, the lipids have the most portion,

whereas the plasma membranes of bacteria, mitochondria and chloroplasts include more proteins than lipid (Pollard, 1990).

1.4 Lipids

A typical plasma membrane consists of lipids in high ratio, which are amphiphilic molecules having a polar head group and hydrophobic carbon chain (Figure 1.2). Although lipids in plasma membrane have this amphipathic property in common, they vary in their chemical structure and function in the membrane. The lipid components affect membrane shape and function, and they also play several key roles in anchoring proteins to the membrane, modifying the membrane proteins, and controlling signal transduction in the cytoplasmic and extracellular space (Pollard, 1990).

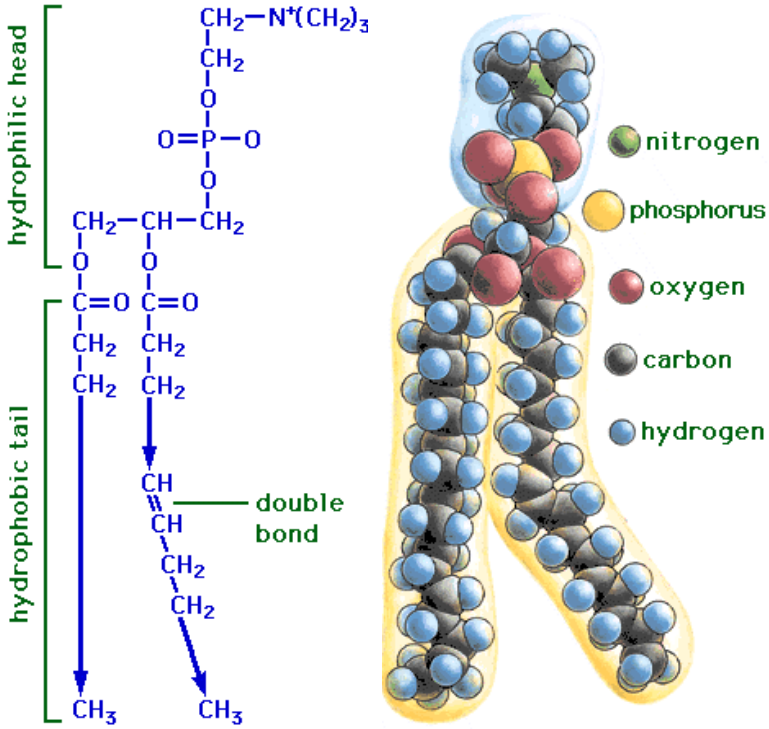

Figure 1.2 : An example of lipid structure (*i.e.*, phospholipid molecule) (Url-1).

1.4.1 Characteristics of lipids

Lipids have two characteristics: A hydrophobic tail region and a hydrophilic head region. The hydrophobic region repels from water while the hydrophilic region attracts to it. Due to their hydrophobic-hydrophilic and van der Waals interactions with the surrounding environment, tail groups self-associate into specific structures such as micelles, liposomes, and lipid bilayer.

Micelles are considerably small spherical structures comprising from an aggregation of surfactant molecules dispersed in a liquid colloid, and they can form when the lipid amount is lower than water. Once lipid bilayers are formed by hydration, liposome structures form in aqueous environment. Lipid molecules generate a bilayer structure where the polar head groups of the lipid molecules face outward and the nonpolar regions in each layer face the core of the bilayer, repelling from the aqueous phase. Lipids in the bilayers have mobile characteristics, and these molecules can change their conformation, rotate on the bilayer surface, diffuse laterally, and flip-flop between two monolayers (Mouritsen, 2005). The lipid molecules provide the cell membrane to be flexible, which is required for their primary functions such as adhesion and migration.

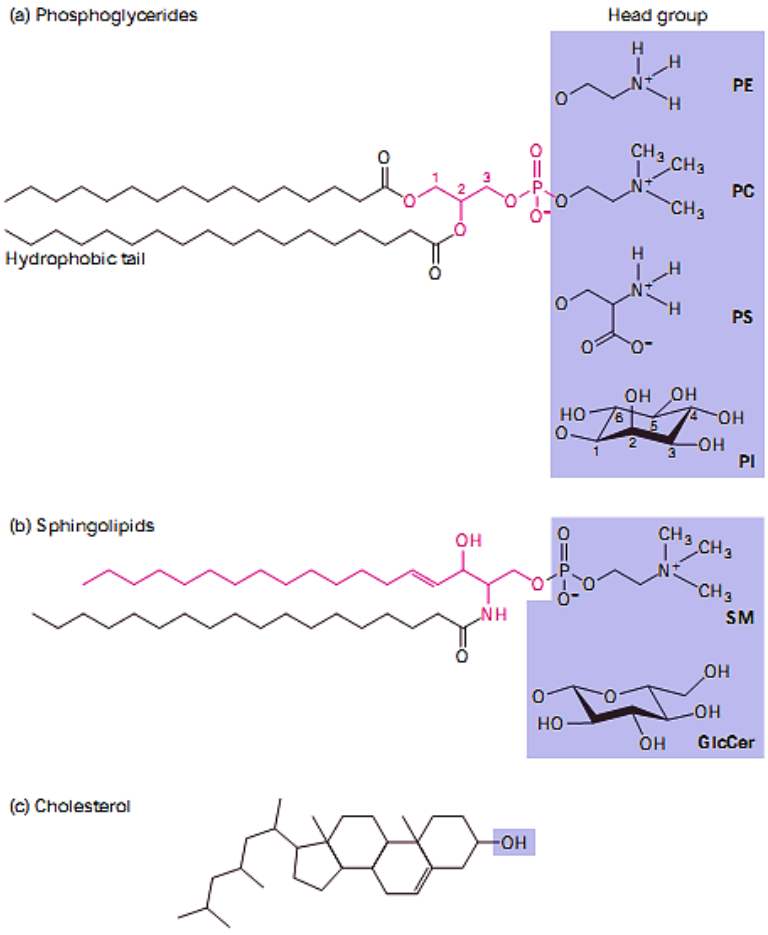

Figure 1.3 : Lipid classification in biological membranes, adapted from (Lodish, 2004).

The lipid bilayer has two crucial features. First, the hydrophobic core generates an impermeable barrier to prevent the diffusion of hydrophilic molecules across the membrane. Besides, this barrier property is controlled by the membrane proteins,

which assist the transportation of specific molecules across this impermeable bilayer. The second feature of the bilayer is related to the stability. The bilayer structure and unity is provided by hydrophobic and van der Waals interactions between the lipid chains. Although the aqueous condition of the membrane can broadly vary in ionic strength and pH, the bilayer structure has the strength to sustain its characteristic structure (Nelson & Cox, 2004).

1.4.2 Lipid classification

There are three classes of lipids reported in literature that form a typical biological membrane (Figure 1.3) (McMullen et al., 2004). All three classes of lipids have amphipathic characteristics as indicated before, and they present a diversity in their chemical composition and specific features.

The most abundant class of lipids in the membranes is phosphoglycerides, which are derivatives of glycerol 3-phosphate (Berg et al., 2002). Typically, a phosphoglyceride molecule comprised from a hydrophobic tail region consisting of two fatty acyl chains esterified to two hydroxyl groups in glycerol phosphate and a polar head group bound to the phosphate group (Figure 1.3a). The two fatty acyl chains vary in the carbon numbers (mostly 16 or 18 carbons) and the saturation degree (Nelson & Cox, 2004). A phosphoglyceride varies according to the nature of its head group, and phosphatidylcholines (PC), the most abundant phosholipids in plasma membrane, comprise from choline group in the head region. The other common phosphoglycerides are phosphatidylethanolamine (PE), phosphatidylserine (PS), and phosphatidylinositol (PI) (Figure 1.3a).

The other lipid class in the biological membranes is the sphingolipids (Figure 1.3b) (Lodish et al., 2004). These lipids are derived from sphingosine, which is an amino alcohol with a long hydrocarbon chain. Sphingolipids contain a long-chain fatty acid bound to the sphingosine amino group. Sphingomyelin (SM) is the most abundant sphingolipid, and its phosphocholine molecule is bound to the last hydroxyl group of sphingosine. Thus, the overall structure of sphingomyeline is quite similar to phosphatidylcholine (Figure 1.3b) (Lodish et al., 2004). Other sphingolipids are glycolipids (*e.g.*, glucosylcerebroside), which have polar head groups made of sugars. The ratio of these glycolipids is approximately 2-10 % of the total lipids in

plasma membranes, and their abundancy is high in nervous tissue (Lodish et al., 2004).

The latter lipid class in biological membranes is steroids, which constitutes from cholesterol and its derivatives (Figure 1.3c) (Berg et al., 2002). Basically, the structure of steroids comprises from a four-ring hydrocarbon. Cholesterol is the most found steroid molecules in animal tissues, and it has a hydroxyl group on one ring, which can interact with water molecule (Figure 1.3c). Cholesterol is particularly rich in the plasma membranes of mammalian cells but it lacks in most prokaryotic cells.

Overall, all three classes of the lipids behave various characteristics in different cell types. Their characteristics are majorly dependent on the exterior environment such as pH and ionic strength. For instance, at neutral pH, some phosphoglycerides (*e.g.*, PC and PE) have no net electric charge, and the others (*e.g.*, PI and PS) have a single net negative charge. On the other hand, the polar head groups in all phospholipids have capability to self-pack together to form a bilayer structure, and their ratio is dependent on the cell type and function (Table 1.1) (Lodish et al., 2004).

Table 1.1: Lipid composition in selected biological membranes, adapted from (Lodish, 2004)

Source/Location	PC	PE+PS	SM	Cholesterol
Plasma Membrane (human erythrocytes)	21	29	21	26
Myelin membrane (human neurons)	16	37	13	34
Plasma membrane (*Escherichia coli*)	0	85	0	0
Endoplasmic reticulum membrane (rat)	54	26	5	7
Golgi membrane (rat)	45	20	13	13
Inner mitochondrial membrane (rat)	45	45	2	7
Outer mitochondrial membrane (rat)	34	46	2	11
Primary leaflet location	Exoplasmic	Cytosolic	Exoplasmic	Both

1.4.3 Role of lipids in biological membrane structure

The lipids have ability to diffuse laterally in a bilayer structure because of their fluidic property. The bilayer fluidity is dependent on the lipid composition, structure

of the phospholipid hydrophobic tails, and environmental conditions such as temperature.

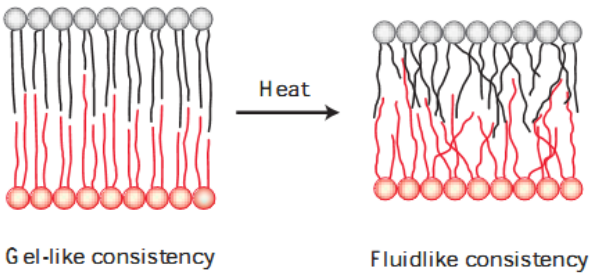

Figure 1.4 : Gel and fluid state of phospholipid bilayer, adapted from (Lodish, 2004).

Molecular interactions (*e.g.,* van der Waals and hydrophobic interactions) cause the nonpolar regions of phospholipids to come each other and aggregate, and the number of carbon chains and saturation degree determine the lipid bilayer structure (Singer & Nicolson, 1972). For instance, long and saturated fatty acyl chains have the greatest ability to aggregate, pack tightly together into a gel-like state (Figure 1.4). Short fatty acyl chains have less surface interaction area, and thus, they form more fluid bilayers (Figure 1.4). Further, temperature is another crucial parameter for bilayer structure (Singer & Nicolson, 1972). For instance, when a gel-like bilayer structure is heated up, the molecular motions of the fatty acyl tails increase, and this causes to change gel-like bilayer structure state to a more fluid state (Figure 1.4). At physiologic temperatures (35-37°C), the hydrophobic region of membranes usually has a low viscosity, and a fluid-like structure is dominant at these temperatures (Lodish et al., 2004).

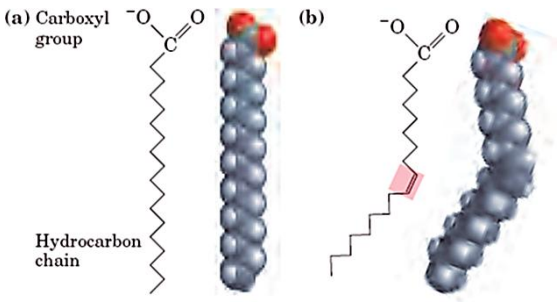

Figure 1.5 : Saturation degree of lipid molecules. a) Saturated lipid. b) Unsaturated lipid, adapted from (Lehninger, 2004).

Saturation degree also affects the fluidity of the phospholipid bilayer, and there are bend-like structures in unsaturated fatty acyl chains to cause more fluid structures

due to their less stable van der Waals interactions with other lipids (Figure 1.5) (Lodish et al., 2004).

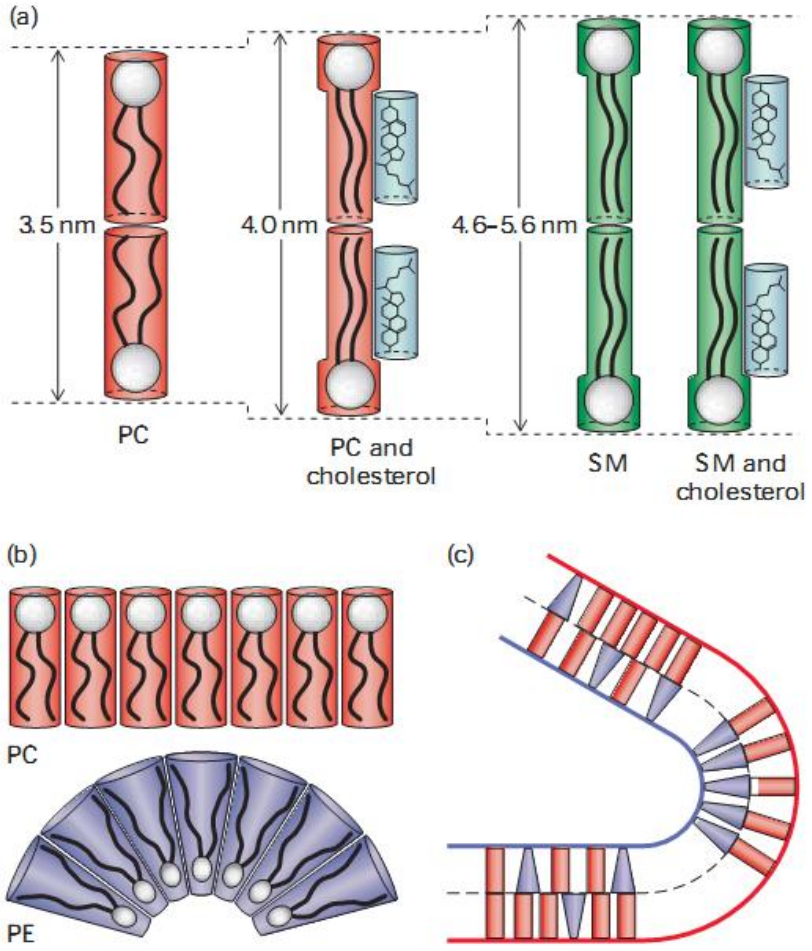

Figure 1.6 : Effect of lipid composition on bilayer thickness and shape. a) Comparison of the lipid sizes on the bilayer structure. b) Phospholipid shape. c) Effect of lipid shape on membrane curvature, adapted from (Lodish, 2004).

On the other hand, the lipid composition is a critical parameter for the bilayer shape and thickness, and it plays key roles in protein integration into the membrane. For instance, sphingomyelin provides a more gel-like and thicker bilayer whereas cholesterol reduces the membrane fluidity and increase the membrane thickness (Figure 1.6a) (Nelson & Cox, 2004). Another parameter is the local curvatures in the bilayer. Local curvatures depend on the sizes of the polar head groups and the length of non-polar hydrophobic carbon tails in phospholipids. Lipids with long tails and large head groups form cylindrical in shape whereas lipids with small head groups present cone shaped structure (Figure 1.6b) (Nelson & Cox, 2004). Thus, the bilayers constructed with cylindrical lipids are quite flat, and those composed of conical lipids

generate curved bilayers (Figure 1.6c). The curvatures play a key role to form highly circular membrane structures such as internal membrane vesicles and microvilli.

As the perspective of membrane lipid composition, cholesterol is an important parameter in preserving and sustaining the fluidity of plasma membrane. In the literature, fluidity is also reported to be essential for normal cell growth and reproduction (Huffer et al., 2011). Cholesterol concentration is another critical parameter for bilayer structure, and it limits the random movement of phospholipid head groups (Bastiaanse et al., 1997). Steroid ring of cholesterol separates and disperses phospholipid tails at low cholesterol concentrations, and this results in slightly more fluid membrane structure (Cooper, 1978). Regular concentrations of cholesterol in biological membranes decrease the membrane fluidity and generate more rigid structures. The lipid composition and concentration of a bilayer structure also affect the thickness, and this property may play a key role for membrane proteins to be localized into the lipid bilayer.

1.5 Membrane Proteins

Membrane proteins are localized within or at the surface of a phospholipid bilayer. Although every biological membrane has similar basic structural components in their structure, the association of proteins into the membrane gains distinctive functions to the membrane. The protein concentration and composition varies in the protein-associated membranes depending on the cell type, function, and subcellular location. For instance, inner membrane of mitochondrial membrane comprises 76% protein whereas myelin membrane only consists of 18%. High phospholipid content in myelin membrane provide electrical insulation to nerve cells from its native environment (Baumann & Pham-Dinh, 2001).

Biological membranes offer a unique hydrophobic condition to associate membrane proteins. Depending on the protein characteristics, some proteins are embedded into the membrane whereas the others are associated with only hydrophilic regions of the membrane (*i.e.*, exoplasmic or cytosolic leaflet of the bilayer). Protein domains localized on the extracellular surface of the membrane usually interact with the other specific molecules such as the external signaling ligands, ions, small metabolites, and adhesion molecules (Lodish et al., 2004). Some domains spanning the membrane can

also form channels and pores to allow the transportation of molecules/metabolites to intra- or extracellular space of the cell. On the other hand, domains localized on the cytosolic face of the plasma membrane have a broad range of functions such as anchoring cytoskeletal proteins to the membrane, and triggering intracellular signaling pathways (Lodish et al., 2004).

1.5.1 Membrane protein classification

Membrane proteins play several crucial functional and structural roles in cell, and they can be classified into three categories depending on their location in the lipid bilayer (Lodish et al., 2004).

Integral membrane proteins, as known as transmembrane proteins, span a phospholipid bilayer multiple times, and they have domains in the cytoplasmic and exoplasmic space of the cell (Figure 1.7). These domains generally constitute water-soluble proteins in their amino acid composition, and interact with aqueous solutions in their three-dimensional structure. On the other hand, these proteins have hydrophobic amino acid content, which is buried into the lipid bilayer, and their side chains protrude to outside of the phospholipid bilayer. Integral proteins are very tightly incorporated with the lipid bilayer, and can be removed by only interfering agents such as detergents, organic solvents, or denaturants (Speers & Wu, 2007). In literature, it is reported that the membrane-spanning domains of all transmembrane proteins consist of at least one α-helices or β-strand (von Heijne, 2006). Further, most of transmembrane proteins have several glycosylation sites to attach complex sugar groups to one or several amino acid side chains, and these sugar chains are generally localized to the exoplasmic domains of the membrane proteins, which play key roles in the cell signaling (Laskey, 1989).

The second class of membrane proteins, lipid-anchored membrane proteins, forms covalent binding with single or multiple lipid molecules (Figure 1.7). The hydrophobic carbon chain of the lipid on one side of the membrane serves the protein to be localized on either inner or outher face of the cell membrane. Without the lipid interaction and binding, the protein does not integrate with the lipid bilayer. Prenylation is the mechanism to attach the proteins to the lipid bilayer, and allows to facilitate the interaction of lipid-anchored membrane proteins with plasma

membrane. Typically, potential attachment sites of these proteins are on the terminal amino group of the protein backbone and the side chain of cysteine residues. Further, the exact function of lipid-anchored proteins has been unknown, but it is reported that these proteins act as an intracellular signal that targets proteins to the apical surface in polarized cells (Karp, 2009).

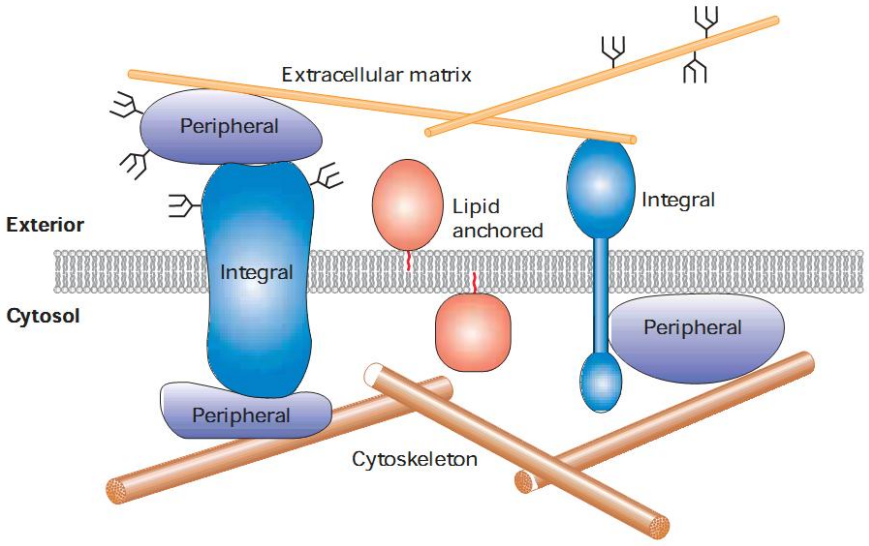

Figure 1.7 : Membrane protein classification in biological membranes, adapted from (Lodish, 2004).

The latter class, peripheral membrane proteins, does not have any interaction with the hydrophobic core of phospholipid bilayer (Figure 1.7). Typically, these proteins are bound to lipid membrane by interacting with either integral membrane proteins (indirectly binding) or lipid head groups (directly binding), and thus, their location is on either the cytoplasmic or the exoplasmic face of the plasma membrane. These proteins can be removed by mild agent treatments such as carbonate at high pH (Fujiki et al., 1982). Further, peripheral proteins may act as regulators of membrane-bound enzymes or may control and limit the mobility of integral proteins by anchoring them (Cafiso, 2005). These proteins interact with cytoskeletal components to support the cellular membranes, and also play a key role in the cellular communication between the interior and exterior section of the cell (Woods & Lazarides, 1988). Additionally, peripheral proteins localized on the outward of the membrane and the exoplasmic domains of integral proteins generally attaches/interacts to the extracellular matrix components (Lodish et al., 2004).

1.5.2 Role of membrane proteins in biological membranes

Membrane proteins have capability either to move freely through the lipid bilayer or attach to cytoskeleton and extracellular matrix. They also present cellular functions including signal transduction, transportation, cell adhesion and communication. Additionally, they also act as transporters, enzymes, receptors, and anchor molecules (Figure 1.8). The other interesting examples for membrane proteins can be pore-forming toxin proteins. These water-soluble proteins present in plant, bacteria, and mammalian cells, and they have several crucial roles in defense system. After their secretion to the target cell, these toxin proteins form pores, and become an integral transmembrane protein in the target cells membrane in order to damage the target cell (Iacovache et al., 2008). Additionally, some of membrane proteins such as multi-drug resistance proteins (MDR) play a key role to deport several xenobiotics from the cytoplasmic space to exoplasmic environment. These proteins provide to resist a broad variety of distinct drugs or chemicals, and gain multi-drug resistance to the organism. For instance, MDRs have ability to transport a wide range of anticancer drugs to out of cells, and their high expression in many tumors makes them as prime suspects in unexplained cases of drug resistance in tumors (Borst et al., 2000).

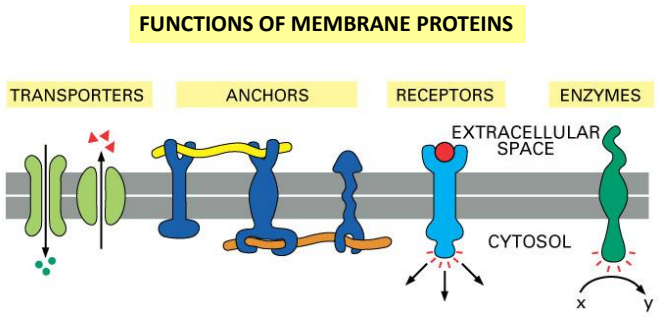

Figure 1.8 : Functions of membrane proteins in plasma membrane (Url-2).

1.5.3 Multi-drug resistance protein (MDR1)

MDR1 protein (P-glycoprotein), a 170 kDa gene product of MDR1 gene, is the one of the most investigated transmembrane proteins (Figure 1.9). This transmembrane protein exists in all cell types, and its expression level is high in gastrointestinal space, blood-brain and blood-testis barrier, adrenal gland and hepatocytes. Although its primary function has not been fully discovered, it is reported that MDR1 protein has several crucial roles in cellular defense mechanism by throwing away

xenobiotics using its ATPase domains located on the cytosolic face (Gottesman & Pastan, 1993).

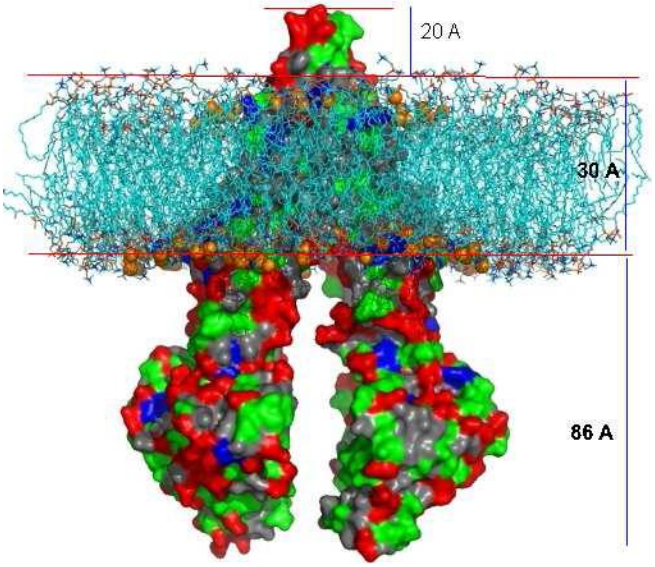

Figure 1.9 : Molecular structure of P-glycoprotein, adapted from (Karasu, 2011).

1.6 Drug-Membrane Protein Interactions

As biological and pharmacological perspective, to discover and evaluate protein-protein and lipid-protein interactions in lipid bilayers allow a better understanding of structural and functional processes (*e.g.*, molecule transport, energy conversion, and cellular signaling) occurring in cell. The membrane proteins, which have vital importance for cells, are targets for 70% of the drugs in the market (Kopec et al., 2005). For instance, asthma drugs bind specific membrane proteins on liver cells; antidepressant drugs provide to transport several specific metabolites across the neural membrane; anesthetic drugs control the activity of specific channel proteins in nervous system. Further, membrane proteins are not only target for drugs, and also several toxins (Gordon et al., 1996).

1.6.1 Statins

Statins are used as hypolipidemic cholesterol-lowering drugs to inhibit 3-hydroxy-3-methylglutaryl-coenzyme A reductase enzyme, which plays a key role in the production of cholesterol in the liver. After their import into the cytoplasm, the mevalonate pathway is blocked, and low density lipoprotein particles are removed from bloodstream in order to reduce blood cholesterol level (Dietschy & Wilson,

1970). Although statins are used to treat several diseases, they increase the number of T cells (Mausner-Fainberg et al., 2008), and this results in to trigger throat cancer (Bates et al., 2006), ovarium cancer (Curiel et al., 2004), hepatocellular carcinoma (Kobayashi et al., 2007), and prostate cancer (Ford et al., 2007).

Typically, statins can be tolerated well in body but their interactions with other drugs cause to several side effects including carcinogenesis, heptoxide, and muscle damage (Christians et al., 1998; Golomb & Evans, 2008; Hsu et al., 1995). In literature, statins also play an inhibitory role on MDR1 protein function, and this interaction was demonstrated using several *in vivo* methods (Wang et al., 2001).

1.7 Model Biological Membrane Systems

The most critical challenge to evaluate and discover membrane protein structure and functionality is the purification of membrane proteins due to their water-insoluble hydrophobic regions, and thus, these proteins cannot conserve their native three-dimensional structure in aqueous solutions. To construct and develop model membrane system will offer to investigate and better-understand not only the function and structure of membrane proteins *in vitro*, and also drug/toxin-membrane protein interactions.

There is a variety of model systems to discover the molecular processes occurring at biological membranes (Richter et al., 2003). These artificial lipid membranes are generally used to characterize biological membrane components (*e.g.*, proteins) and membrane active compounds (*e.g.*, ligands). There are several model membrane systems including micelles, bicelles, nanodiscs, liposomes, black lipid films, solid-supported membranes, and so on (Figure 1.10) (Richter et al., 2003).

McConnell and co-workers pioneered in model membrane technology, which has been widely used in basic studies of membrane processes and possible biotechnological applications (McConnell et al., 1986). During the past decade, the applications of surface-based membrane systems have considerably increased, and allowed to work with membrane receptor-integrated lipid bilayer systems for prestigious platforms based on biosensor and microfluidic technologies (Castellana & Cremer, 2006; Lundquist et al., 2010).

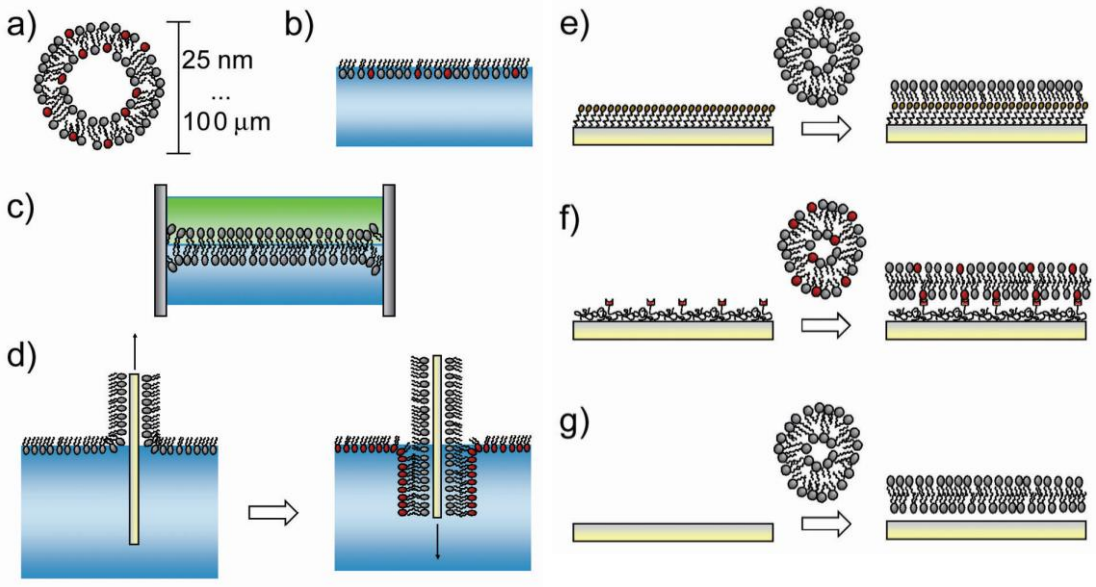

Figure 1.10 : Model membrane systems. a) Liposomes, b) lipid monolayers at the air-water interface, c) black lipid membranes, d) mono and multi-layers of lipids produced by Langmuir-Blodgett method, e) solid-supported lipid membranes, f) polymer-supported bilayer lipid membranes, g) spontaneous spreading of liposomes or membranes on solid support material, adapted from (Richter, 2003).

1.7.1 Liposomes

Liposomes are lipid vesicles in spherical shape formed by single or multiple lipid bilayers in an aqueous condition. They are generally formed by phospholipid molecules, and present energy-favorable structures in aqueous solution by using their hydrophilic and hydrophobic interactions (Torchilin, 2006). Diversity of the liposomes depends on the number and the size of bilayers such as large multilamellar vesicles (MLVs) or large and small unilamellar vesicles (LUVs and SUVs) (Figure 1.11) (Jesorka & Orwar, 2008; Maestrelli et al., 2006). A single lipid bilayer size is approximately 4-5 nm, and a unilameller liposome size varies 20-500 nm depending on the encapsulated aqueous volume. The liposome production methods rely on several parameters including:

- The physiochemical characteristics of lipids involved in liposome production;
- The nature of the medium where lipid vesicles are formed;
- Extra processes requirement involved in the application of the liposome formation;

- Optimum size, polydispersity and shelf-life of liposomes for the desired application;

- Batch-to-batch reproducibility, efficiency, and possibility to form large-scale production of liposomes (Gomez-Hens & Fernandez-Romero, 2006; Mozafari et al., 2008).

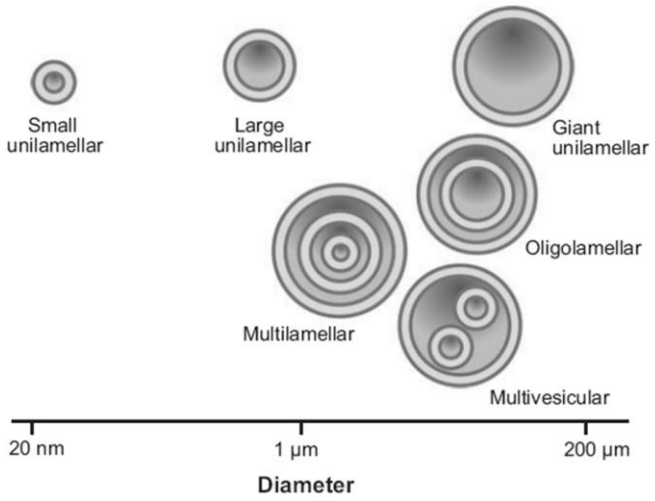

Figure 1.11 : Classification of liposomes, adapted from (Jesorka, 2008).

Liposome structure and size allow to encapsulate and immobilize water soluble or insoluble molecules inside and/or integrate to the liposome. This opportunity also makes the liposomes to be used in controlled drug delivery applications such as anticancer therapy (Chang et al., 2009), and thus, liposomes assist to increase the effectiveness and circulation time of drugs (Gabizon & Papahadjopoulos, 1988). As a model membrane perspective, liposomes have ability to be modified in a desired manner that can mimic the structure and function of cellular membranes as in their native condition. By modifying the liposome surface, it is also possible to target the specific cells and cellular components (Hale et al., 1980). However, the lack of the accessibility to inner side of the liposome membrane restricts the utility of liposomes for electrochemical and surface-based applications.

1.7.2 Black lipid membranes

Black lipid membrane is another most useful membrane model, which was first described by Mueller in 1962 (Mueller et al., 1962). Since this membrane system permits simultaneous access to the solution and electrical control for both sides of the bilayer, it reasonably presents physiological conditions and mimics an actual cell

membrane (Romer & Steinem, 2004). In membrane research, black lipid membranes are used as recognition elements and host matrixes for membrane proteins (Mueller et al., 1962).

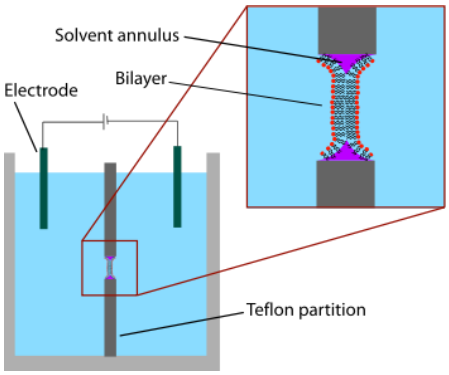

Figure 1.12 : Black lipid membrane production (Url-3).

Typically, black lipid membranes consist of three components: Lipid bilayer, a ring component, and microlenses (Figure 1.12). Contrast to liposome formation, black lipid membrane is formed by spreading a lipid solution in a small hole (Ø 0.5mm) between two walls separating two distinct aqueous environments. Black lipid membrane systems contribute temporarily evolution of membrane lipids according to their phase behavior in fluid conditions as in their native conditions (Shalaev & Steponkus, 1999).

Black lipid membranes allow to access and control both sides of the membrane, and they are convenient for electro-chemical measurement (Romer & Steinem, 2004). Beside to these advantages, black lipid membrane systems suffer from several challenges in their production and characterization. As production aspect, the physical stability of black lipid membranes is quite low, and affected by the residues inside the bilayer. For instance, material properties of the bilayer including thickness (Fettiplace et al., 1971), elasticity (Raghunathan et al., 2012), and electrical properties (Coster & Laver, 1986) are main limitation factors to reproduce these membrane systems. However, black lipid membranes have size limitations, and so, it is impossible to produce large lipid bilayers (Ries et al., 2004). As characterization aspect, there is no convenient optical technique for characterization of the static and dynamic structure of black lipid membranes (Benz & Janko, 1976). Every black lipid membrane has also unique properties depending on lipid composition, supporting material characteristics, and the production methodology. Nevertheless, black lipid membrane system has been tremendously precious method in membrane research.

1.7.3 Solid-supported lipid membranes

Solid-supported lipid membrane system is an alternative technique to black lipid membrane system in order to immobilize lipid bilayers on a solid surface such as glass, silicon, mica, quartz, and gold surfaces (Castellana & Cremer, 2006). Langmuir-Blodgett transfer (Osborn & Yager, 1995) and liposome spreading techniques (Janshoff & Kunneke, 2000) assist to construct such supported lipid membranes on a planar surface.

Lipid membranes immobilized on a solid surface have a major advantage in their long-term and high mechanical stability (Purrucker et al., 2001). Another crucial advantage is that these membrane systems can be monitored and characterized by several surface-sensitive analyzing tools and electrochemical analyzing devices. However, the distance between the solid support and the lipid bilayer restricts or prevents the incorporation of large transmembrane-spanning proteins (Castellana & Cremer, 2006). Transmembrane proteins in lipid bilayers have hydrophilic regions that jut out from the lipid membrane, and therefore, the drawbacks in the native behavior of the transmembrane proteins may resulted in denaturation, structural alteration and problems in the function when the protein contacts with the solid support (Castellana & Cremer, 2006). The lack of a well-defined ionic reservoir is also a major obstacle for generating the native condition of the membrane proteins (Pucadyil & Schmid, 2010). However, ion transfer experiments cannot be monitored with such lipid membrane systems. (Castellana & Cremer, 2006).

To improve the described problems for solid-supported lipid bilayers, hybrid bilayers have been developed (Lingler et al., 1997). For this aim, the lipid bilayer is produced with two steps: The production of monolayer on solid surface and the deposition of the lipid monolayer on it. To produce the first monolayer, alkanethiol chemistry is performed, and a spacer alkanethiol monolayer is immobilized on a metal support surface. Following the alkanethiol monolayer step, a phospholipid monolayer is deposited either by Langmuir-Blodgett transfer or by liposome vesicle fusion techniques. Thiol/lipid constructed bilayers are stable in air, and establish an improved barrier towards charge transfer. However, thiol/lipid hybrid membranes have much higher rigidity than that of the biological membranes in their native condition. Adding to this challenge, the structure of such hybrid membranes does not

allow to form a water reservoir between the bilayer and the metal support surface. Due to these conformational restrictions, thiol-based supported lipid membranes are unstable for the incorporation of the integral proteins.

1.7.4 Polymer-supported bilayer lipid membranes

Polymer-supported bilayer membranes are produced to benefit from the most advantageous properties of unsupported bilayer lipid membranes and solid-supported bilayer lipid membranes. Thus, these membrane platforms utilize bilayer fluidity and stability, accessibility to various characterization techniques, and the possibility of integration and evaluation of membrane-incorporated proteins.

Contrast to hybrid membranes, polymer cushions separate the lipid bilayer from the solid surface, and they support the membrane by increasing the water content between the bilayer and the solid surface. For doing this, water-rich gels (Ide et al., 2006), covalently bound spacers (Raguse et al., 1998), and hole spanning membranes (Schmidt et al., 2000) can be utilized between the solid support and the hydrophilic region of the membrane.

Since last decade, the applications on polymer-supported bilayer membranes have been considerably increased. For instance, one of the most interesting studies for polymer-supported bilayer membranes was reported by Wagner and co-workers (Figure 1.13) (Wagner & Tamm, 2000). In this experiment, a linear polyethyleneglycol (PEG) polymer, spacer molecule, was immobilized between the solid support and one side of lipid molecules in the bilayer (Wagner & Tamm, 2000). This method provided to construct stable structures, and generated a water reservoir between the lipid bilayer and the support material. Thus, this model membrane model allowed to integrate and characterize membrane proteins (Wagner & Tamm, 2000). However, polymer-supported bilayer lipid membranes generate low impedance compared to biological membranes, and such low impedance restricts the biosensor applications of polymer-supported membranes. These membranes may also have some defects in the bilayer that can prevent the incorporation of membrane-spanning proteins. Therefore, such structural and functional properties need to be solved with another model membrane system.

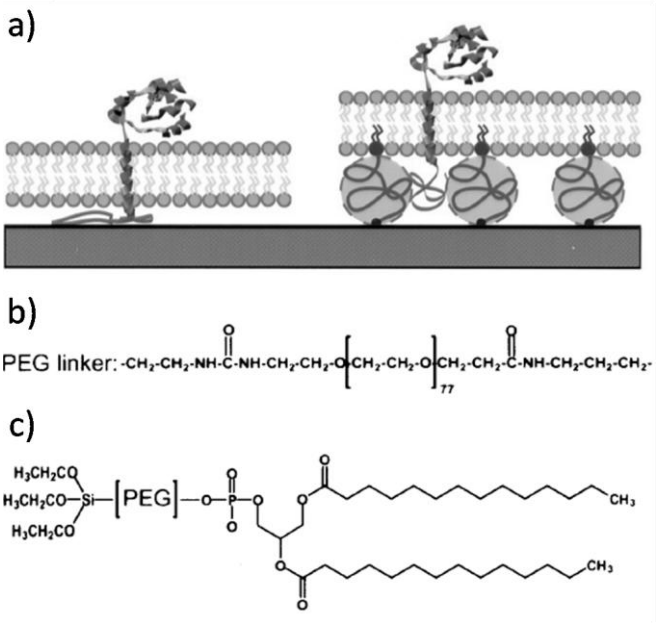

Figure 1.13 : Design of a polymer-supported lipid bilayer. a) Polymer-supported lipid bilayers were designed to form a space between the lipid bilayer and the support substrate b) Chemical structure of the spacer (polyethyleneglycol (PEG)) molecule was shown. c) Structure of a lipid polymer with a silane group for covalent binding to the solid support surface, adapted from (Wagner, 2000).

1.7.5 Tethered lipid bilayer membranes

To overcome the challenges in the lipid bilayer platforms mentioned before, tethered lipid bilayer membranes were developed in recent decade (Giess et al., 2004). In this platform, the inner leaflet of the lipid bilayer is covalently bound to a solid support via a spacer group. The spacer group serves as a cushion that elevates the bilayer from the surface, prevents for surface roughness effects, and can act as an ion reservoir under the membrane. Further, this membrane system presents better stability compared to black lipid membranes and the other supported-lipid membrane platforms, and it can be stable for several days or even weeks as reported (Vockenroth et al., 2008).

There are several different techniques to form tethered lipid bilayer membranes (Giess et al., 2004). These membrane systems are prepared either in a multiple-step procedure or a simple one-step reaction. Multiple-step procedure requires several surface reactions such as the grafting of a polymeric spacer molecule and coupling of lipids to the polymeric structure (Giess et al., 2004). The latter procedure usually uses more synthetic attempts. In this concept, anchor lipids, which are covalently

coupled to a spacer group with its polar head group, are used to construct an artificial bilayer system. This anchor group can react with a solid substrate with a chemical bonding like thiol chemistry on metal surfaces or silane-coupling to oxide substrates (Atanasov et al., 2005; Giess et al., 2004). The durability, stability and accuracy of the constructed membrane depend on several parameters such as surface roughness, grafting density of the anchor lipids and their chemical composition. For instance, higher grafting density generally causes higher electrical resistances of the bilayer structure. However, the increase in the grafting density can frustrate the incorporation of complex membrane proteins with large domains. These parameters need to be optimized in order to observe well balance between grafting density, suitable anchor chemistry, and the length of the spacer group. For this aspect, there are several experiments to increase the stability and allow the insertion of complex membrane protein. For instance, thiol-lipid molecules have been used to preserve the stability (Atanasov et al., 2005). The thiol-lipid molecule comprises lipid derivatives, which are modified at their head groups with a hydrophilic spacer consisting of a thiol or disulfide group for covalent binding to the support surface. These molecules can simultaneously react with metal surfaces, and generates self-assembled monolayers. Fusion of the liposomes on the self-assembled monolayer tends to form the tethered lipid bilayers on the support surface.

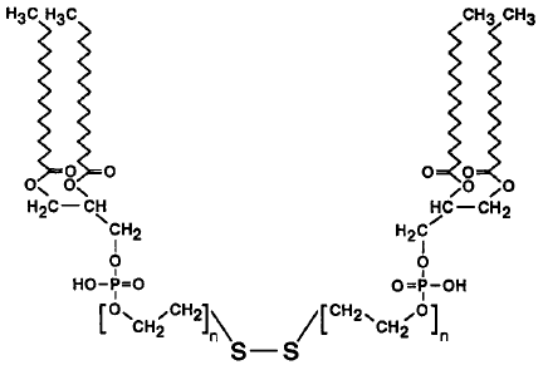

Figure 1.14 : Chemical structure of the thiol-lipid molecule synthesized by Vogel and co-workers, adapted from (Lang, 1994).

In the literature, Vogel and co-workers pioneered to reveal tethered lipid bilayer formation concept. In this study, they produced a thiol-lipid molecule consisting of 1-3 ethyleneglycol residues, which acted as a hydrogel, and a thiol end group was used for covalent linkage to metal surfaces (Figure 1.14) (Lang et al., 1994). After the formation of self-assembled monolayer, highly stable lipid bilayer structure was

formed by depositing a second monolayer of different phosphatidylcholine. Additionally, Knoll and his colleagues produced for the first time an oligopeptide molecule as a spacer molecule bound to the polar head group of the lipid (Figure 1.15a), and constructed a peptide-tethered lipid bilayer structure for bacteriorhodopsin enzyme insertion into the membrane (Figure 1.15b) (Naumann et al., 1995). It was reported that the activity of the enzyme was preserved if the enzymes were properly incorporated on a platform, which has adequate space between the solid support and lipid bilayer (Naumann et al., 1995). Further, the results indicated that the enzymes in the lipid bilayer system had comparable kinetic activities to those in liposomes, and the peptide spacer apparently prevented protein denaturation as well (Naumann et al., 1995).

Overall, tethered lipid bilayer membranes provide the opportunity of an aqueous compartment between the lipid bilayer and the solid support surface (*e.g.*, metal surfaces). Thus, this model membrane system forms a water-containing sub-membrane space, which reduces the hydrophobic effects of the metal surface, and accommodates an extracellular space for the incorporation of complex membrane proteins. This region generates a reservoir for ion transport, and preserves the native structure of the membrane protein *in vitro* conditions.

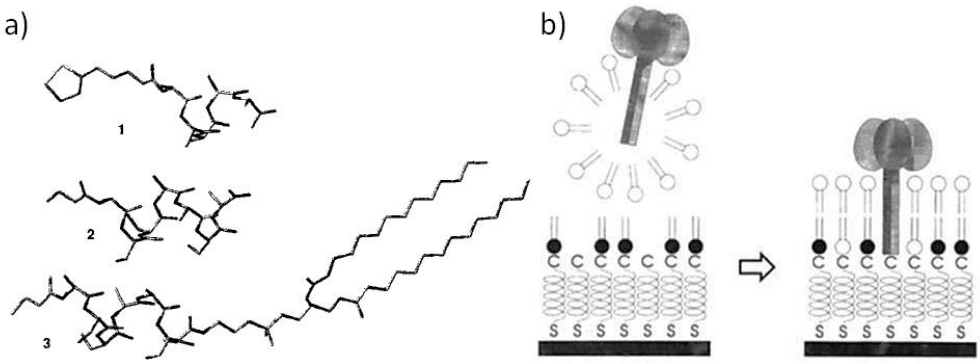

Figure 1.15 : Tethered lipid bilayer platform presented by Knoll and co-workers. a) Oligopeptide modified spacer molecule. b) Schematic illustration of the fusion of liposomes with bacteriorhodopsin enzyme and the construction of tethered lipid bilayer structure, adapted from (Naumann, 1995).

1.8 Characterization Methods for Model Membrane Systems

The increasing interest on lipid membranes has been fed by the numerous surface-sensitive characterization techniques based on several optical and mechanical sensing

methods such as Surface Plasmon Resonance (SPR), Quartz Crystal Microbalance-Dissipation (QCM-D), Atomic Force Microscopy (AFM), Transmission Electron Microscopy (TEM), Total Internal Reflection Fluorescence Microscopy (TIRF), Electrochemical Impedance Spectroscopy (EIS), Cyclic Voltammetry (CV), Fluorescence Recovery After Photobleaching (FRAP), and Fourier Transform Infrared Spectroscopy (FTIR) (Richter et al., 2003). These characterization methods aid to discover the physico-chemical and structural properties of the lipid layers in aqueous media. In the following sections, the most common characterization technologies based on optical, mechanical and microscopic detection were described in detail.

1.8.1 Surface plasmon resonance

Surface Plasmon Resonance Spectroscopy (SPS) or SPR was first introduced for biosensor applications by Lundström in 1983 although this technology had already been used to characterize organic layers on metal surfaces for several years. In the past decade, SPR-based sensing platforms has been widely utilized as an intensely powerful and quantitative detection system in order to evaluate the biomolecular interactions at the interface between a variety of analytes and several ligands such as protein-ligand, protein-protein, protein-DNA and protein-lipid membrane. This platform also provides several kinetic parameters including equilibrium constants and energetics, and hence, it can employ these parameters in high sensitive and label-free biochemical assays (Wang et al., 2012).

1.8.1.1 Principle

SPR is an optical phenomenon that evaluates electromagnetic waves along the boundary of two media with different dielectric constants. Before to elaborate the surface plasmon phenomena, basics of total internal reflection of planar electromagnetic wave at interface between the materials with different refractive indices ($n_1 > n_2$) should be comprehended in details (Figure 1.16).

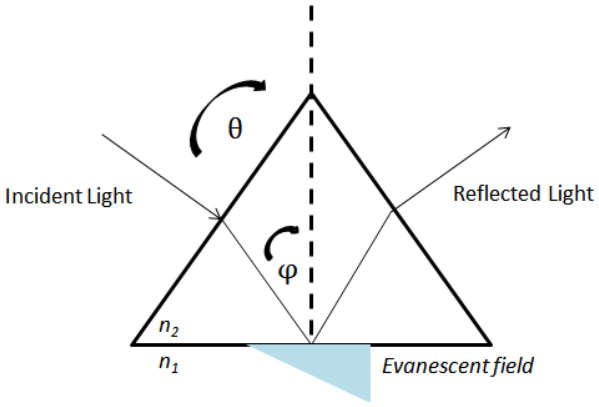

Figure 1.16 : Total internal reflection mode and evanescent field excitation.

In this schematic, a light beam passes from the material/condition with high refractive index (n_2) through the material/condition with low refractive index (n_1), and some of the light reflects from the interface (Sapsford, 2010). When the ray of light strikes the interface at an angle larger than the critical angle, the light approaches total internal reflection (Sapsford, 2010). The relationship between the reflected light intensity and the incidence angle can be described using the equation governed by Snell's law:

$$\sin\theta = \frac{n_2}{n_1} \qquad \textbf{(1.1)}$$

The reflection (R) is termed as a function of the incidence angle, and reflection spectrum is defined as:

$$R = \frac{I_r}{I_0} \qquad \textbf{(1.2)}$$

where I_r is the intensity of the reflected and I_0 is the intensity of the excitation light. On the other hand, more detailed investigation of the electric field distribution at the close vicinity of the interface demonstrates that the light intensity does not lose totally, when total internal reflection happens above the critical angle (θ_c). A harmonic wave with an amplitude perpendicular to the interface is also observed to move parallel to the surface, and this electromagnetic distribution is termed as an evanescent wave. The decay length (l) is described as a function of the angle of incidence, and this parameter is defined as:

$$l = \frac{\lambda}{2\pi\sqrt{(n.\sin\theta)^2 - 1}} \quad \textbf{(1.3)}$$

When one of the materials is coated a conducting film such as gold, the light is not totally reflected, and some of the light is lost. In this condition, a second angle exists higher than the critical angle where the loss is the highest, and the reflected light intensity is minimum. This angle is called as surface plasmon resonance angle (θ_{spr}) (Lofas et al., 2011). This angle is formed by the oscillation of plasma at the metal film surface, and these oscillating plasma waves are termed as surface plasmons. When incident light wave vector couples with the surface plasmon wavelength, the electrons on the metal film resonate, and there is a loss of energy that causes a decrease in the intensity of the reflected light. Further, the resonance angle differs with the different dielectric material, which is attached to the metal film surface, or with the different quality of the same dielectric surface. The amplitude of the wave vector is dependent on the angle where it strikes the interface, and an evanescent electrical field related to plasma wave moves through the medium from the metal surface. Since this phenomenon allows to evaluate the interactions between the media and metal film surface, the signals obtained by biochemical interactions are investigated with the resonance angle that changes dynamically as a response of biochemical process.

To excite and generate surface plasmons on a metal-dielectric surface, the incident light requires to provide photons that meet the energy and momentum conservation laws. In detail, the incident photon's momentum and energy should couple to the plasmon's momentum and energy for the excitation of the charge-coupled oscillations. There are several light coupling techniques such as waveguide, grating, and prism coupling methods (Velasco-Garcia, 2009).

1.8.1.2 Coupling methods

Waveguide coupling

Waveguide set-up can be used to couple light for the excitation of surface plasmons (Figure 1.17). The plasmon excitation needs the photons to match the momentum defined as:

$$\beta_{waveguide} = Re(k_z) \quad \textbf{(1.4)}$$

where βwaveguide is the propagation constant for the specified waveguide mode and k_z is the wave vector for the surface plasmon modes at the metal-sensing medium interface. A small portion of the light moves through the metal layer to the metal-sensing medium interface, and stimulates surface plasmons. Thus, the intensity of propagating wave is increased in the planar waveguide structure. This coupling strategy is realized in a narrow wavelength range and demonstrates itself as a dip in the transmitted light spectra (Dostálek et al., 2001; Toyama et al., 2000). During any binding events on the sensing surfaces, this effect can evaluated and monitored in the transmitted light spectra as a shift in the dip position (Hoa et al., 2007; Suzuki et al., 2005).

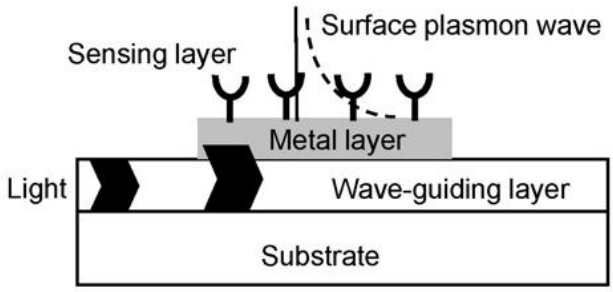

Figure 1.17 : Waveguide coupling, adapted from (Velasco-Garcia, 2009).

Grating coupling

In the grating coupling method, the periodic structure of the grating diffracts light into several beams multiplying in different directions (Figure 1.18). The beam directions are determined by the grating period and the wavelength of the incident light, and so, the surface plasmons are excited in the conditions defined as:

$$m\frac{2\pi}{\Lambda} + k_0 = \pm Re(k_z) \quad \textbf{(1.5)}$$

where m is a function of the grating order, Λ is the grating period, and k_0 is the component of the incident light parallel to the interface. Transmitted or reflected light from grating coupled biosensors can be studied under intensity, wavelength or angular interrogation (Byun et al., 2007; Homola et al., 1999; Singh & Hillier, 2006).

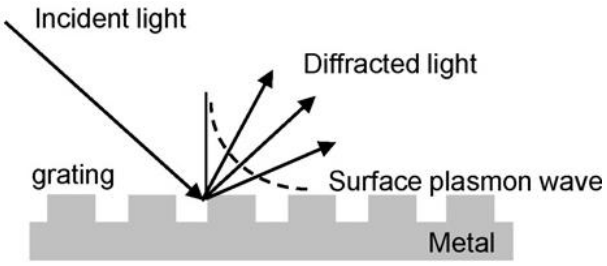

Figure 1.18 : Grating coupling, adapted from (Velasco-Garcia, 2009).

Prism coupling

This coupling method is the most common way to speed up the momentum of light. In this coupling method, the photons are not directly matched with the metal/dielecetric interface, and they are coupled to the evanescent light at prism base, which has high refractive index. For the excitation of surface plasmons, there are two pioneering configurations (*i.e.*, Otto and Kretschmann configuration), using a prism surface. In these configurations, a second dielectric layer provided by a prism generates two interfaces. In Otto configuration, a dielectric layer is sandwiched between a metal film layer and the prism (Figure 1.9a) (Otto, 1968). For instance, the evanescent field connects approximately a 200 nm wide air space between the prism and the metal film layer, and the plasmons are excited at the metal-air interface. This configuration is beneficial for surface plasmon applications in solid phase media. The space between metal and prism surface reduces the plasmon efficiency, and however, it is less convenient for applications with solutions.

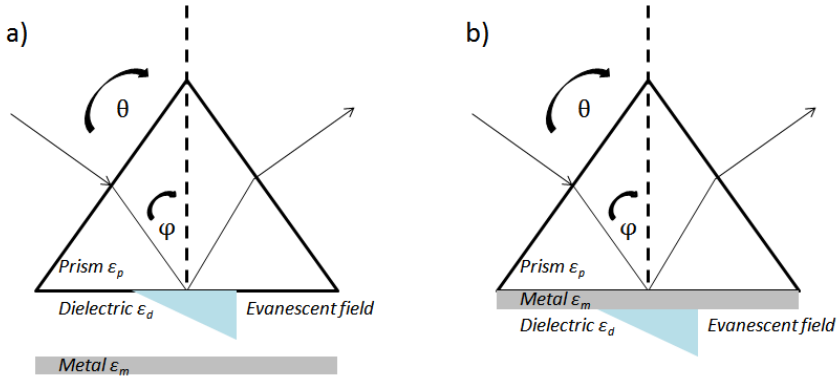

Figure 1.19 : Prism coupling methods for Surface Plasmon Resonance. a) Otto configuration. b) Kretschmann configuration.

In biological applications, the most practical and broad version for surface plasmon excitation method is derived from Kretschmann configuration (Figure 1.9b) (Kretschmann & Raether, 1968). In this configuration, prism surface with a high

refractive index is modified by a thin metal layer (*e.g.*, gold, silver) (~50 nm), which is attached to a low refractive index dielectric. The light beam is reflected at the prism base under an incidence angle, which is higher than the critical angle. The evanescent field matches with the surface plasmon, and this causes a resonance. The resonance is adjusted by tuning the incidence angle. During the tuning, the plasmon resonance indicates a sharp dip in the reflectivity spectrum at the resonance angle. Upon the changes on the metal thin film layer, the reflectivity spectrum changes and results in a variation in the plasmon angle.

1.8.1.3 Surface plasmon resonance measuring methods

Surface plasmon technologies offer several different recording modes, (*i.e.*, scan and kinetic modes), and they are two most common techniques to evaluate the shift in the resonance angle of plasmon excitation caused by changes in interfacial refractive index. In the scan mode, the light intensity is monitored and analyzed at the prism base as a function of the incidence angle (Figure 1.20a). Kinetic mode allows to analyze the changes in reflectivity as a function of time at a constant angle, and monitors any changes such as surface reactions and binding events in real-time (Figure 1.20b).

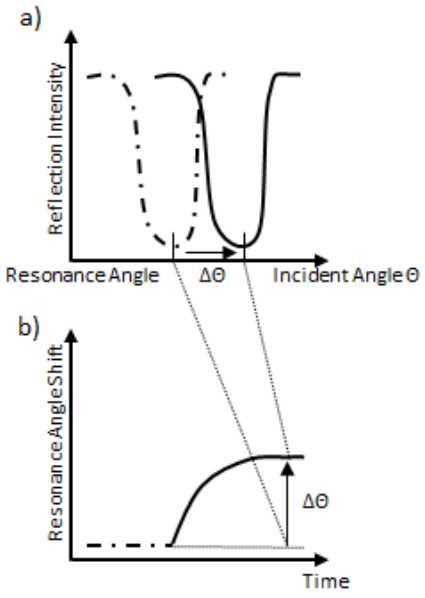

Figure 1.20 : Surface plasmon resonance curves. a) Scan mode. b) Kinetic mode.

1.8.2 Quartz crystal microbalance

QCM provides a high-resolution mass sensing technology based on the piezoelectric material, and it measures very small mass changes on the quartz crystal resonator in

real-time. In 1880, the physical phenomenon of this technology was first discovered by Jacques and Pierre Curie (Curie & Curie, 1880). When a mechanical stress was carried out to a piezoelectric material (*e.g.*, quartz crystal), a voltage proportional to the stress was generated. In 1959, Sauerbrey proved that quartz crystal oscillation frequency depending on the mass change at the sensor surface, and he coined the term as quartz crystal microbalance (Sauerbrey, 1959).

Until now, as a methodology, QCM is sensitive to measure at solution-surface interface, and thus, it evaluates analyte/material characteristics for analytical chemistry and electro-chemistry applications. As a technique, QCM has possessed a broad detection range, and presented a versatile platform for various analyte/material characterizations. The detection range covers from the binding of small molecules or polymer films (low mass end detection range) to the binding of much larger masses such as complex biopolymers, macromolecules, and cells (the upper end detection range) (Marx, 2003). Further, this technology provides critical information about energy dissipation features of the analyte/material bound on the sensor surface, and it presents mass and energy dissipation characteristics of films and membranes on the oscillating quartz crystal sensor surface.

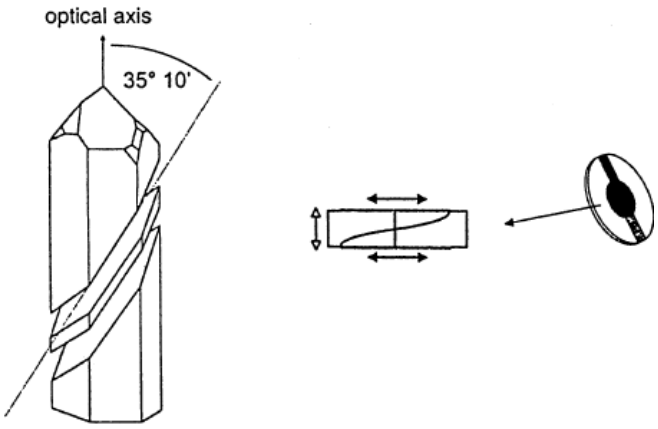

Figure 1.21 : AT-cut of a quartz crystal, adapted from (Janshoff, 2000).

1.8.2.1 Principle

QCM is a mechanical characterization method that measures mass effect on the oscillating quartz crystal, and the mass binding causes a decrease in the crystal's oscillation frequency. The quartz crystal, which is commonly used in QCM applications, requires a specific crystal cut with a few tenths of a mm in thickness and an angle of $\theta = 35° 15`$ from the crystallographic Z-axis. This specific crystal is

called as AT-cut crystal (Figure 1.21) (Janshoff et al., 2000). This geometry allows a stable oscillation with nearly no temperature variations in frequency at 25°C. QCM is in a shear mode device, consisting of a thin piezoelectric AT-cut quartz crystal disk and a pair of electrodes. Typically, AT-cut quartz crystal oscillates to indicate a pure shear motion of the surfaces. The surfaces move parallel, and the thickness of the disk does not change (Figure 1.22). Due to the piezoelectric property of the quartz crystal, the application of a voltage across the crystal leads to a corresponding mechanical strain.

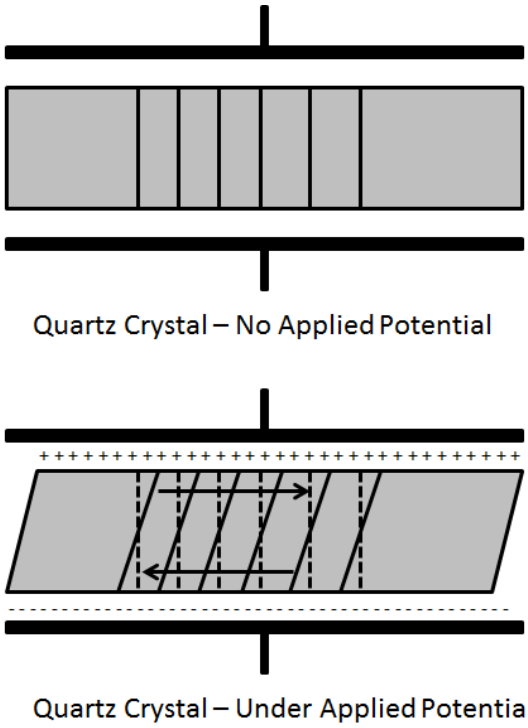

Figure 1.22 : A schematic illustration of thickness shear formation of quartz crystal under a voltage applied.

The applied electric field to the quartz crystal stimulates the re-orientation of the dipoles of the crystal, and this effect results in a lattice strain and shear deformation at the resonance frequency (Liu et al., 2011). The directional shear deformation depends on the applied potential direction, and its extension is affected by the applied potential magnitude. For instance, the adverse polarity generates an identical strain in the adverse direction, and this vibration effect on the quartz crystal causes a transverse acoustic wave. When a mass load is applied on the quartz crystal surface, the surface electrodes can present only odd harmonics such as n=1, 3, 5, 7, and so on. On the other hand, a standing wave effect is formed when the acoustic wavelength reaches to twice the thickness of the crystal sensor. Hence, the resonance frequency

and the crystal thickness have a correlation, and they can be described by the following equation:

$$f_n = n.f_0 \quad \textbf{(1.6)}$$

$$f_0 = \frac{C_t}{\lambda} = \frac{C_t}{2d_q} \quad \textbf{(1.7)}$$

where n is an odd harmonics (n=1, 3, 5,7…), f_0 is the fundamental frequency, C_t is the transversal velocity, λ is the wavelength, and d_q is the thickness of the quartz plate.

To evaluate and understand the situation of mass load of pure elastic mass on the surface, Sauerbrey defined an equation:

$$\Delta f = \frac{-2\Delta m f^2}{A(\mu\rho_q)^{0.5}} = -C_f \Delta m \quad \textbf{(1.8)}$$

where Δf is the measured resonant frequency decrease (Hz), Δm is the elastic mass change (g), f is the intrinsic resonance frequency of quartz crystal (Hz), A is the electrode area (0.196 cm^2 in many applications), μ is the shear modulus of quartz (2.947 x 10^{11} dyn/cm^{-2}), and ρ_q is the density of quartz (2.648 $g.cm^{-3}$). This formula indicates a C_f parameter, the integrated QCM sensitivity, having a value of 0.903 Hz/ng for ca. 9 MHz crystal. In QCM sensitivity, Sauerbrey equation is effective only for small mass (not greater than 2% of the crystal mass) bound to the crystal surface (Vashist & Vashis, 2011).

Overall, QCM technique depends on the operation of circular quartz crystals in the thickness shear mode of oscillation in many applications. Any mass added to the sensor surface will cause to oscillate with the same lateral movement and frequency. The decrease in the frequency indicates a deposition of mass on the sensor surface. The mass sensitivity relies on the thickness of the crystal, which designates the resonant frequency. Further, QCM allows to evaluate the viscoelastic properties of the film adjacent to the quartz surface as the perspective of resonance frequency and dissipation (Lucklum & Hauptmann, 2000). Dissipation is defined as the ratio of

energy lost per oscillation cycle divided by total energy stored in the oscillator (Cho et al., 2010).

$$D = \frac{E_{lost}}{2\pi E_{stored}} \quad \textbf{(1.9)}$$

When the size and flexibility of the material on the resonator increases, the dissipation parameter also increases. By using Sauerbrey equation and theory, both frequency and dissipation parameters present an information to quantify and separate the viscoelastic variations regarding shear viscosity and storage modulus of the adsorbed materials (Dixon, 2008). Further, frequency and dissipation plots indicate the conformation and structural characteristics of the adsorbed material, and thus, the mass load is approximated by frequency parameter and the viscoelastic characteristics is estimated by dissipation parameter (Dixon, 2008).

1.8.3 Atomic force microscopy

AFM has become a modern characterization tool to evaluate and explore the topography of any kind of solid surfaces in a nanometric point of view since it was first introduced by Binning, Quate and Gerber in 1986 (Binnig et al., 1986). AFM is a versatile device that offers to present the mechanical characteristics of the surfaces, image visualization, and the interaction forces. This force spectroscopy mode also offers to understand the intermolecular forces at close vicinity of the surfaces, and so, this mode plays a key role in a broad range of biological, chemical, and physical processes such as chemical and physical adsorption, wetting, coating, catalysis, cell adhesion, rigidity, and so on (Deng et al., 2010). Further, the image visualization mode provides three-dimensional images of the surface ultrastructure with high resolution under physiological conditions, and it requires minimal sample preparation compared to the other visualization methods such as scanning electron microscopy (Chang et al., 2009).

AFM probes the sample surface using a sharp tip, a couple of microns long and frequently less than 100 Å in diameter, and this tip is located at the close vicinity of the surface. The tip is connected at the free end of a cantilever, which is 100 to 200 μm long, and the forces between the tip and the sample surface lead to bending or deflection in the cantilever (Figure 1.23). Scanning system is equipped with a

detector, which measures the cantilever deflections during the scanning. The scanned data, which is derived from the detector, is transferred to a computer, and converted to surface topography map.

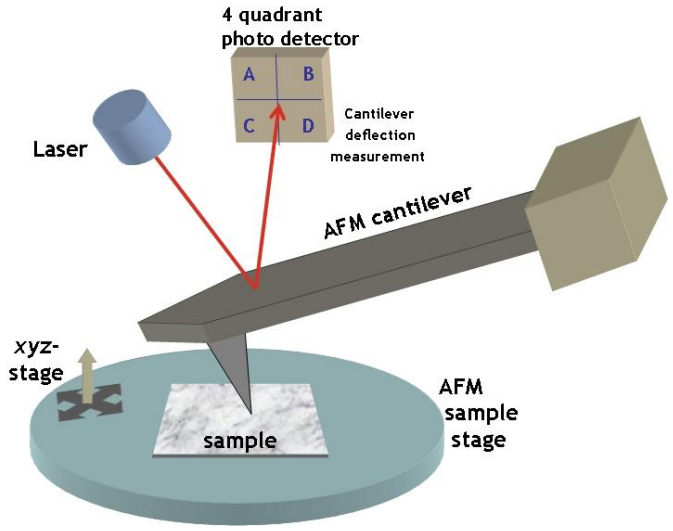

Figure 1.23 : A schematic illustration of a typical Atomic Force Microscopy set-up, adapted from (Kim, 2010).

Further, AFM has capability to be used for the applications of insulators and semiconductors as well as electrical conductors. Multiple forces usually contribute to the deflection of an AFM cantilever, and the most common interaction is an interatomic force, which is caused by van der Waals forces (Cappella & Dietler, 1999). The distance between the tip and the samples is a critical parameter to evaluate the forces on the sample.

1.8.3.1 Atomic force microscopy imaging modes

AFM imaging modes are classified in two separated groups: Static mode (contact mode) and dynamic mode (non-contact and tapping mode). When AFM imaging modes are compared as the aspect of the tip distance to sample surface, the cantilever is above less than a few angstroms from the sample surface, and the interatomic force between the two contents (cantilever and sample) is repulsive in the contact mode. In the non-contact mode, the cantilever is above about tens of nanometers from the sample surface, and the interatomic force between the contents is moderate. In the tapping mode, the cantilever is above about a few nanometers from the sample surface, and the interatomic force between the contents is attractive (Figure 1.24).

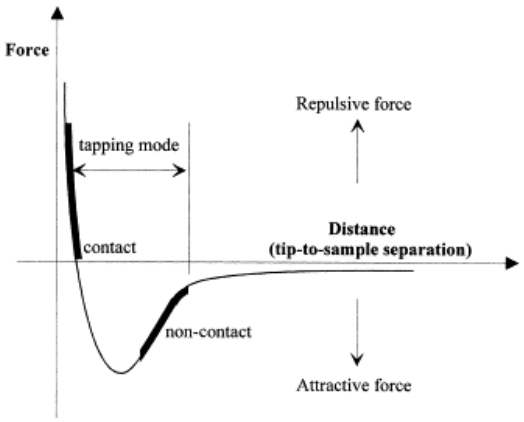

Figure 1.24 : Comparison of Atomic Force Microscopy imaging modes, adapted from (Kim, 1999).

Static mode (Contact mode)

In static mode (contact mode), the cantilever is contacted and dragged the sample surface, and the topography is measured directly using the deflection of the cantilever (Figure 1.25a). In this mode, an AFM tip is connected to the end of a cantilever with a low spring constant, and physically contacts with the sample. The surface structure can be visualized at a constant height or at constant force, and these measurements provide quantitative dimensions to evaluate accurate surface roughness measurements, the height of the sample surface, and the thickness of biological layers. This imaging mode can be performed in high scan speeds, and it presents atomic resolution of the sample. However, contact mode is intensely influenced by frictional and adhesive forces, and so, this mode can damage and distort actual topography of the sample.

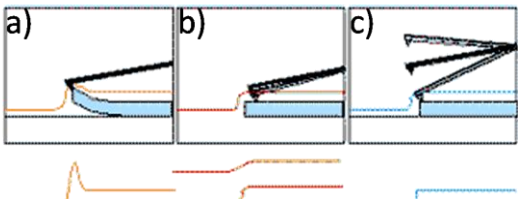

Figure 1.25 : Atomic Force Microscopy imaging modes. a) Contact mode, b) non-contact mode, and c) tapping mode (Url-4).

Dynamic mode (Non-contact mode and tapping mode)

There are two different regimes in dynamic mode scanning: Non-contact mode and tapping modes. In the non-contact mode, the cantilever is externally driven to oscillate at or close vicinity of its fundamental resonance frequency (Figure 1.25b). Similar to contact mode, non-contact mode can be used to visualize the topography

of insulators and semiconductors as well as electrical conductors. During the scan, this method presents little or no damage on the sample topography. The total force between the tip and the surface is quite low (~10-12 N), and such low measurement force is advantageous to evaluate soft or elastic samples. Further, this imaging mode protects possible contamination to the sample, and provides actual imaging of the sample in its native condition. However, non-contact imaging generally results in low resolution, and it can also be hindered by the contaminant layer which can interfere with oscillation. Slower scanning speed in non-contact mode avoids to contact with fluid layer, and this mode is typically used for highly hydrophobic samples with minimal fluid content.

Tapping mode (AC mode or intermittent contact mode) was developed to achieve high resolution without inducing destructive frictional forces both in air and fluid content. In the tapping mode, the cantilever is oscillated up and down at close to its resonance frequency, and located above the surface with a quiet little fraction of its oscillation period (100 to 200 nm) (Figure 1.25c). During the scan, the lateral forces are significantly reduced. The very soft and fragile samples can be successfully imaged using this technique. However, the scan speed is lower than that of contact mode.

1.8.3.2 Atomic Force Microscopy Force Measurements

AFM tip is localized at the end of a cantilever, and the amount of force between the tip and sample surface is dependent on the spring constant (stiffness) of the cantilever and the distance between the tip and the sample surface. This force can be described using Hooke's Law:

$$F = -kx \tag{1.10}$$

where F is force (N), k is spring constant (N/m), and x is cantilever deflection (m). By measuring the interaction force between AFM tip and the sample, force-distance curves are plotted to evaluate the sample's physical characteristics. In AFM force measurement, the tip connected to a cantilever is driven to move over the sample surface in normal direction. Vertical position of the tip and the corresponding deflection of the cantilever are generated by the force between the tip and sample.

Such a force measurement can be plotted as the cantilever deflection versus displacement (Figure 1.26). The force measurements are calculated using multiplying the cantilever deflection with the spring constant. The distance measurements are calculated using subtracting the cantilever deflection from the height position.

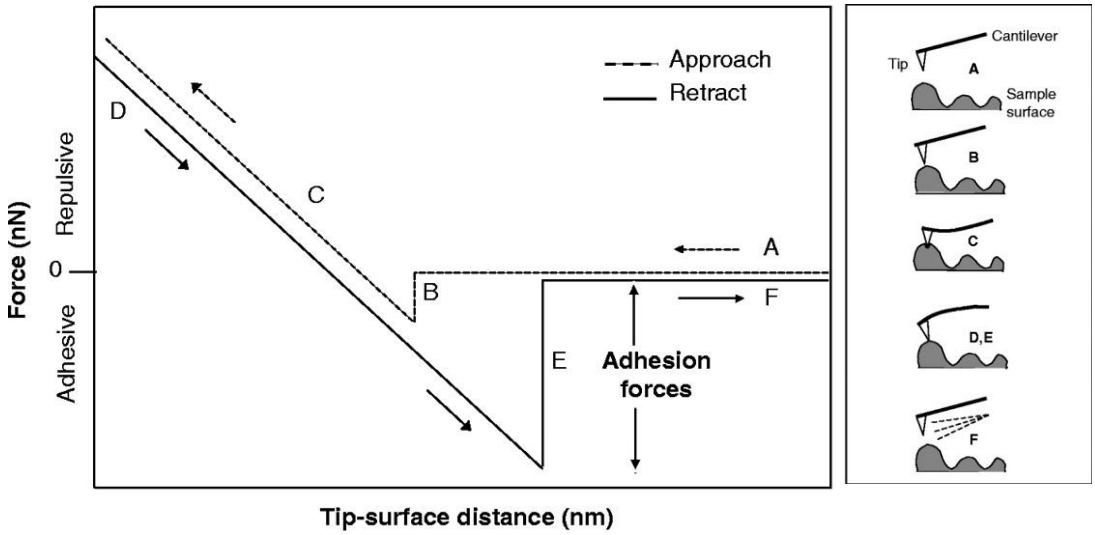

Figure 1.26 : Evaluation of various probe-sample interactions using Atomic Force Microscopy force curves, adapted from (Shahin, 2005).

The force-distance curves offer several critical information regarding the physical properties of the sample surface. The approach of force-distance curve can be utilized to evaluate the forces, including van der Waals forces and hydrogen bonding (Hinterdorfer & Dufrene, 2006). When the tip is moved back (retracted) from the surface, the curve often indicates a hysteresis called as "pull-off" force. Pull-off force can be used to calculate approximately surface energy of solids or the binding forces between complementary molecules. The force-distance curve is also used to evaluate the thickness of mixed monolayer and bilayer formation in model membrane systems.

2. MATERIALS AND METHODS

2.1 Materials

The following chemicals were purchased and used without further purification: Phosphatidylcholine (PC) (P3556), 3,3′-Dithiodipropionic acid di(N-hydroxysuccinimide) (DTSP) (D3669), pravastatin (P4498), P-glycoprotein (P-gp, MDR1) (M9194), monoclonal anti-P-glycoprotein (anti-MDR1) clone F4 (P7965) antibody, anti-Pin-1 Mouse monoclonal antibody (WH0005300M1), 100 mL round bottom flask (Z510424) (Sigma-Aldrich, St. Louis, MO, USA); dimethyl sulfoxide (DMSO) (1029521000) and chloroform (1070242500) (Merck, Whitehouse Station, NJ, USA); 1,2-distearoyl-sn-glycero-3-phosphoethanolamine-N-[amino (polyethylene glycol)-2000] (ammonium salt) (DSPE-PEG) (880128P) (Avanti, Alabaster, AL, USA). SPR (Reichert SPR slides) and QCM gold-coated surfaces (QSX301) were purchased from Reichert (Depew, NY, USA) and Q-Sense (Västra Frölunda, Sweden), respectively.

2.2 Preparation of Liposomes

In liposome production, PC molecules were used as model lipid molecule to mimic eukaryotic cell membranes due to their high abundance in animal and plant cell membranes (Henneberry, Lagace, Ridgway, & McMaster, 2001). To prepare liposomes, lyophilized PC was first dissolved in chloroform. The stock concentration was adjusted to 1 mg/mL, and stored at 4°C for further use. To produce thin lipid film, a round bottom flask (capacity: 100 mL) with low surface roughness value was used. First, PC solution (100 μL) was poured into the round bottom flask, and then, the flask was rotated under N_2 gas atmosphere to allow the evaporation of chloroform. Thin film layer formed on the flask surface was stored at 4°C overnight for further use.

Liposome production was carried out using phosphate buffered saline (PBS, 0.1 M, pH: 7.4). To prepare 1M PBS stock solution, 8.01 g of NaCl, 0.2 g of KCl, 1.78 g of

$Na_2HPO_4 \cdot 2H_2O$, and 0.27 g of KH_2PO_4 were dissolved in 1L of distilled water, and pH was adjusted to 7.4. This stock solution was diluted 10 times before the experiments. Liposomes were generated by the hydration of thin lipid films using the buffer solution, and the bulks of liquid crystal-like bilayers became fluid and swell. For doing this, 5 mL of 0.1 M PBS solution was used, and the film layer was detached during agitation with a vortex. The phospholipids were self-closed to form large lipid vesicles in order to avoid the interaction of water with their hydrophobic tail region. Once lipid vesicles were formed, the size of the vesicles could be changed by different techniques. In the literature, there is a variety of liposome production methods such as Lipid Hydration Method, Sonication Method, Solvent Spherule Method, French Pressure Method, Freeze Thaw Method, Microfluidization Method, Extrusion Method, and so on (Sessa & Weissman.G, 1968; Wagner & Vorauer-Uhl, 2011).

Figure 2.1 : Avanti Mini-Extruder (Url-5).

In this study, lipid extrusion technique was preferred to produce unilamellar lipid vesicles with a narrow size distribution in order to evaluate the optimum conditions for the construction of lipid bilayers, and to discover drug-membrane protein interactions. In lipid extrusion technique, a lipid suspension was forced through a polycarbonate filter membrane with a defined pore size to produce lipid vesicles having a diameter close to the pore size of the filter used. This technique also provided the homogenity of the liposome in their size distribution in the suspension. During this process, the extrusion should be performed at a temperature above the phase transition temperature (Tg) of the lipid. For PC, room temperature could be used since the Tg of PC is 16-19°C (Adhikary et al., 1995; Wang et al., 2010).

Avanti Mini-Extruder, which allows to efficiently and rapidly prepare unilamellar vesicles in the desired diameter using a filter membrane, was used in this study (Figure 2.1). The whole system consists of a holder block, two syringes, 100 nm pore size of polycarbonate membranes, teflon supports, and outer cases. The holder also allows to extrude unilammellar vesicles at high temperatures for the lipids with Tg above room temperature. Extrusion through filter membranes with 100 nm pores generally produces LUVs with a mean diameter of 120-140 nm as reported by the manufacturer (Figure 2.2).

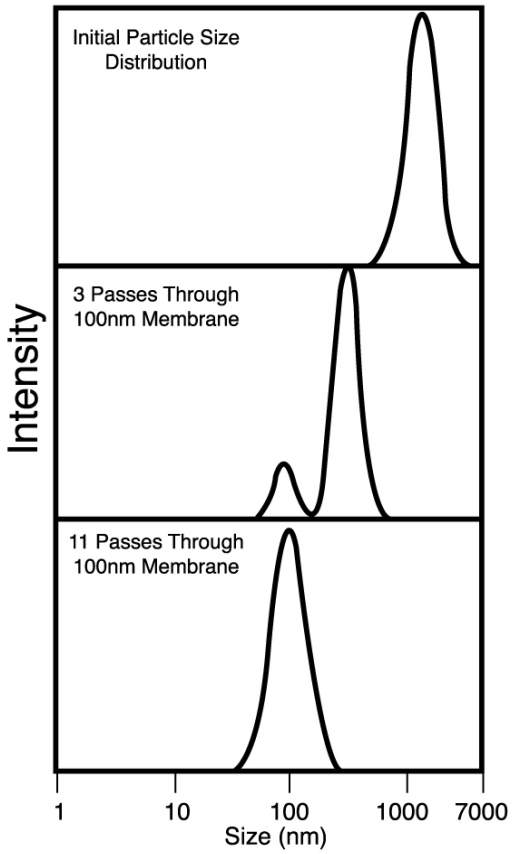

Figure 2.2 : Extrusion of lipid solution through a filter membrane with 100 nm pores, and the effect of extrusion number on the size distribution of the produced liposomes (Url-6).

To produce LUVs with ca. 100 nm diameter, the lipid solution was passed through the filter with an odd number (*e.g.,* 3, 5, 7, …15) in order to avoid any contamination of the sample by unpacked lipid molecules and liposomes in different size, which might not have passed through the filter. To narrow down the size distribution, and optimize the liposome production, the lipid solution were extruded 15 times through a 100 nm polycarbonate membrane in each experiment. The liposome suspension was then stored at 4°C overnight for further use.

2.3 Preparation of MDR1-incorporated Liposomes

To prepare protein-incorporated liposomes, MDR1 protein stock solution was first prepared. For this, 10 μL of MDR1 cell membrane fragment was dissolved in 1 mL of EGTA-Tris buffer (0.1 M, pH 7.0), and stored at -20°C for further use. To evaluate the effect of protein amount on the lipid bilayer construction, a variety of MDR1 protein amounts (0.7 μL to 4 μL) was added to the suspension solution before liposome production. Following this step, MDR1 protein-incorporated liposome production was performed as described in the preparation of liposome section using Avanti Mini-Extruder.

2.4 Characterization and Optimization of Tethered Lipid Bilayers on Gold-coated Surface

To construct and characterize each binding event, SPR and QCM-D were used as characterization methods, and the optimum conditions were determined. These methods allowed to real-time monitor the binding of the molecules and the construction of tethered lipid bilayer platform. Additionally, layer-by-layer modifications and the lipid bilayer construction were visualized by liquid-AFM system.

2.4.1 Characterization of tethered lipid bilayers by surface plasmon resonance

In SPR characterization, the whole process was monitored in real-time by Reichert SR7000 SPR system (Depew, NY, USA) coupled with a peristaltic pump (Masterflex Model 7550-50 Vernon Hills, IL, USA) (Figure 2.3). The connection between the peristaltic pump and the system was provided by Tygon tubings. The system has a fixed light source that illuminates through a sapphire prism and the gold-coated surface, and simultaneously records the plasmon angle and the changes in the refractive index upon binding events on the reaction chamber. A custom version of National Instruments LabVIEW® data acquisition and instrument control software was used to record data for plasmon response versus time, and to control/monitor the collection of data and system. As a SPR sensor surface, BK7 glass slides modified with 1 nm of chromium and 50 nm of gold were used.

Figure 2.3 : Reichert SR7000 Surface Plasmon Resonance system (Url-7).

Before each experiment, the whole system and gold-coated SPR surfaces were cleaned. The gold-coated surfaces were washed out with acetone, and dried under N_2 gas atmosphere before mounting to the system. The sapphire prism surface must be extremely clean with no visible dust and particles prior to mounting of a new sensor slide. Therefore, the prism surface was cleaned with 70% ethanol, and then, ethanol was allowed to evaporate at room temperature. The sensor slide was mounted to the system after the cleaning of prism surface. To minimize the refractive index variations between the prism and the gold-coated surface, a matching oil with same refractive index of gold-coated surface (n=~1.5) was used. Before the measurements, the tubings in the system were washed with 0.1% sodium dodecyl sulfate (SDS) and degased distilled water. To reduce the possible bubble formation, degased distilled water was pumped through the system. Then, temperature was adjusted to 25°C, and the flow rate for all solutions was set to 0.1 mL/min. During each binding event, refractive index changes were measured as micro refractive index unit (μRIU) for every 3 seconds, and SPR sensitivity was set to 0.75 μRIU. Average monitoring time for the tethered lipid bilayer construction was ca. 70 minutes in SPR measurements. After the completion of each experiment, tubings were cleaned with 0.1% SDS and degased distilled water.

2.4.2 Characterization of tethered lipid bilayers by quartz crystal microbalance-dissipation

In QCM-D characterization, the binding events and viscoelastic properties of the lipid layers were monitored in real-time by QCM-D (KSV QCM Z500, Finland) coupled with Masterflex peristaltic pump (Figure 2.4). The connection between the peristaltic pump and the system was provided by Tygon tubings. QCM-D monitors and records data regarding the frequency and energy dissipation response of the

freely oscillating sensor. As a QCM-D sensor, gold-coated QCM crystals were used. QCM sensor consists of a thin quartz slide sandwiched between a pair of electrodes. Due to the piezoelectric characteristics of quartz, the crystal is excited to oscillation by applying an AC voltage across the electrodes. To real-time monitor the binding events and evaluate the viscoelactic properties, the changes in frequency (Δf) and dissipation (ΔD) parameters were measured at 15, 25, 35, 45 MHz, simultaneously. The adsorbed mass per area, Δm, was calculated according to the Sauerbrey equation (Sauerbrey, 1959). To evaluate the theoretical liposome behavior and lipid bilayer formation, -ΔD/Δf ratio was utilized as reported in the literature (Bendas, 2010; Ye, Konradi, Textor, & Reimhult, 2009).

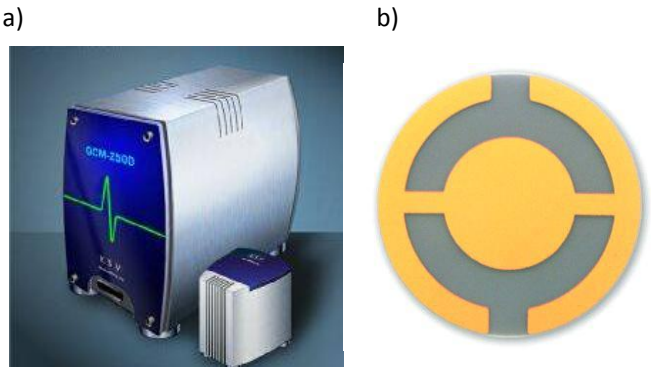

Figure 2.4 : Quartz crystal microbalance system. a) KSV QCM Z500 system (Url-8). b) Gold-coated quartz crystal slide (Url-9).

Before sampling, QCM-D system and gold-coated crystals were cleaned. The gold crystals were washed out with absolute acetone, and dried under N_2 gas atmosphere before mounting the slide to the system. The reaction chamber and tubings were cleaned with 0.1% SDS, ethanol, and degased distilled water successively. Following the cleaning, the reaction chamber was dried with N_2 gas, and then, the sensor crystal slide was mounted. Before the measurements, the reaction chamber was loaded with degased distilled water to reduce possible air-bubble formation. System temperature was adjusted to 25°C, and the flow rate for all solutions was set to 0.1 mL/min. Average monitoring time for tethered lipid bilayer construction was ca. 800 minutes in QCM-D measurements. After the completion of each experiment, tubings were cleaned with 0.1% SDS, ethanol, and degased distilled water, respectively.

2.5 Construction of Tethered Lipid Bilayers on Gold-coated Surface

Construction of tethered lipid bilayers was performed in three steps: Activation of gold-coated surface (Figure 2.5a), attachment of the tethering layer (Figure 2.5b), formation of protein-free lipid bilayer (Figure 2.5c) and membrane protein-inserted lipid bilayer (Figure 2.5d). Apart from the first step, the whole process was monitored by characterization devices (*i.e.*, SPR and QCM).

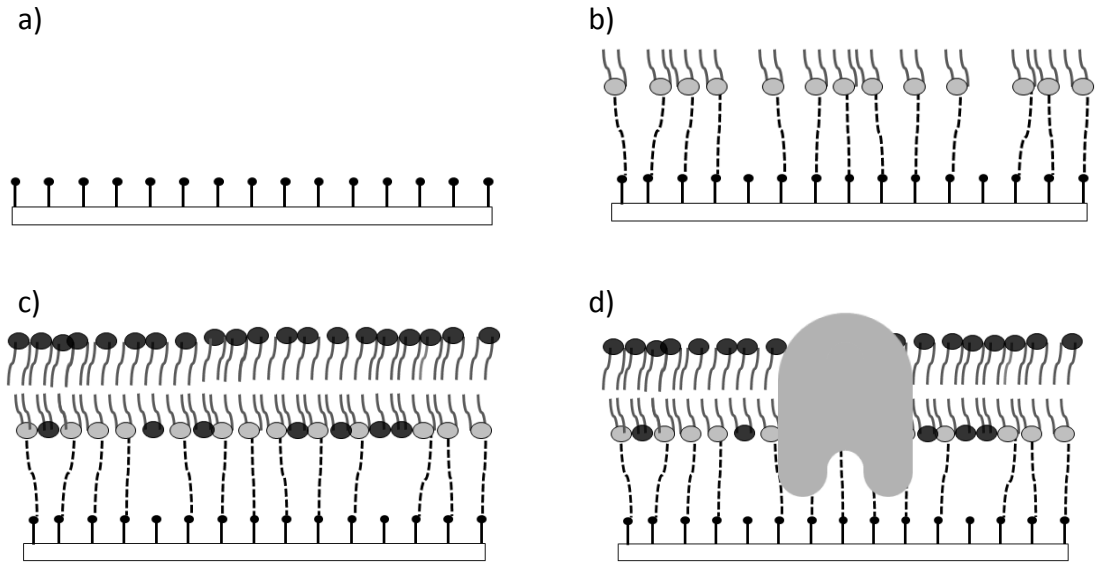

Figure 2.5 : Construction of tethered lipid bilayer on gold-coated surfaces. a) Activation of gold-coated substrate with DTSP. b) DSPE-PEG modification. c) Construction of protein-free lipid bilayer. d) Formation of membrane protein-incorporated lipid bilayer.

2.5.1. Activation of gold-coated surfaces

For the activation step, gold-coated surfaces were modified by DTSP, which is a homobifunctional cross-linking reagent containing a cleavable disulfide linkage and succinimide groups at the end (Figure 2.6). This reagent is typically coupled to molecules containing primary amines by amide bonds buffered at pH 6.5-8.5. For this step, gold-coated surfaces were placed in a beaker containing 1 mM of DTSP dissolved in DMSO, and incubated at room temperature overnight. The surfaces were then washed out with acetone to remove weakly attached DTSP molecules, and dried with N_2 gas before mounting the surface to the characterization device.

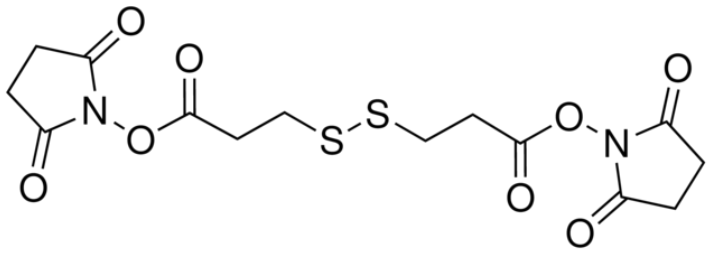

Figure 2.6 : Chemical structure of 3,3′-Dithiodipropionic acid di(N-hydroxysuccinimide) (DTSP) (Url-10).

2.5.2 Construction of tethering layer

For further modifications, DTSP-activated slides were mounted to characterization device, and DSPE-PEG, a modified lipid molecule with an amino group on the phosphate end (Figure 2.7), was incubated on the surface to attach at the succinimide groups of DTSP molecules. To minimize air-bubble formation in the reaction chamber, all solutions were degased before the experiment. To evaluate the effect of DSPE-PEG concentration, lyophilized DSPE-PEG molecules were dissolved in degased distilled water as 1 mg/mL, and then, aliquoted to the various concentrations from 0.01 to 0.06 mg/mL. DSPE-PEG solutions were pumped through the reaction chamber using a peristaltic pump. The binding of DSPE-PEG molecules was monitored in real-time by either SPR or QCM-D, and the solutions were passed until the surface coverage reached to the saturation. Then, the surface was washed out with degased distilled water to remove weakly bound/unbound DSPE-PEG molecules from the surface. In all experiments, the real-time data was simultaneously monitored and recorded to evaluate the binding events.

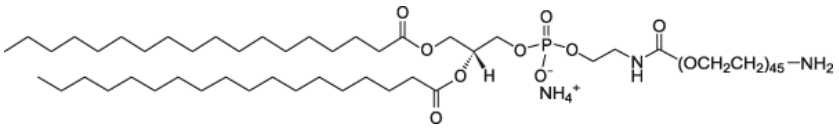

Figure 2.7 : Chemical structure of 1,2-distearoyl-sn-glycero-3-phosphoethanolamine -N-[amino (polyethylene glycol)-2000] (ammonium salt) (DSPE-PEG) (Url-11).

2.5.3 MDR1 protein-free lipid bilayer formation on tethered layer

After the completion of DSPE-PEG layer, the buffer in the system was changed with PBS, and a background signal was obtained in PBS condition. To construct the last layer of the tethered lipid bilayer platform, liposome solution was pumped through the reaction chamber, and this application was continued until saturation was

observed. Following the saturation, a second PBS wash was performed to remove weakly bound/unbound liposomes from the surface. In all experiments, the real-time data was simultaneously monitored and recorded to evaluate MDR1 protein-free lipid layer formation.

2.5.4 MDR1 protein-incorporated lipid bilayer formation on tethered layer

To evaluate protein-incorporated lipid bilayer formation, a broad amount range of MDR1 protein-loaded liposome solution from 0.7 μL to 4 μL was pumped through the reaction chamber instead of MDR1 protein-free liposome solution, and weakly bound/unbound liposome were removed with PBS. In all experiments, the real-time data was simultaneously monitored and recorded to evaluate MDR1 protein-integrated lipid layer formation.

2.6 Evaluation of Orientation and Membrane Protein Insertion by Antibody Binding

To confirm the functional orientation and integration of proteins in lipid bilayers, anti-MDR1 monoclonal antibody was used, and the binding events were monitored in real-time by SPR. To check the existence of non-specific binding, the interaction of anti-MDR1 monoclonal antibody was also evaluated with MDR1 protein-free lipid layers. To evaluate anti-MDR1 antibody specificity for MDR1 protein, anti-Pin-1 mouse monoclonal antibody was used as another control antibody, which is known to have no interactions with MDR1 protein.

To evaluate protein integration, tethered lipid bilayer platform was first constructed until MDR1 protein-incorporated lipid layer formation step under the optimum conditions observed by SPR and QCM-D. The protein-free and protein-incorporated tethered lipid bilayer system was incubated with 1:1000 (v:v) of anti-MDR1 antibody. For another negative control, 1:1000 (v:v) of anti-Pin-1 mouse monoclonal antibody was used on MDR1 protein-incorporated tethered lipid bilayer system. After the application of the antibody solution, a second PBS wash followed this step to remove the weekly bound/unbound antibody molecules. In all experimets, the real-time data was simultaneously monitored and recorded to evaluate antibody binding events.

2.7 Evaluation of Drug-Membrane Protein Interaction in Tethered Lipid Bilayers

As another functionality analysis, pravastatin (statin-based drug), was used to evaluate drug- MDR1 protein interactions (Figure 2.8). The system was limited to work with water soluble molecules, and thus, the other statin molecules such as simvastatin and lovastatin were not suitable to be used in this platform. Such statin molecules could only dissolve in organic solvents, and these solvents damage the stability of the lipid bilayer construction.

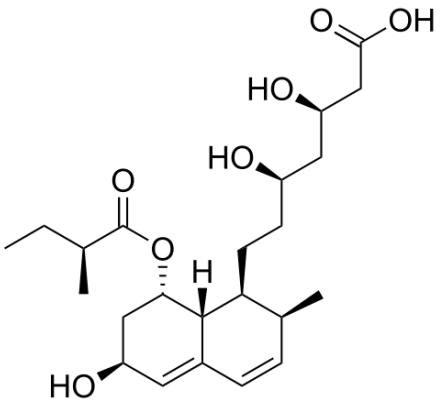

Figure 2.8 : Chemical structure of pravastatin molecule (Url-12).

To perform statin experiments, pravastatin was first dissolved in PBS (0.1 M, pH: 7.4), and the stock concentration was set to 1 mg/mL. To monitor the drug-membrane protein interactions, tethered lipid bilayer platform was constructed on SPR gold-coated slides until the protein-incorporated lipid layer formation under optimum conditions, and the aliquoted concentrations of pravastatin solutions (0.01 and 0.05 mg/mL in PBS) were circulated/passed through the reaction chamber. After the application of the drug solution, PBS wash followed this step to remove the weekly bound/unbound pravastatin molecules. To evaluate the binding events, the real-time data was simultaneously monitored and recorded in all binding events by using SPR system.

2.8 Visualization of Tethered Lipid Bilayers by Liquid-Atomic Force Microscopy

In AFM characterization, the samples were prepared on SPR gold-coated slides and gold (111)-coated mica surfaces. For the visualization and characterization of the

layer-by-layer modification, NanoMagnetics Instruments AQUA non-contact-AFM system (Beytepe, Ankara, Turkey) was used in Physics Department at Istanbul Technical University (Figure 2.9).

Figure 2.9 : NanoMagnetics Instruments AQUA non-contact-AFM system (Url-13).

To construct the tethered bilayers for AFM imaging, the surfaces were first activated with DTSP at room temperature overnight, and self-assembled monolayer structure was generated. To minimize the evaporation during the activation step, the surfaces were kept under DMSO atmosphere, which was provided using DMSO solution in a closed-box. The surfaces were washed out with acetone after DTSP activation. DSPE-PEG layer was first investigated under distilled water condition, and for doing this, DSPE-PEG solution was dropped and covered on DTSP activated surfaces. DSPE-PEG solution was incubated on the surfaces at room temperature for 30 minutes under PBS atmosphere, and thus, possible evaporation of PBS was minimized. PBS atmosphere was provided using same princible with the generation of DMSO atmosphere. Weekly bound/unbound DSPE-PEG molecules were then removed using PBS. To evaluate the conformation of DSPE-PEG changes in different conditions (liquid and air), the surface was also dried under N_2 gas atmosphere, and monitored by AFM. Then, the surface was wetted with PBS, and analyzed by liquid-AFM system again. To evaluate lipid bilayer construction, DSPE-PEG-activated surface was incubated with liposome solution at room temperature for 90 minutes under PBS atmosphere. The surface was then washed out with PBS to remove weakly bound/unbound liposomes. To visualize and evaluate protein-incorporated lipid bilayers, MDR1 protein-inserted liposome solution was used, and

the samples were analyzed under PBS condition. All layers were monitored by liquid-AFM with non-contact mode, and after each experiment, the surfaces were disposed.

3. RESULTS AND DISCUSSION

To incorporate membrane proteins with large hydrophilic domains into lipid bilayer, a well-defined ionic reservoir between lipid bilayer and solid support surface is required. This space provides a native environment for the membrane protein to be stable and functional in its three-dimensional conformation. Here, a tethered lipid bilayer membrane platform was constructed to provide such native conditions for membrane protein-incorporated bilayer systems. To generate an adequate reservoir space, gold-coated support surfaces were first activated with DTSP molecule, and incubated overnight. Although DTSP molecule binds on the gold surfaces via thiol groups in an hour, it was reported that self-assembled monolayer formation takes long time (Diao et al., 2001). After the activation, lipid bilayer was elevated from the support surface by using a spacer molecule, which was a modified lipid molecule with an amino group on the phosphate end. MDR1 was used as a model membrane protein, and protein-incorporated lipid bilayer platform was further evaluated with statin-based drugs in order to understand the interactions between MDR1 protein and statins.

3.1 Evaluation of Spacer Molecule Binding

After the surface activation, spacer molecule (*i.e.*, DSPE-PEG) was bound on the gold-coated surfaces, and the binding events were real-time monitored using the changes in the optical thickness and resonator frequency.

3.1.1 The effect of spacer molecule binding on optical thickness

Changes in optical thickness, which was caused by DSPE-PEG molecule binding, were monitored using SPR system, and the data was collected in real-time as μRIU (micro refractive index unit). Spacer molecule concentration ranging from 0.01 to 0.06 mg/mL was evaluated, and all SPR characterization measurements were performed with at least three independent experiments and reported as the average values ± standard deviation (Table 3.1). The results indicated that the optical

thickness increased with increasing concentrations. The effects of various spacer concentrations on the binding kinetics were plotted in Figure 3.1. After PBS washing step, unbound/weakly bound DSPE-PEG molecules were removed, the remained spacer layer was calculated as μRIU. The spacer layer, which was obtained at the lowest spacer concentration (0.01 mg/mL) showed a high signal decrease after the washing step. For the other concentrations, on the other hand, signal was not observed to decrease significantly (Figure 3.1).

Table 3.1 : Optical thickness values of the constructed spacer layers.

DSPE-PEG Concentration (mg/mL)	Optical Thickness Values (μRIU)
0.01	327 ± 22
0.02	837 ± 31
0.03	909 ± 51
0.04	1098 ± 90
0.05	1113 ± 69
0.06	1130 ± 55

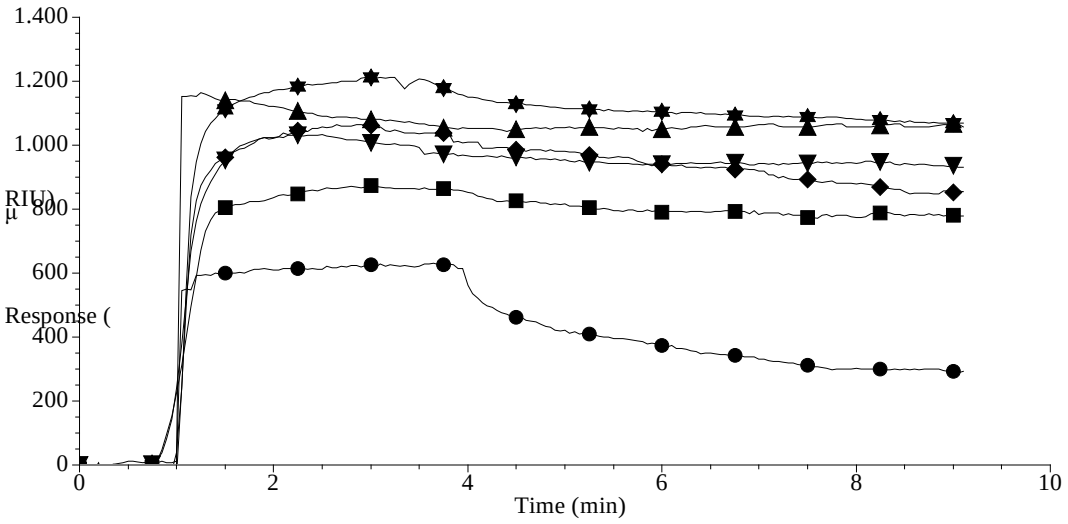

Figure 3.1 : Real-time SPR analysis for the binding effect of various DSPE-PEG concentrations (● 0.01; ■ 0.02; ♦ 0.03; ▲ 0.04;▼ 0.05; ★ 0.06 mg/mL) on DTSP-modified surfaces.

Spacer molecule consists of a PEG chain (Figure 2.7), and this probably influenced the molecular conformation and binding rather than lipid molecules (DSPE) in this hybrid complex. In literature, it was reported that variations in PEG concentration affected the conformation of PEG molecules (Lin et al., 2010). In low concentrations, the surface coverage would also be low, and the distance between the individual molecules restrict their interaction. The intramolecular interactions

between PEG molecules would then be more pronounced. In these conditions, their conformation could be demonstrated as “mushroom-like” structure, and thus, these molecules spread to cover a larger area (Figure 3.2a). They would be assumed in a spherical shape, and their height from the surface would be low. When the concentration was increased, on the other hand, PEG molecules could interact with each other so intermolecular interactions would be dominant rather than intramolecular interactions. Thus, “brush-like” conformation would be observed (Figure 3.2b). The conformational structure changes to extended polymeric chains, which elongates in vertical direction from the surface.

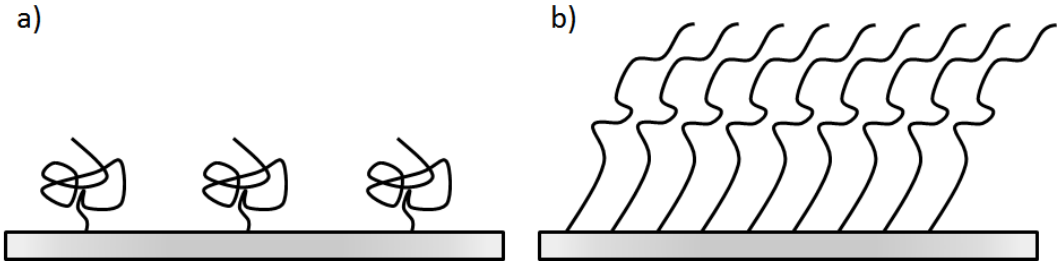

Figure 3.2 : The illustration of DSPE-PEG concentration effect on the conformation. a) Mushroom-like structure. b) Brush-like structure.

Upon the lights of theoretical and experimental results, a drastic change in optical thickness was observed between 0.01 and 0.02 mg/mL concentrations, and the conformational transition from the mushroom to brush-like was thought to be the reason for that observation. At higher concentrations, there was a gradual increase in optical thickness was seen after the washing step. These changes in conformation and the angle of the polymer chains with the surface can affect the liposome spreading and lipid bilayer formation, which would be evaluated in the following sections.

3.1.2 The effect of spacer molecule binding on resonator frequency

Changes in resonator frequency, which was caused by DSPE-PEG molecule binding, were monitored in real-time using QCM-D. The data was collected in Hz, and plotted as frequency change (Δf) versus time (Figure 3.3). Spacer molecule concentration ranging from 0.01 to 0.06 mg/mL was evaluated as performed in SPR experiments. All QCM characterization measurements were evaluated with at least three independent experiments, and the results were reported as the average values ± standard devaition (Table 3.2).

Table 3.2 : QCM-D frequency values of the constructed spacer layers.

DSPE-PEG Concentration (mg/mL)	QCM-D Frequency Values (f)
0.01	45 ± 9
0.02	175 ± 11
0.03	218 ± 11
0.04	254 ± 12
0.05	255 ± 7
0.06	295 ± 7

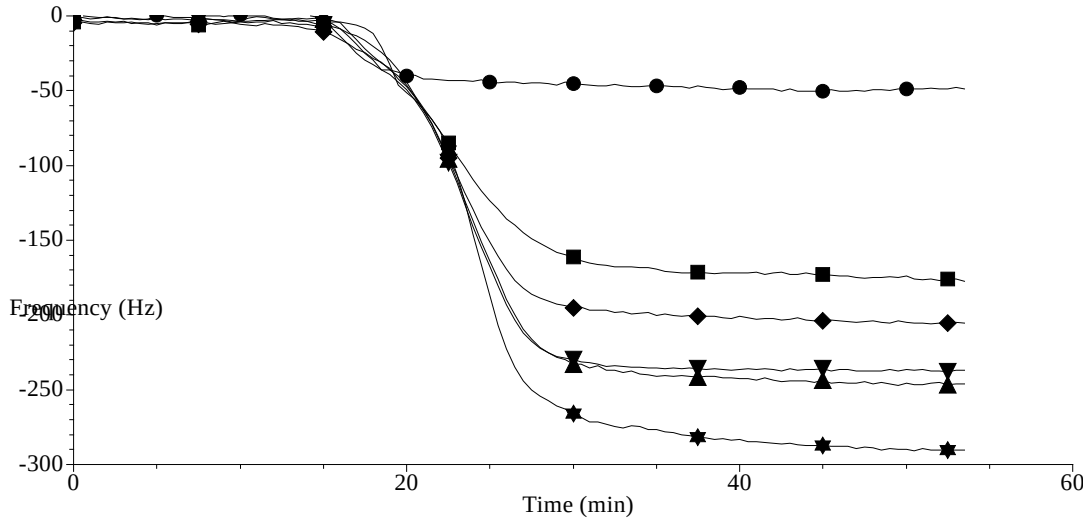

Figure 3.3 : Real-time QCM-D frequency analysis for the binding effect of various DSPE-PEG concentrations (● 0.01; ■ 0.02; ♦ 0.03; ▲ 0.04;▼ 0.05; ★ 0.06 mg/mL) on DTSP-modified surfaces.

Any mass load on QCM-D resonator leads to a decrease in the frequency of oscillation, and the incremental concentration will cause more mass load on the resonator. In this experiment, QCM-D resonator frequency indicated that incremental concentrations of spacer molecule resulted in higher dumping in the frequency (Figure 3.3). On the other hand, PBS wash did not cause high changes as observed in SPR experiments. The long duration of QCM-D experiments compared to SPR experiments (ca. 6 fold), might cause the removal of unbound/weakly bound DSPE-PEG molecules from the surface during the application of DSPE-PEG solution through the QCM reaction chamber. Overall, QCM results supported the data obtained by SPR experiments, and these results indicated a damping in resonator frequency depending on the incremental mass load on the sensor surface.

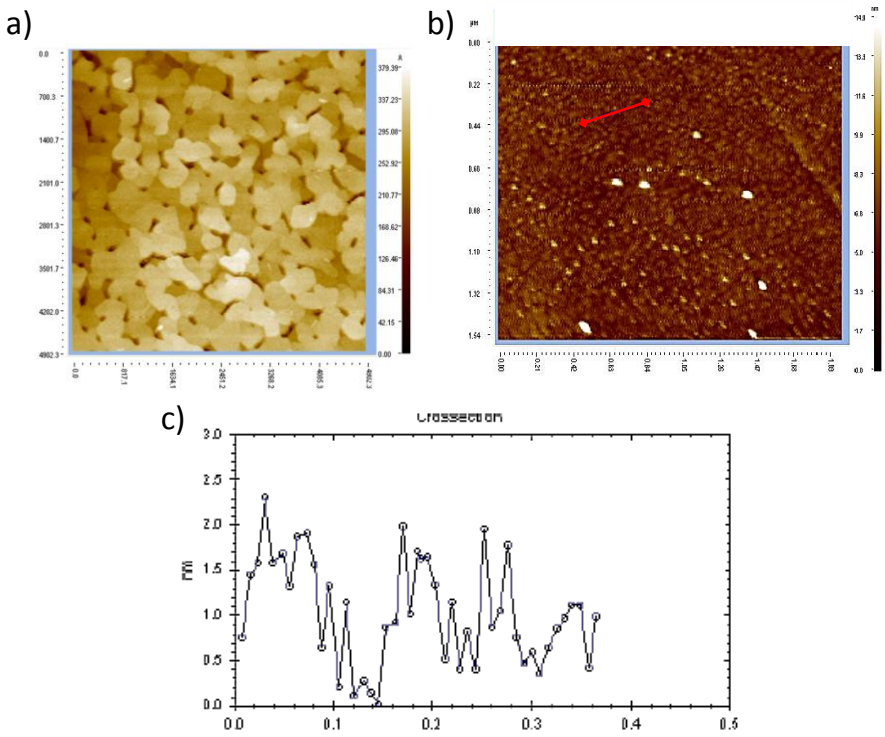

Figure 3.4 : Visualization of unmodified support surfaces. a) AFM image of Au(111)-coated mica surface. b) AFM image of gold-coated SPR surface. c) Crossection analysis of the selected region indicated on SPR surface.

3.1.3 Visualization of spacer molecule binding by liquid-atomic force microscopy

The binding of spacer molecule onto gold-coated surfaces was visualized using liquid-AFM system. For doing this, unmodified gold-coated SPR surface and Au(111)-coated mica surface were first analyzed to understand the characteristics of two distinct surfaces, and AFM analysis were evaluated with at least ten independent experiments. Au(111)-coated mica surfaces presented lower than 1 nm of roughness value (Figure 3.4a) whereas this parameter for SPR surfaces was observed more than 8 nm (Figure 3.4b). Such high roughness value of the SPR surfaces might be correleated with deformations on the BK7 glass surface, which was used as a base of gold-coated SPR surface. In literature, abrasive machining processes during the cutting and shaping of glass slides generally cause surface damages and result in residual cracks and deformation on the top surface (Lv et al., 2012). However, the deposition method of two distinct metal layers (*i.e.,* cromium and gold) can also cause to increase the surface roughness. Large area scans (~1.5 µm x ~2.0 µm) also indicated that this surface had some defects, which might affect the binding area for

surface activator molecule (*i.e.*, DTSP) (Figure 3.4b). On the other hand, as reported in literature, mica material provided a flat surface in atomic level (Wang et al., 2002), and crystalic gold structures were uniformly deposited on mica surface as shown in Figure 3.4a. For further topographical analysis, a uniformly coated region on SPR surface was selected, and this region was used to evaluate the effect of surface activator and the other modifications. Cross-section analysis presented lower than 2.3 nm of roughness on this selected area (Figure 3.4c).

Before the binding of spacer molecule, the surfaces were first modified using DTSP reagent, which naturally breaks its disulphide bond and interacts via thiol bonding to gold-coated surfaces (Figure 3.5a). Interestingly, thiol groups selectively bind to the center of three gold atoms (Figure 3.5b), and organizes uniformly oriented self-assembled monolayer structure (Fenter et al., 1994; Schreiber, 2000) (Figure 3.5c). On the other hand, washing direction was a critical parameter for self-assembled monolayer conformation, and thus, DTSP immobilized surfaces were carefully washed in order to obtain directional orientation in self-assembled monolayer formation. Further, it was reported that this reagent interacts and generates self-assembled monolayer onto Au(111) structures (Fenter et al., 1994; Hobara et al., 2001; Schreiber, 2000). In this study, commercially available SPR surfaces, which comprised from a cocktail of different gold structures other than Au(111), were used. Besides to the structural defects on SPR surfaces, it was theoretically realized that the immobilization capability of SPR surfaces for DTSP molecules was expected to be lower than that of completely Au(111)-coated mica surfaces, and this theoretical expectation was further evaluated in the following sections.

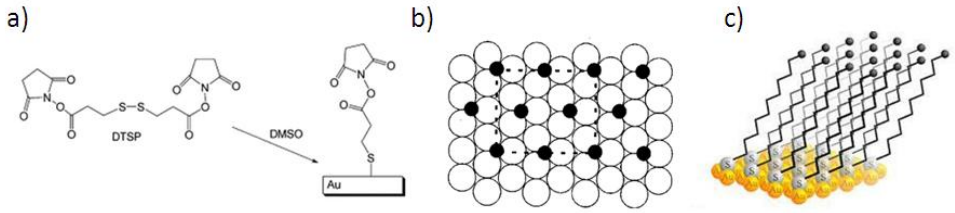

Figure 3.5 : Binding of DTSP on gold-coated surface. a) Binding reaction of DTSP molecules on gold surface. b) Possible DTSP binding sites on gold-coated surface. c) Self-assembled monolayer formation by DTSP molecues.

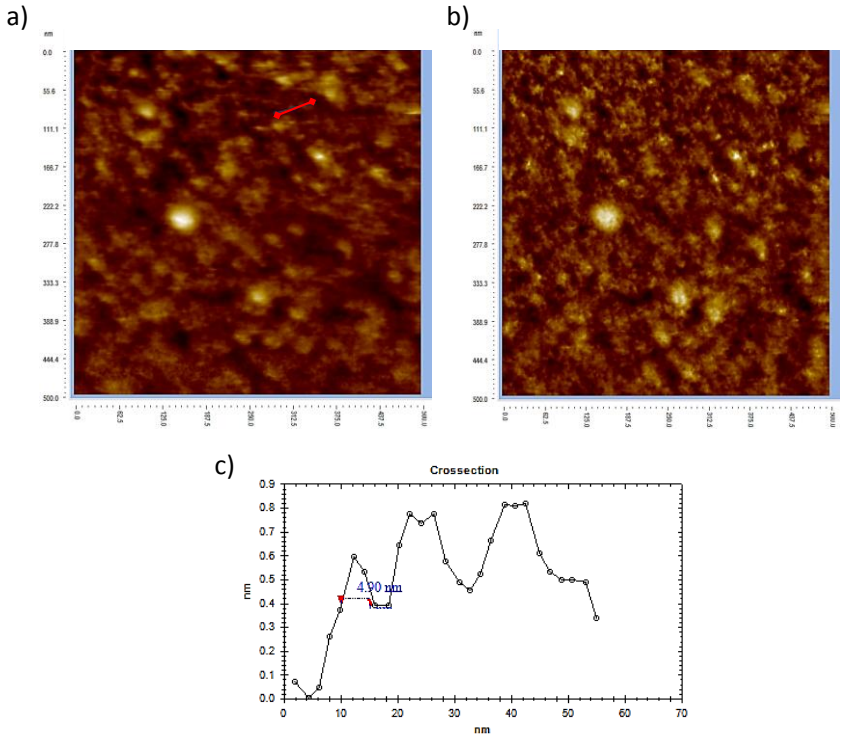

Figure 3.6 : Visualization of DSPE-PEG binding onto gold-coated SPR surface. a) Topography analysis of DSPE-PEG coated surface. b) Dissipation analysis of DSPE-PEG coated surface. c) Cross-section analysis of the selected region indicated in topography image.

To visualize the conformation of spacer molecule, gold-coated surfaces were modified using 0.03 mg/mL of DSPE-PEG in optimum conditions, which were obtained in SPR and QCM studies. Gold-coated SPR surfaces were first evaluated in terms of topography and dissipation characteristics using liquid-AFM system in PBS environment (0.1 M, pH 7.4). Topography parameter presents an image of the surface in nanometric scale. Dissipation parameter indicates the loss of energy during cantilaver scans the surface, and demostrates mechanic characteristics of the surface. As a result of topography analysis, DSPE-PEG molecules typically generated condensed structures (Figure 3.6a). Adding to this, viscoelastic layer formations were also visualized at some regions, which were shown as lighter color in the figures (Figure 3.6a and 3.6b). Further, a uniformly coated area was selected on the SPR surface, and the surface roughness was observed as lower than 1 nm (Figure 3.6c). These results indicated that the surface roughness reduced after the spacer molecule binding, and nearly smooth, and flat surface was obtained. Additionally, large area scans (500 nm x 500 nm) were performed, and the roughness criteria was investigated using roughness avearage parameter, which is used to explain for an

area between the roughness profile and its mean line, or the integral of the absolute value of the roughness profile height over the evaluation length. Roughness average parameter was observed as 0.683 nm. This parameter was further evaluated and compared with layer-by-layer modifications on the surface in the following sections.

The modifications on Au(111)-coated mica were evaluated to analyze the spacer molecule binding on more flat surface, and thus, the surfaces roughness effect on DSPE-PEG binding and conformation was investigated in detail. Topography analysis presented similar results with DSPE-PEG modification on SPR surface (Figure 3.7a). Since SPR surfaces have some structural defects and high roughness value, more smooth and uniform coating was observed on mica surfaces, and it was topographically realized that spacer molecules widely diffused on Au(111) crystals (Figure 3.7a). The flocculation of spacer molecules, however, was rarely observed as well (Figure 3.7a). Dissipation analysis on smaller area scans (225 nm x 225 nm) was performed to evaluate the conformation of spacer molecule, and upon the light of this analysis, a directional behavior was clearly observed as in the experiments with SPR surfaces (Figure 3.7b).

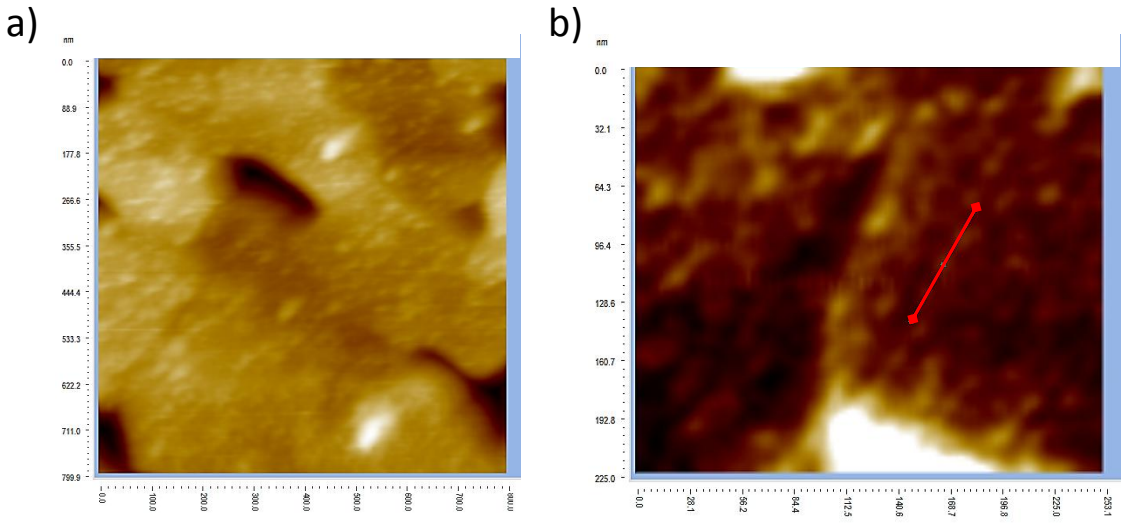

Figure 3.7 : Visualization of DSPE-PEG binding onto Au(111)-coated mica surface. a) Topography analysis of DSPE-PEG coated surface. b) Dissipation analysis of DSPE-PEG coated surface.

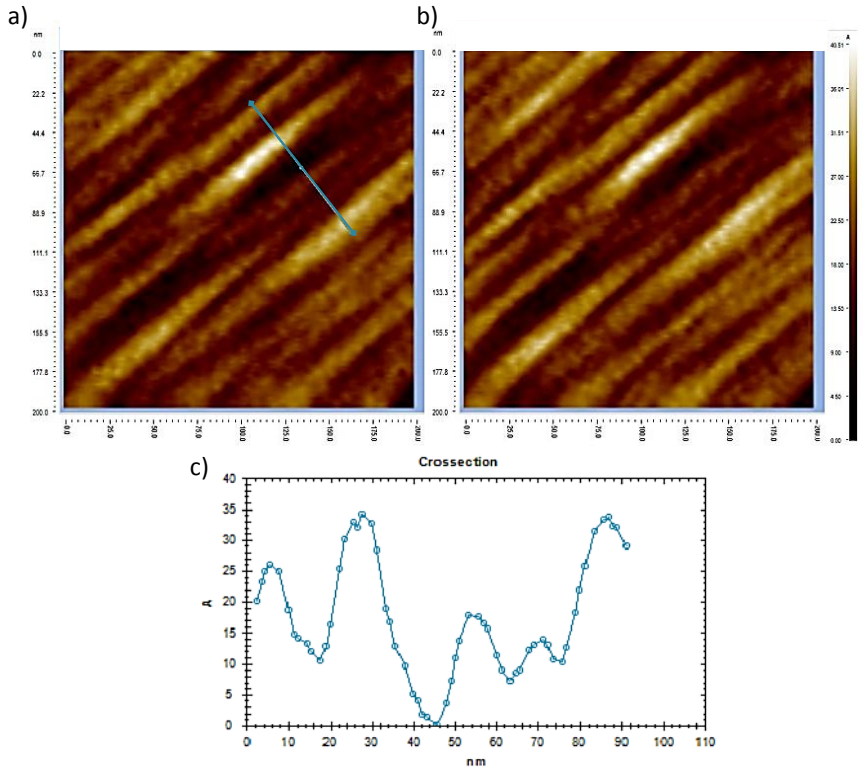

Figure 3.8 : Visualization of incubation time effect on DSPE-PEG conformation. a) Forward scan of AFM imaging. b) Backward scan of AFM imaging. c) Crossection analysis of the selected region indicated on forward scan image.

To evaluate incubation time effect on DSPE-PEG conformation, regular incubation time was increased to more than 2 hours under PBS condition (0.1 M, pH 7.4). In this experiment, forward and backward scans on the same region of SPR surface were carried out to demonstrate the directional behavior of spacer molecule. Liquid-AFM imaging indicated similar results with the experiments of regular incubation time, and the directional behavior was clearly observed in dual-scanning experiments (Figure 3.8a and 3.8b). Additionally, the dimensions of spacer molecule were calculated, and each polymer chain on the surface was observed ca. 14 nm in width and ca. 88 nm in height under PBS conditon. In literature, the length of one PEG residue was reported as 3.5 Å (Kenworthy et al., 1995). The total number of PEG residues in the spacer molecule is 45 (Hansen et al., 2003), and theoretical length of the spacer molecule is ca. 16 nm. This result implied that PEG residues presented an extension and expansion in the conformation in aqueous conditions. The conformational behavior of polymer residues is variable in different conditions, and it is dependent on pH and ionic content of the medium (Nataliya M Samoshina et al., 2011). Additionally, as disscussed in Section 3.1.1, intermolecular interactions

between PEG residues existed in the optimum conditions for spacer molecule (0.03 mg/mL of DSPE-PEG), and "brush-like" conformation, in which thin and long polymeric chains extended through vertical direction, was observed in liquid-AFM analysis (Allen et al., 2002; Jokerst et al., 2011; Kenworthy et al., 1995).

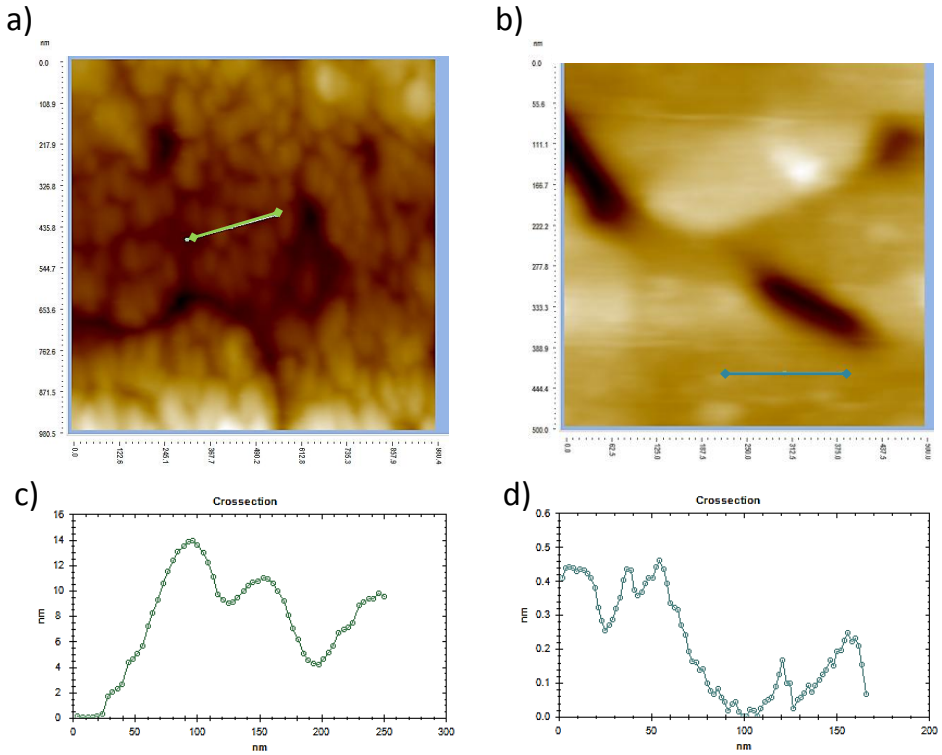

Figure 3.9 : Visualization of different condition effects on DSPE-PEG conformation. a) Conformational behavior of spacer molecule in air condition. b) Conformational behavior of spacer molecule in aqueous condition. c) Cross-section analysis of the selected region indicated on air condition image. d) Cross-section analysis of the selected region indicated on aqueous condition image.

To visualize the effect of different conditions on DSPE-PEG conformation, Au(111)-coated mica surfaces were used to avoid the surface roughness effect. For doing this, the spacer molecule modified mica surfaces were first dried using N_2 gas atmosphere and analyzed using AFM system in air condition. Then, the surfaces were re-hydrated with PBS solution (0.1 M, pH 7.4) to evaluate the changes in aqueous condition. As a result of this experiment, polymeric spacer molecule flocculated and formed a rough structure in air condition (Figure 3.9a) as opposed to the polymer covered surface in aqueous condition (Figure 3.9b). Therefore, re-hydration allowed to regenerate the directional behavior and uniform coating on the surface (Figure 3.9b). AFM images were further analyzed in two distinct conditions, and

crossectional analysis indicated that ca. 14 nm and ca. 0.4 nm of roughness were observed for polymeric structures in air and aqueous conditions, respectively (Figure 3.9c and 3.9d). In literature, Au-tethered-PEG layers were furthered investigated in PBS and 20% of 2-propanol in PBS conditions by using AFM system, and it was observed that while PEG chains presented "brush-like" structure in PBS, the addition of propanol to the buffer caused PEG chains to be collapsed (Backmann et al., 2010). In the presented study, DSPE-PEG molecules were investigated in both dehydrated and rehydrated conditions, and, it was observed the polymer chains presented a highly rough structure in dehydrated form whereas re-hydration allowed the polymer chains to gain their previous "brush-like" structure.

Additionally, the height of immobilized layer in different conditions was calculated by digging the surface with AFM tip (Figure 3.10a and 3.10b). For doing this, AFM tip was first used to dig a small area (100 nm x 100 nm) on the SPR surface, and then, the surface was visualized using AFM system. Immobilized layers were calculated in air and aqueous conditions, and the heights were observed ca. 50 nm and ca. 12 nm, respectively (Figure 3.10c and 3.10d). As a result of this experiment, spacer molecules generated a highly condensed structure in aqueous condition whereas it demonstrated a flocculated structure in air condition. In literature, it was reported that the behavior of PEG residues could change in different conditions, and this behavior could easily monitored in air/water transition (Jebrail et al., 2008). Therefore, in aqueous conditions, PEG residues presents highly complex intermolecular interactions, which contact to the other residues, and generates a uniform and smooth distrubution on the support material.

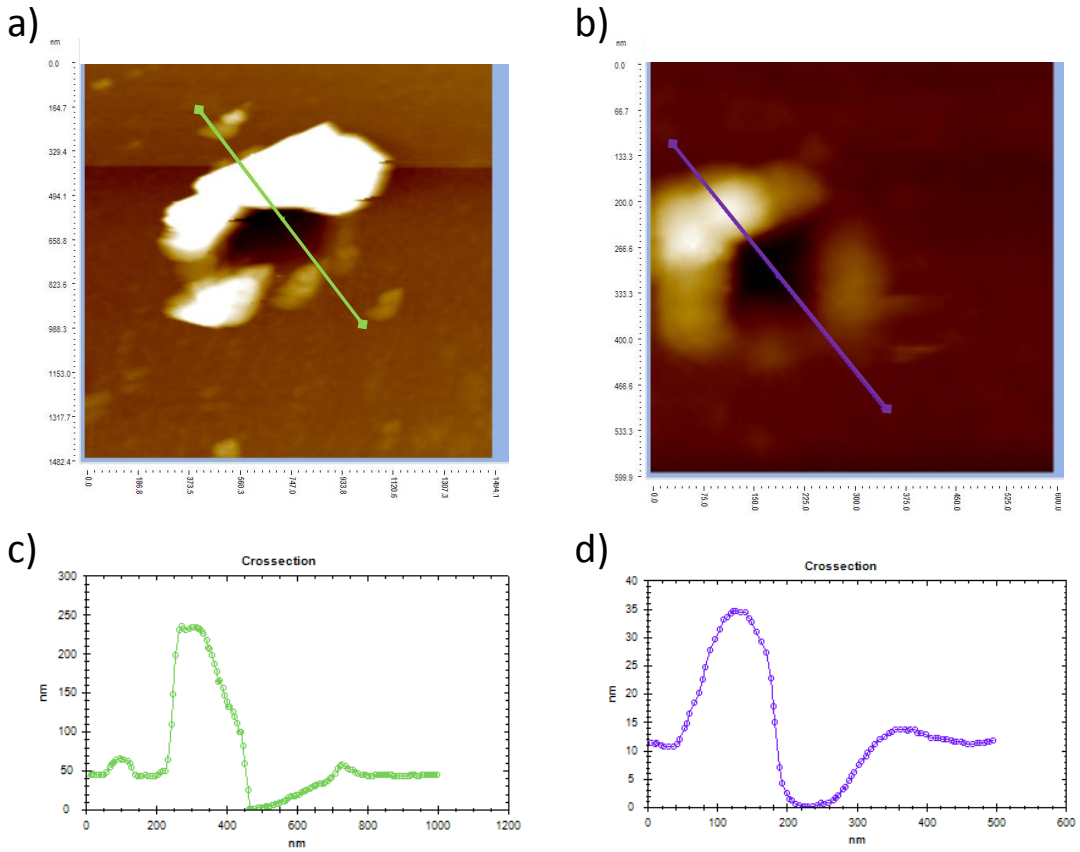

Figure 3.10 : Height measurements of DSPE-PEG layer. a) Visualization of the height measurement in air condition. b) Visualization of the height measurement in aqueous condition. c) Height measurement of the selected region indicated on air condition image. d) Height measurement of the selected region indicated on aqueous condition image.

3.2 Evaluation of MDR1 Protein-Free Liposome Binding/Spreading and Lipid Bilayer Formation

For lipid bilayer platform, PC molecules were preferred as model lipid molecule to mimic eukaryotic cell membranes due to their high abundance in animal cell membranes (Henneberry et al., 2001). Liposome binding/spreading and lipid bilayer formation were monitored in real-time using SPR and QCM-D in order to evaluate the effects of binding events and lipid layer characteristics (*e.g.*, viscoelasticity and rigidity) on optical thickness, resonator frequency, and dissipation parameters.

3.2.1 Characterization of DSPE-PEG concentration effect on liposome binding/spreading by surface plasmon resonance

To evaluate the spacer concentration effect on liposome binding/spreading, a fixed concentration of liposome solution was incubated on tethered layer, which was generated by the various concentrations of DSPE-PEG molecules. All SPR measurements were evaluated with at least three independent experiments.

Application of various concentrations of the spacer molecules resulted in different liposome binding/spreading characteristics (Figure 3.11). For instance, at the highest concentration of the spacer molecule (0.06 mg/mL), liposome binding first increased, and then, excessive amount of liposomes were easily removed during washing step. Therefore, the optical thickness signal returned the beginning signal after the first washing step (Figure 3.11). It was realized that liposomes could not attach on this concentration of DSPE-PEG molecules. Liposomes probably presented weak interactions with dense tethered layer, and therefore easily removed from the surface in washing steps. However, 0.05 mg/mL of DSPE-PEG condition, another high concentration, presented low change in the optical thickness beginning from the experiment (Figure 3.11). At low spacer concentrations (0.01 and 0.02 mg/mL), the spreading of liposomes either did not cause a drastic increase in the optical thickness from the beginning or the sudden decrease in washing step (Figure 3.11). On the other hand, the highest optical thickness was observed at 0.03 and 0.04 mg/mL of DSPE-PEG concentrations (Figure 3.11). After washing step, the signal levels did not change, and the surface was saturated after 30 minutes. According to SPR optical thickness results, 0.03 and 0.04 mg/mL of spacer conditions presented the optimum liposome binding results (Figure 3.11).

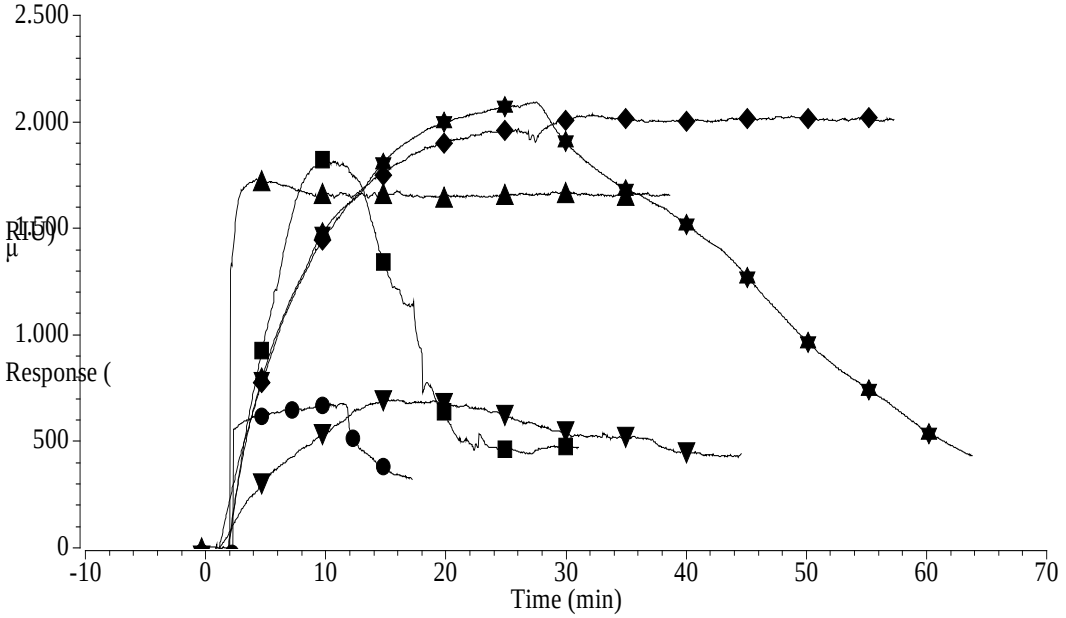

Figure 3.11 : Real-time SPR analysis of the liposome binding/spreading on the surfaces modified by various DSPE-PEG concentrations (● 0.01; ■ 0.02; ♦ 0.03; ▲ 0.04;▼ 0.05; ★ 0.06 mg/mL).

3.2.2 Characterization of DSPE-PEG concentration effect on liposome binding/spreading and lipid bilayer formation by quartz crystal microbalance

Frequency changes on QCM resonator were monitored in real-time in order to evaluate liposome binding/spreading on the tethered layer. All QCM measurements were evaluated with at least three independent experiments.

Mostly, QCM frequency change presented similarity with the results obtained by SPR. For instance, low amount of DSPE-PEG on the surface demonstrated that liposomes could not effectively bind on the tethered layer as observed in SPR experiments (Figure 3.12). On the other hand, higher spacer concentrations (0.04 to 0.06 mg/mL) presented different kinetic curves in QCM experiments but the signal levels for these concentrations reverted to the beginning level after washing step, which was comparable to the results obtained by SPR experiments (Figure 3.12). Overall, liposome binding/spreading on the tethered layer formed by 0.03 mg/mL of DSPE-PEG concentration presented the highest signal level in both characterization methods (*i.e.*, SPR and QCM), and this concentration was preferred to continue in the following experiments (Figure 3.12). Additionally, it was noticed that this minor

difference between SPR and QCM results could depend on the different active surface areas, which were used in both characterization devices. In 0.03 mg/mL DSPE-PEG concentration, the liposome binding/spreading caused 1968 ± 126 μRIU of a signal increase in SPR measurements, and 489 ± 91 Hz of a signal decrease in QCM frequency measurements.

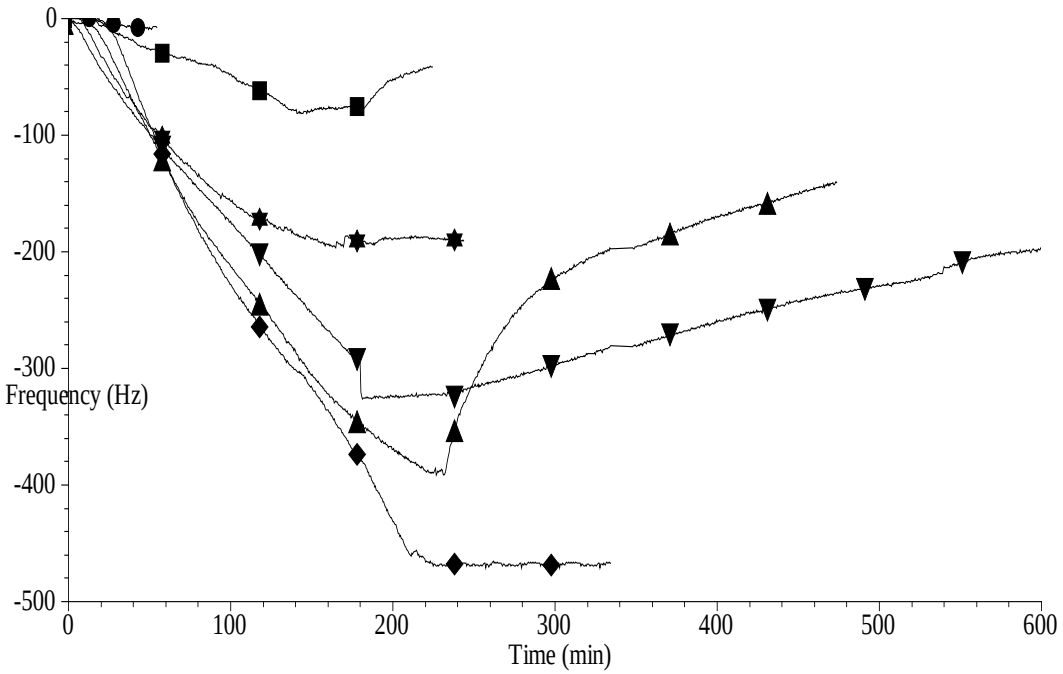

Figure 3.12 : Real-time QCM frequency analysis of the liposome binding/spreading on the surfaces modified by various DSPE-PEG concentrations (● 0.01; ■ 0.02; ♦ 0.03; ▲ 0.04; ▼ 0.05; ★ 0.06 mg/mL).

QCM frequency response in liposome binding/spreading experiments resulted in high signal changes compared to the previous experiments (ca. 30 Hz) (Reimhult et al., 2003; Stalgren et al., 2001). In literature, the liposome layer is typically separated above 1-2 nm from the support surface, and such narrow reservoir is considerably lower than the space which is formed by polymeric molecules (Groves et al., 1997; Sackmann, 1996). Additionally, such narrow space is not adequate to incorporate transmembrane proteins with large hydrophilic domains such as MDR1, and thus, the reservoir gap is further increased to provide a sufficient space for these membrane proteins. For instance, dioctadecylamine was used as anchor polymer to tether lipid bilayers in order to investigate the construction of a tethered bilayer system on glass surface. It was reported that although the presence of the polymer caused to reduce the fluidity, the polymer provided more stable structure to the bilayer system

compared to polymer-free platforms (Naumann et al., 2002). Further, PEG molecules had been used to construct lipid bilayers on glass and gold-coated surfaces in the literature (Merzlyakov et al., 2006; Munro & Frank, 2004; Wagner & Tamm, 2000). For instance, Wagner and co-workers successfully incorporated cytochrome b5 and annexin V proteins into lipid bilayers, which were tethered by PEG polymer (Wagner & Tamm, 2000). As a result of this experiment, it was realized that lipid bilayer systems, which were directly constructed on the solid support, prevented the mobility of membrane proteins. Therefore, it was obviously demonstrated that lipid bilayer system required a tethering layer in order to elevate the bilayer, and conserve the native conformation of proteins. Further, PEG tethers and PEG-lipid hybrid (DMPE-PEG) complexes were also investigated to understand/discover the interactions of PEG with surface and liposomes (Munro & Frank, 2004). In this experiment, PEG tethers without lipid molecules interfered to liposome spreading, and the liposomes remained intact on the surface instead of generation lipid bilayer on the surface. Overall, the presence and concentration of PEG molecule are critical parameters to construct a tethered lipid bilayer system for transmembrane proteins with large hydrophilic domains, and this step requires further optimization to provide native conditions for such proteins.

To understand the lipid layer characteristics and lipid bilayer formation, dissipation parameter of QCM-D platform was utilized (Figure 3.13), and ΔD and Δf values were first calculated to determine the viscoelastic properties of the constructed lipid bilayers. In the literature, $-\Delta D/\Delta f$ value was reported to understand liposome behavior on solid surface (Hopfner et al., 2008; Keller & Kasemo, 1998; Khan et al., 2008; Reimhult et al., 2002). High $-\Delta D/\Delta f$ value indicates that the presence of high water content causes an increase in elasticity when the liposomes remained intact on the surface. The liposomes lose their water content and form a more rigid layer when they are deformed and fused onto the surface. The deformation of liposomes also results in the loss of entropy, and a more attractive surface potential is generated for a lipid bilayer formation.

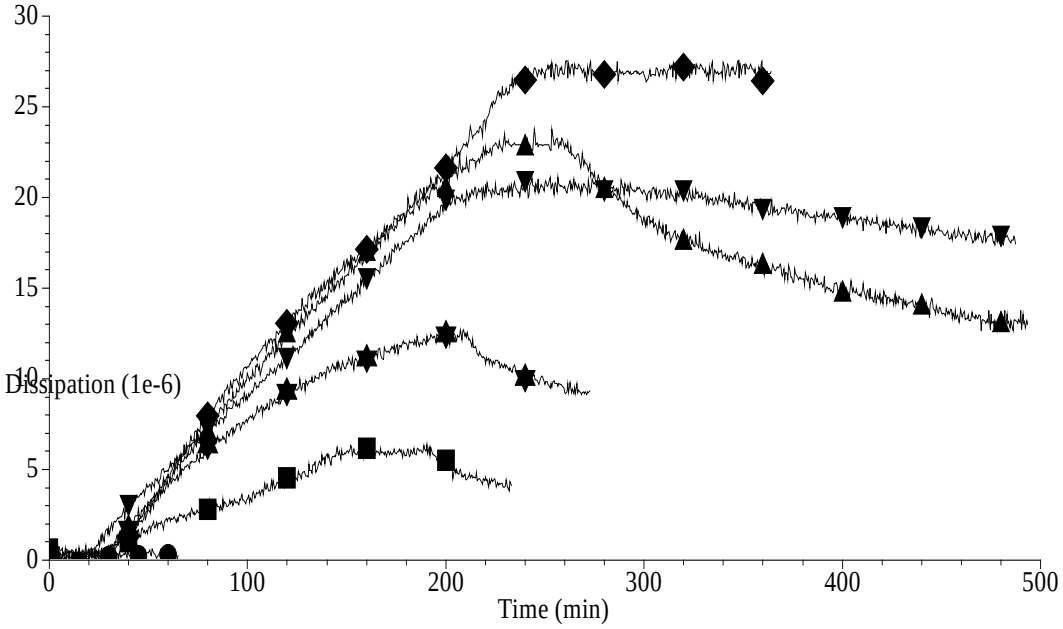

Figure 3.13 : Real-time QCM-D dissipation analysis of liposome binding/spreading on the surfaces modified by various DSPE-PEG concentrations (● 0.01; ■ 0.02; ♦ 0.03; ▲ 0.04; ▼ 0.05; ★ 0.06 mg/mL).

Table 3.3 : Liposome behavior in various concentrations of DSPE-PEG molecule.

DSPE-PEG Concentration (mg/mL)	-ΔD/Δf Ratio	Liposome Behavior
0.01	4.03 ± 3.53	non-deformed
0.02	5.71 ± 1.13	non-deformed
0.03	1.85 ± 0.15	flattened and bilayer formation
0.04	6.16 ± 2.58	non-deformed
0.05	5.20 ± 0.61	non-deformed
0.06	3.38 ± 1.20	partial deformation

To evaluate lipid bilayer formation in the presented tethered lipid bilayer platform, -ΔD/Δf ratios were compared with a control value of -ΔD/Δf, which was reported in the previous experiments (Bendas, 2010; Ye et al., 2009). BSA was used as a control, and its ratio was observed as 1.3 ± 0.76 Hz. In the literature, -ΔD/Δf ratios of 3–4 and higher values predict non-deformed liposomes on the surface, whereas -ΔD/Δf ratios of 1–2 (control value) and lower values indicate bilayer formation (Bendas, 2010). Additionally, -ΔD/Δf ratio of ~2 indicates a strong binding and flattening of liposomes on solid surface (Bendas, 2010). In this study, -ΔD/Δf ratio calculations were presented in Table 3.3. At high (0.04 and 0.05 mg/mL) and low (0.01 and 0.02 mg/mL) DSPE-PEG concentrations, liposomes bound without any deformation and remained intact onto the surface. At 0.06 mg/mL of DSPE-PEG

concentration, liposomes presented partial deformation compared to the control. At 0.03 mg/mL of DSPE-PEG concentration, liposomes deformed and generated a flattened structure. This concentration indicated a variation between 1 and 2, and resulted in a dual-characteristic, flattening of liposomes and bilayer formation.

In the presented platform, liposomes were not directly spread on a solid surface such as SiO_2 but onto a lipid layer with a polymer cushion, whereas these calculations were generally used on a solid surface without any modification. For instance, SiO_2 is one surface that liposomes can spontaneously spread and form lipid bilayer structure. The investigations based on lipid bilayer formation on these surfaces were summarized as: (i) liposomes start to attach to the surface; (ii) liposomes begin to deform and partially form lipid bilayers when the liposome amount reaches a critical level such as saturation; (iii) all liposomes form lipid bilayer structure (Reimhult et al., 2006). On the other hand, liposome interaction with DSPE-PEG chains was indicated a crucial parameter for tethered lipid bilayer formation in the presented platform. Thus, molecule concentration and conformation of the modified layer play a key role to construct lipid bilayers, and affect the liposome behavior.

Further, the mass load caused by liposome binding/spreading was calculated using Saurebrey's equation, which was explained in detail in Introduction section (Sauerbrey, 1959). To calculate the mass load, the data found at the optimum conditions (0.03 mg/mL of DSPE-PEG concentration) were used, and the mass load of the liposomes was observed as 2.9 ± 0.8 μg/cm^2 (Bendas, 2010). Theoretically, the expected mass load was calculated based on the molecular weight and head group size of PC, and reported as ~ 2.1 μg/cm^2 (Bendas, 2010; Reimhult et al., 2003). Such excessive amount of mass load implied that the majority of liposomes deformed and spontaneously fused to either construct a lipid bilayer or form partial local multilayers (Bendas, 2010; Hopfner et al., 2008; Reimhult et al., 2003; Reimhult et al., 2006; Stalgren et al., 2001). On the other hand, one should keep in mind that this theoretical estimation is efficiently performed for solid and homogenously distributed layer conditions. Apparently, the constructed lipid layer in this study does not provide such solid layer, as generated by BSA. Additionally, homogenous distribution and/or any defects on the lipid layer could not be evaluated with QCM-D and SPR experiments, and thus, liquid-AFM assisted to visualize the surface properties of the constructed lipid layer as described in the following sections.

3.2.3 Visualization of liposome binding/spreading and lipid bilayer formation by liquid- atomic force microscopy

Optimum conditions for DSPE-PEG concentration were used to evaluate liposome binding/spreading and lipid bilayer formation on the support surface. All experiments were performed under PBS condition (0.1 M, pH 7.4), and analyzed using liquid-AFM system. As a support material, gold-coated SPR surface and Au(111)-coated mica surface were utilized to evaluate the surface roughness effect on liposome binding/spreading and lipid bilayer formation. AFM analysis was evaluated with at least ten independent experiments.

Application of liposomes onto the tethered layer provided more flat surface compared to the previous layer, which was formed by DSPE-PEG (Figure 3.14a and 3.14b). Visually, mica surfaces allowed to generate uniform distribution of liposomes whereas few defects and non-homogenous distribution were observed on SPR surfaces (Figure 3.14a and 3.14b). Due to the defects and high roughness on SPR surfaces, the variations on the constructed layer was observed. Quantitatively, a random area was selected to evaluate the roughness differentiation on the constructed layer, and lower than ca. 1.5 nm of surface roughness value was observed on AFM images (Figure 3.14c and 3.14d). On this selected area, SPR surface majorly presented ca. 0.5 nm roughness, and some flocullation were however, observed as well (Figure 3.14c). On the other hand, mica surfaces mostly presented ca. 1 nm roughness value, and some variations in the roughness was also observed (Figure 3.14d). On the other hand, overall roughness value was observed as 0.452 nm for roughness average. Comparing to previous constructed layer (*i.e.,* DSPE-PEG modification), this parameter reduced and presented more flat surface. In literature, the height of lipid bilayer, which was designed for MDR1 insertion, was reported as ca. 3 nm (Karasu, 2011), and well-organized lipid bilayer was theoretically expected to be less than 3 nm of roughness. As the results obtained by QCM-D experiments, the roughness value quantitatively supported that the most of liposomes could be deformed and fused to either form a lipid bilayer or form partially local multilayers on the support surface. As AFM perspective, lipid bilayer formation and local multilayers were visually observed.

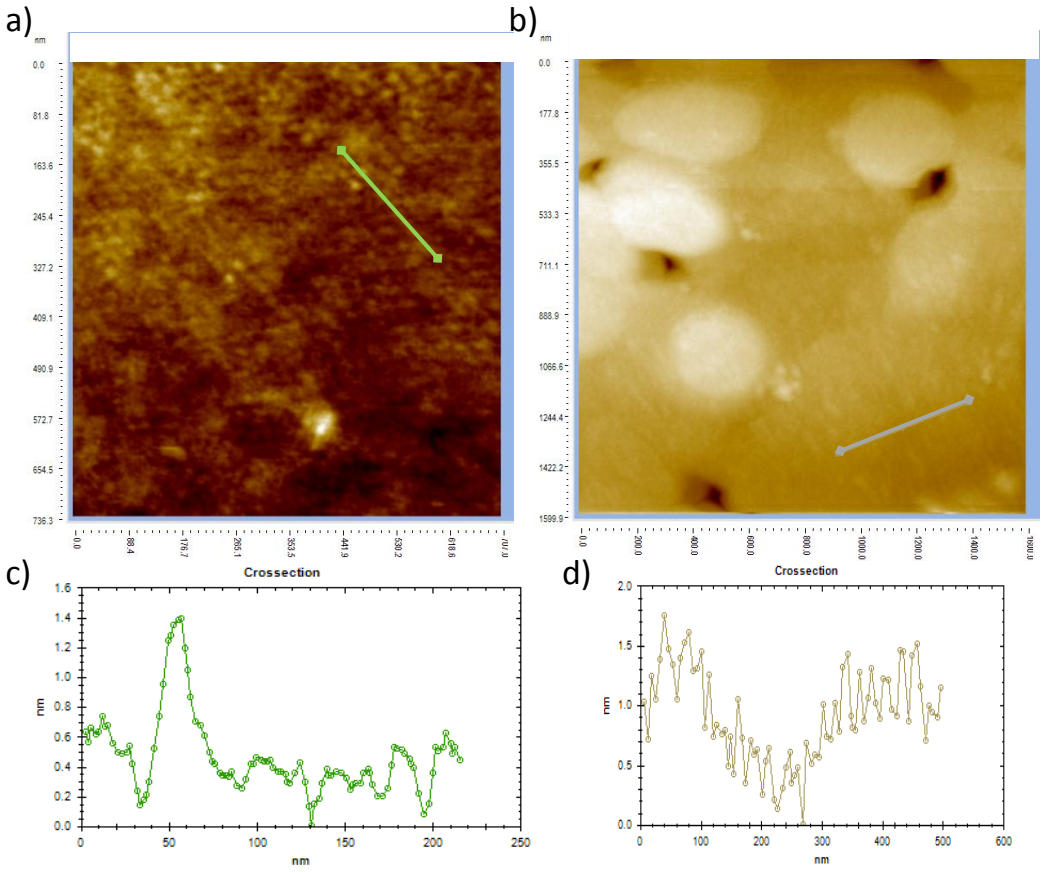

Figure 3.14 : Visualization of lipid bilayer formation on various surfaces. a) Lipid bilayer formation on gold-coated SPR surface. b) Lipid bilayer formation on Au(111)-coated mica surface. c) Cross-section analysis of the selected region indicated on gold-coated SPR surface image. d) Cross-section analysis of the selected region indicated on Au(111)-coated mica surface image.

3.3 Evaluation of MDR1-incorporated Liposome Binding/Spreading and Lipid Bilayer Formation

To monitor MDR1-incorparated liposome binding/spreading and lipid bilayer formation, SPR and QCM-D based characterization methods were performed, and the binding events and lipid layer characteristics were evaluated using optical thickness, resonator frequency, and dissipation parameters.

3.3.1 The effect of MDR1 amount on liposome binding/spreading by surface plasmon resonance

Various volumes of MDR1 protein ranging from 0.7 to 5.0 µL were tried to understand the effect of MDR1 amount on liposome behavior. All SPR measurements were evaluated with at least three independent experiments.

To test the effect of protein amount, 0.04 and 0.03 mg/mL of DSPE-PEG-coated surfaces were chosen to observe the effect of different surfaces on the spreading of protein-incorporated liposomes. After washing step, protein-loaded liposomes were removed from the surface prepared by 0.04 mg/mL of DSPE-PEG, and thus, this concentration did not provide a stable platform for protein-incorporated lipid bilayer systems. The layer formed using 0.03 mg/mL of DSPE-PEG was shown to be stable, and so, it was used in further studies. Kinetic curves showed that liposomes containing low (0.7 μL) and high (3.0 – 5.0 μL) amount of MDR1 were either fully removed from the surface or not efficiently constructed on the support surface (Figure 3.15). Although 0.9 and 2.0 μL of MDR1-loaded liposomes presented a successful construction, 1.0 μL of MDR1 resulted in the highest binding capability and provided the optimum conditions for protein-loaded liposome binding/spreading (Figure 3.15).

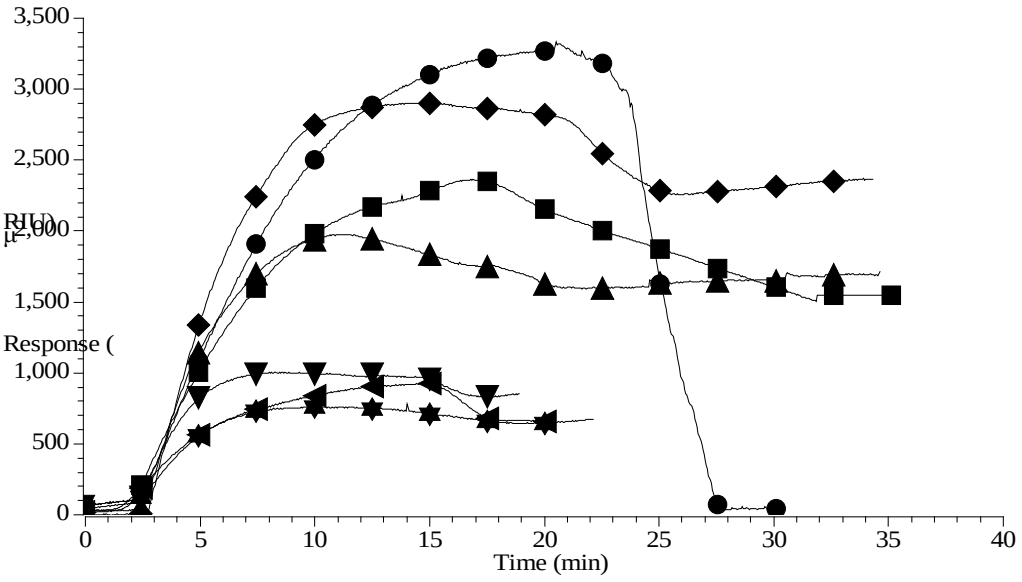

Figure 3.15 : Real-time SPR analysis for the binding/spreading of various MDR1 amount-loaded (● 0.7; ■ 0.9; ♦ 1.0; ▲ 2.0;▼ 3.0; ★ 4.0; ◄ 5.0 μL) liposomes on the surfaces modified by 0.03 mg/mL of DSPE-PEG.

Additionally, the effect of MDR1 amount on lipid bilayer/spreading obviously presented a special trend, which was plotted in Figure 3.16 using the collection of three independent experiment results, and these results indicated that the presented tethered lipid bilayer system was reproducible.

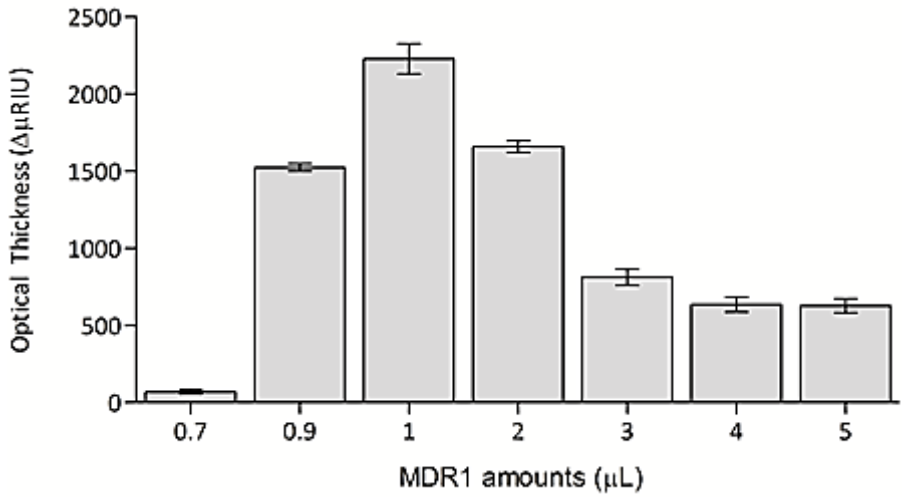

Figure 3.16 : The effect of various MDR1 amount-loaded liposomes on the optical thickness.

3.3.2 The effect of MDR1 amount on liposome binding/spreading and lipid bilayer formation by quartz crystal microbalance

In QCM frequency experiments, various amounts of MDR1 protein ranging from 0.7 to 4.0 μL were analyzed to evaluate the effect of MDR1 amount on liposome behavior (Figure 3.17 and 3.18). All QCM measurements were evaluated with at least three independent experiments.

The frequency experiments showed that low (0.7 μL) and high (2.0-4.0 μL) amounts of protein caused small changes in resonator frequency during the application of the protein-loaded liposomes (Figure 3.17). Although 0.9 μL of MDR1-loaded liposomes first presented a high binding tendency, it was observed that these liposomes loosely bound on the surface, and this mass load was easily removed from the surface after washing step (Figure 3.17). Further, dissipation analysis was carried out to understand the effect of protein amount on the liposome behavior (Figure 3.18). QCM characterization method implied that 1.0 μL of MDR1-loaded liposomes resulted in the highest damping in frequency and dissipation change, and provided the optimum conditions as observed in SPR experiments. Overall, high amount of protein-incorporated liposomes obstructed the construction of lipid bilayer, and thus, 1.0 μL of MDR1 conditions were preferred in following experiments and analyses.

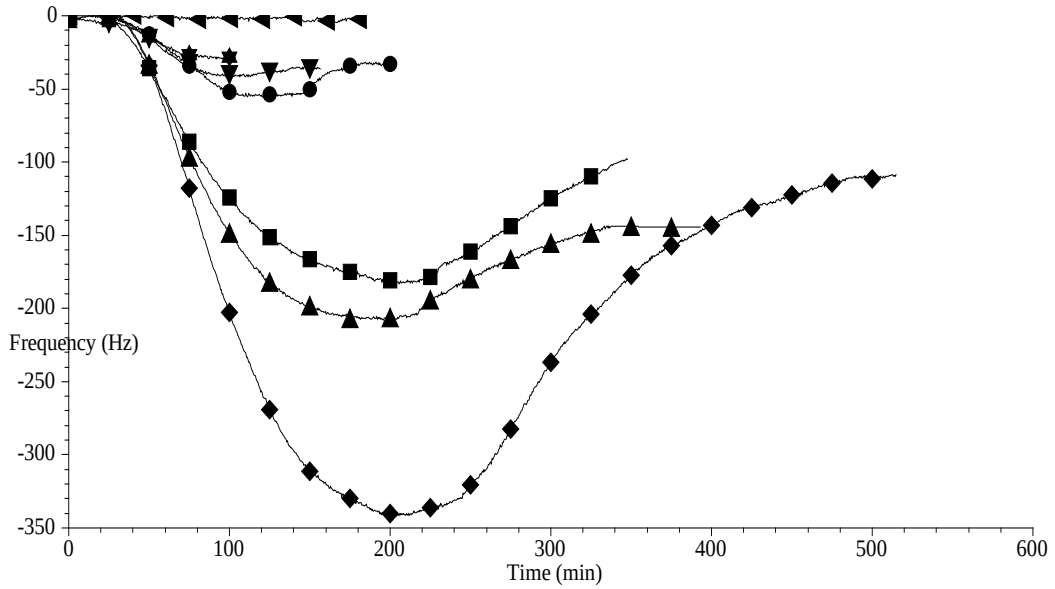

Figure 3.17 : Real-time QCM frequency analysis for the binding/spreading of various MDR1 amount-loaded (● 0.7; ■ 0.8; ♦ 0.9; ▲ 1.0;▼ 2.0; ★ 3.0; ◄ 4.0 µL) liposomes on the surfaces modified by 0.03 mg/mL of DSPE-PEG.

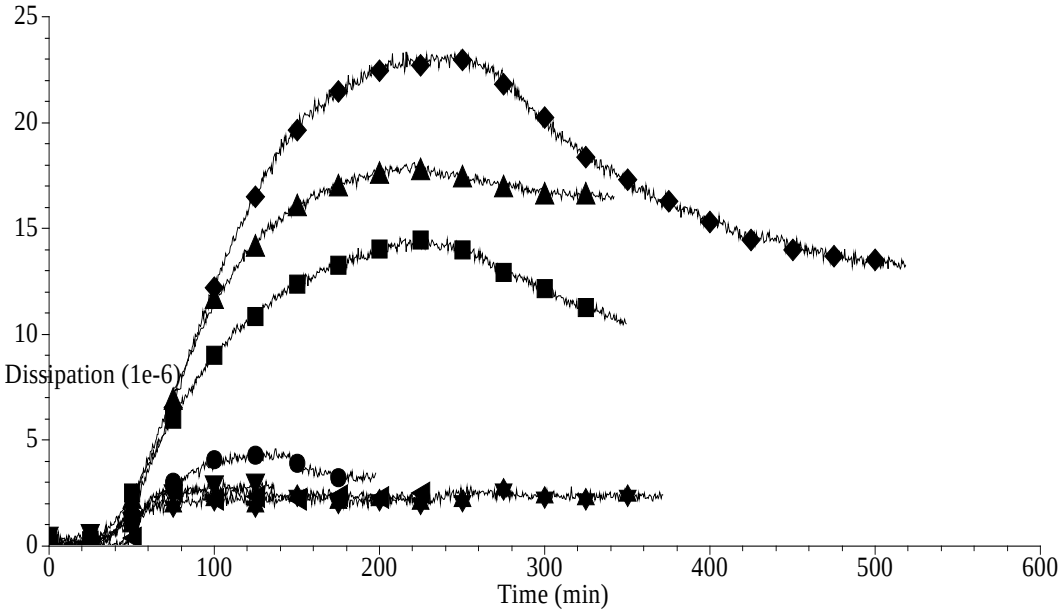

Figure 3.18 : Real-time QCM dissipation analysis for the binding/spreading of various MDR1 amount-loaded (● 0.7; ■ 0.8; ♦ 0.9; ▲ 1.0;▼ 2.0; ★ 3.0; ◄ 4.0 µL) liposomes on the surfaces modified by 0.03 mg/mL of DSPE-PEG.

The binding/spreading of MDR1-free and MDR1-loaded liposomes was also investigated using QCM dissipation characteristics. To compare these two distinct conditions, liposomes were incubated on the tethered layer, which was formed by

0.03 mg/ml of DSPE-PEG. As a result of the dissipation analysis, MDR1-loaded liposomes indicated lower dissipation value compared to the protein-free conditions (Figure 3.19). Highly viscoelastic layers have a tendency to increase the damping frequency whereas rigid layers cause to a decrease in frequency (Keller & Kasemo, 1998; Reimhult et al., 2003; Reimhult et al., 2006). Thus, the presence of MDR1 protein reduced the viscoelasticity of the constructed layer, and eventuated in a more rigid structure. Most probably, the presence of proteins in lipid layers also caused to hinder the movement of phospholipids, and so, such large macromolecule led to form a solid structure instead of an elastic structure.

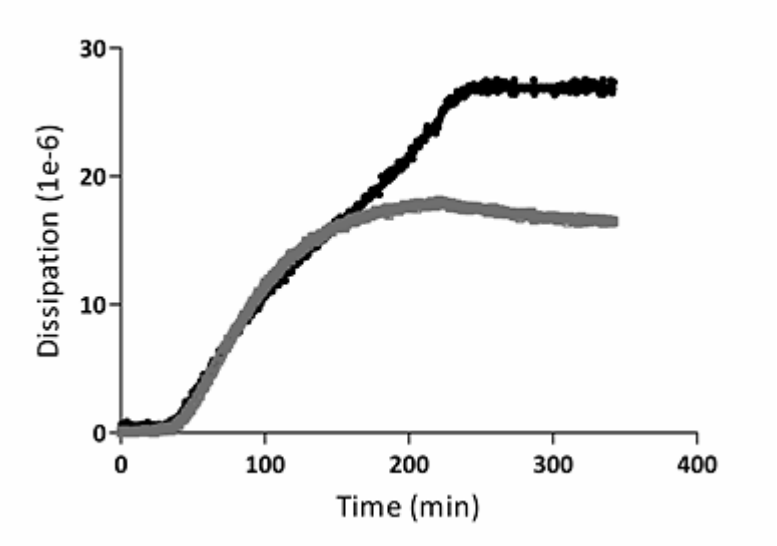

Figure 3.19 : The comparison on dissipation characteristics of MDR1-free (black) and MDR1-incorporated liposomes (gray).

In literature, protein-loaded liposomes were spread on SiO_2 surfaces, and in this case, both frequency and dissipation levels increased compared to protein-free conditions (Graneli et al., 2003). These results implied that the increase in the protein amount caused to increase the number of intact liposomes on the surface, and thus, these two behavioral characteristic values increased (Graneli et al., 2003). On the other hand, when hydrophilic regions of the transmembrane protein were enzymatically cleaved to evaluate the liposome behavior, it was observed that the removal of the outward regions stimulated lipid bilayer formation. This study showed that large membrane protein-loaded liposomes could not be directly spread on the support surface (Graneli et al., 2003). In this thesis, the tethered lipid bilayer system allowed to integrate MDR1 protein, which has a large hydrophilic domain, into the lipid membrane. Long PEG chains were probably assisted to not only elevate the lipid layer from the

surface, and also, allow the liposomes to deform and resulted in lipid bilayer formation. In the presented platform, the presence of proteins only hindered the mobility of phospholipids membrane as in their native environment. This could also be advantage since the restriction of phospholipid movement could increase the stability of the formed bilayer.

Further, the mass load caused by MDR1-loaded liposomes was analyzed using Sauerbrey's equation, and a value of 2.55 $\mu g/cm^2$ was calculated. The protein-loaded liposomes led to an increase of 0.45 $\mu g/cm^2$ compared to the protein-free liposome conditions. The active QCM area was 20 mm^2, and thus, the total mass load was calculated as 88 ng or 15600 molecules/μm^2 (Molecular weight of MDR1 is 170 kDa).

3.3.3 Visualization of MDR1-incorporated lipid layers by liquid-atomic force microscopy

Liquid-AFM system was performed under PBS condition (0.1 M, pH 7.4) to confirm MDR1 integration into the lipid layers. For doing this, MDR1-incorporated lipid layers were constructed on gold-coated SPR surface. AFM analysis was evaluated with at least ten independent experiments.

Application of MDR1-loaded liposomes onto the tethered layer increased roughness average value from 0.452 nm to 1.562 nm (Figure 3.20a). These results indicated the integration of MDR1 protein into the lipid bilayer system. Theoretically, the dimensions of MDR1 protein in lipid bilayers were reported as ca. 2 nm at exoplasmic section of the membrane and ca. 8.6 nm at cytoplasmic section (Karasu, 2011), and these values also supported the roughness changes, which was observed in AFM analysis. Typically, several structures with ca. 1.2 – 2.8 nm were found on the lipid layer. When a small area was selected to analyze in detail, ca. 1.2 nm of jut-up regions were observed (Figure 3.20b). Further, theoretical dimensions implied that the protein was mostly integrated with its native orientation, and MDR1-incorporated lipid bilayer system was further evaluated with antibody binding in the following section.

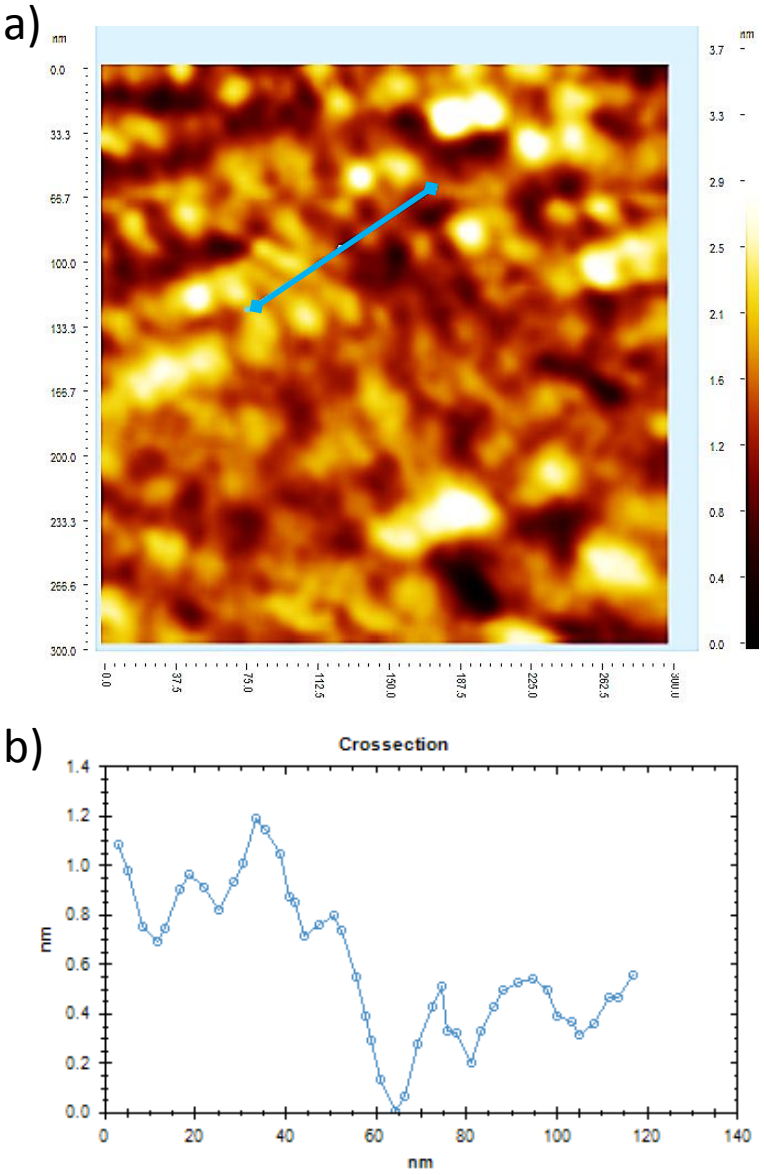

Figure 3.20 : Visualization of MDR1-incorporated lipid bilayers. a) MDR1-incorporated lipid bilayer formation on gold-coated SPR surface. b) Cross-section analysis of the selected region indicated on SPR surface image.

3.3.4 Evaluation of orientation and membrane protein insertion by antibody binding

Specific anti-MDR1 human monoclonal antibody analysis was carried out to confirm the orientation and the integration of MDR1 in lipid bilayers. The binding events were monitored in real-time by SPR system. All SPR measurements were evaluated with at least three independent experiments.

As a result of antibody experiments, specific anti-MDR1 monoclonal antibody caused an increase of 841 ± 20 μRIU in the optical thickness (Figure 3.21). To evaluate the specificity of antibody to MDR1 protein, two different controls were also carried out. As first control, anti-MDR1 monoclonal antibody was evaluated on MDR1-free lipid layers, and there was no experimentally binding observed, and the signal level remained at the noise level (Figure 3.21). As second control, anti-Pin-1 (G8) mouse monoclonal antibody, which is known no interaction with MDR1, was evaluated. Similar to the first control, there was no relative change in the optical thickness observed. Overall, antibody analysis indicated that MDR1 was successfully and efficiently inserted into the lipid bilayer without damaging the native structure of the protein.

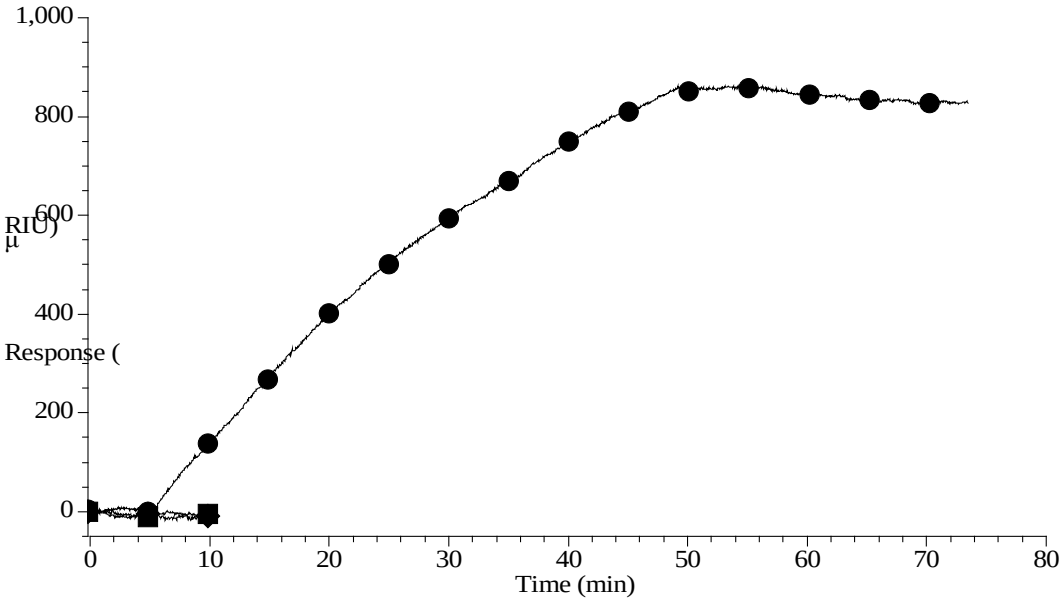

Figure 3.21 : Antibody binding experiments. (●) anti-MDR1 human monoclonal antibody binding on MDR1-incorporated lipid bilayers; (■) anti-MDR1 antibody binding on MDR1-free lipid bilayers; (▲) anti-Pin-1 (G8) mouse monoclonal antibody binding on MDR1-incorporated lipid bilayers.

3.3.5 Evaluation of statin-MDR1 interaction

To evaluate drug-membrane protein interactions in real-time, statin molecules were carried out onto MDR1-incorporated lipid bilayer system, and the binding events were monitored in real-time using SPR system. All SPR measurements were evaluated with at least three independent experiments.

Several statin molecules (*i.e.*, pravastatin, lovastatin and simvastatin) with different characteristics in their water solubilities were evaluated in this experiment. For instance, pravastatin has more hydrophilic and polar structure, and can be dissolved up to 10 mg/mL in water. Due to the water solubility aspect, pravastatin differs than the other statin molecules such as cerivastatin, fluvastatin, atorvastatin, lovastatin and simvastatin, and the hydrophilicity level of the listed statin molecules decreases, respectively (Serajuddin et al., 1991). As opposed to pravastatin, lovastatin (0.4 μg/mL soluble in water) and simvastatin (0.76 μg/mL soluble in water) are two of the most lipophilic statin molecules, and their solubility is 200 times lower than that of pravastatin. For instance, lovastatin is successfully dissolved in ethanol up to the 10 mg/mL concentration, whereas simvastatin is dissolved in ethanol and DMSO as 20 mg/mL. Additionally, simvastatin can be dissolved as 0.5 mg/mL in DMSO-PBS mixture (1:1) if the statin molecule is first treated with DMSO (Url-14).

In drug-membrane protein interaction experiments, it was noticed that simvastatin and lovastatin experiments interfered to the stability of the tethered lipid bilayer system since these statin molecules could be only dissolved in organic solvents such as ethanol. Thus, the experiments could not be efficiently performed using these statin molecules. Further, DMSO-PBS (1:1) solution was tested as a solvent to prepare simvastatin samples (0.5 mg/mL). Since SPR has high sensitivity at the close vicinity of the sensor surface, the solution interfered to the refractive index parameter, and high variations in refractive index hindered the reliability of the results. Thus, simvastatin solution in DMSO-PBS (1:1) could not be used to evaluate statin-MDR1 interactions.

In this experiment, only water-soluble statin molecules, pravastatin, could be used to test its interactions with the presented tethered lipid bilayer system. Two different concentrations (0.01 and 0.05 mg/mL) of pravastatin was analyzed to evaluate the concentration effect on statin binding (Figure 3.22). Since low concentrations resulted in low signal or at noise ratio level, the data was calculated using the collection of three independent experiment results. At low concentration of pravastatin (0.01 mg/mL), the binding events were recorded for 10 minutes, and the refractive index resulted in ~20 μRIU (Figure 3.22). At lower concentrations than 0.01 mg/mL, the signal level remained at the noise signal level. Higher

concentrations (*e.g.*, 0.05 mg/mL) of pravastatin was analyzed for 2 minutes till the stabilization of the signal, and it resulted as ~60 μRIU change in optical thickness (Figure 3.22). Overall, the interactions between pravastatin and MDR1 protein were evaluated, and the concentration effect on the statin binding (0.01 and 0.05 mg/mL) was demonstrated. Five times increase in pravastatin concentration resulted in approximately 3 times change in the optical thickness. It was noticed that excessive amount of statin molecules could saturated the corresponding binding sites on MDR1 protein. Additionally, contrast to pravastatin molecule, more lipophilic and non-polar statin molecules (*i.e.*, simvastatin and lovastatin), could not be efficiently carried out on the presented lipid bilayer platform due to the organic solvent content in their solutions. In sum, the results showed that the interaction studies could only be performed by water-soluble drugs on the constructed model membrane system.

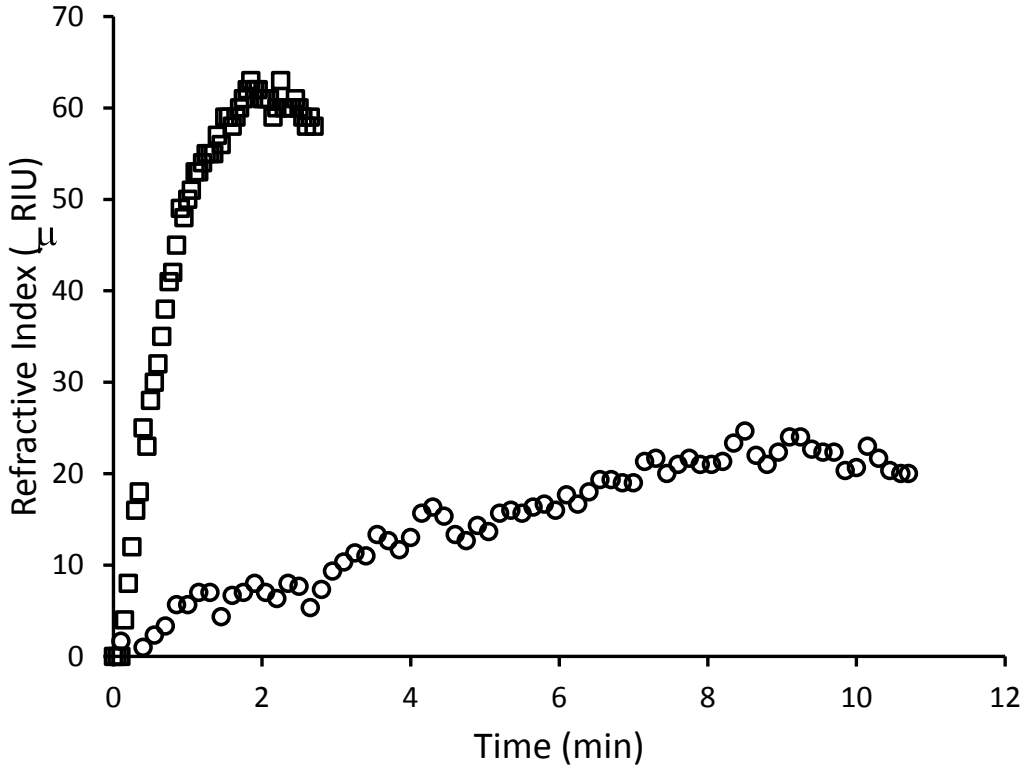

Figure 3.22 : Real-time SPR analysis for (□) 0.05 mg/mL and (○) 0.01 mg/mL of pravastatin interaction on MDR1-incorporated lipid bilayers.

4. CONCLUSION

Biological membranes, only a few nanometers thick, present a complex structure, which consists of lipids, proteins and carbohydrates. Membrane proteins play key roles in several cell progresses such as the control of molecule transportation, biological energy conversion, cellular division, signal trafficking, communication, adhesion, and recognition. Thus, any deficiencies in the structure and function of membrane proteins cause several diseases from diabetes to cancer (Hien et al., 2010; Koehn et al., 2008). Therefore, these proteins have a great portion in drug design researches, and they are used as the target of many drugs. On the other hand, it is necessary to develop cell membrane mimicking systems to investigate membrane proteins. Model membrane systems present an invaluable opportunity to mimic biological membranes *in vitro*, and also allow the functional reconstruction of membrane proteins with large domains in cytoplasm (*i.e.*, integral proteins). Tethered lipid bilayer membrane system is one of the most attractive model membrane platforms, and it generates an extra subspace for the cytoplasmic section of the large integral proteins. The aim of the thesis is to construct a model membrane system (*i.e.*, tethered lipid bilayer platform) for membrane protein research, and present an alternative method to study drug-membrane protein interactions *in vitro*.

For this purpose, a tethered lipid bilayer platform was constructed to investigate membrane proteins (*e.g.*, MDR1), which have large domains in cytoplasmic space, on model membrane systems. For doing this, a modified lipid (*i.e.*, DSPE-PEG) was used as a spacer molecule to elevate lipid membrane from the gold support surface. The binding/spreading and lipid bilayer formation of protein-free and protein-loaded liposomes were evaluated using SPR and QCM-D characterization methods, and the platform was visualized using liquid-AFM system in order to investigate the lipid layer characteristics *in vitro* conditions. Additionally, drug-protein interactions were evaluated on the presented tethered lipid bilayer platform. To the best of our knowledge, there was no previous study to investigate the interactions between statin-based drugs and MDR1 on model membrane systems.

To construct spacer layer, DSPE-PEG concentrations ranging from 0.01 to 0.06 mg/mL were evaluated, and according to the characterization experiments (*i.e.,* SPR and QCM-D), the binding of DSPE-PEG molecule increased with the increased concentrations. Low concentrations of PEG molecules present intramolecular structures (mushroom-like regime) whereas high concentrations allow to interact with each PEG residues, and result in intermolecular structure (brush-like regime) (Lin et al., 2010). Characterization methods demonstrated a drastic change between 0.01 and 0.02 mg/mL concentrations, which resulted in a conformational transition from the mushroom to brush-like regimes. Brush-like structure is necessary to deform liposomes and fuse them to each other for lipid bilayer formation, and the extension of the spacer allows to elevate the lipid layer from the support surface in order to generate a reservoir space for transmembrane proteins. To evaluate the lipid layer formation, a fixed volume and concentration of liposomes were tested, and high (0.05 and 0.06 mg/mL) and low (0.02 and 0.03 mg/mL) concentrations of DSPE-PEG molecule did not provide a significant lipid layer formation, and resulted in a drastic decrease/increase in the optical thickness and frequency parameters after washing. SPR and QCM-D experiments demonstrated that 0.03 mg/mL of DSPE-PEG concentration was critical to form lipid bilayer structure and provide optimum conditions. To visualize the conformation of spacer molecule in the optimum concentration, liquid-AFM system was performed, and the spacer molecules typically provided condensed structures and a directional behavior, which was generated by DTSP molecule. To perform further analysis on spacer molecule characteristics, DSPE-PEG coated surface was first dried, and then, re-hydrated. Changes in the condition affected the structural behavior of spacer molecule, and resulted in the collapse of molecules on the surface and a rough structure formation in air condition. Re-hydration allowed the regeneration of the layer and uniform coating on the surface as observed previously. Thus, the constructed spacer layer holds a potential to be stored in the dried form, and this layer can be used after re-hydration for further experiments. Additionally, the height of the spacer molecule in various conditions was calculated, and observed as ~50 nm and ~12 nm in air and aqueous conditions, respectively. As a result, spacer molecules generated more condensed and complex structure in aqueous condition. Therefore, the structural behavior of spacer molecule was evaluated, and the viscoelastic property of PEG chains in spacer molecule caused to decrease the roughness of the unmodified gold-

coated surfaces. Thus, DSPE-PEG layer presented more flat surface to construct a lipid layer in the following steps. Additionally, the directional behavior of DSPE-PEG molecules probably assisted to not only elevate the lipid layer from the surface, and also, enabled the liposomes to deform and form lipid bilayer on the surface.

To evaluate liposome binding/spreading and lipid bilayer formation, the effect of DSPE-PEG concentration was analyzed, and it was observed that spacer concentration highly affected the construction of the lipid layer platform and high surface coverage was found to be as ineffective as low coverage. In addition, QCM-D analysis allowed to evaluate the lipid bilayer formation in more detail, and indicated liposome deformation and the generation of flattened structure, which resulted in the construction of a lipid bilayer-like structure at optimum DSPE-PEG concentration. The other concentrations resulted in either non-deformation or partially deformation of liposomes, and thus, intact lipid vesicles were remained instead of lipid bilayer formation. Liquid-AFM system was also performed to visualize and analyze the lipid bilayer structure, and the overall roughness parameters presented that the lipid layer generated more flat surface than the previous surface formed by spacer molecule. AFM analysis supported the results obtained by QCM-D experiments, and indicated liposome deformation and lipid bilayer formation. For the construction of protein-incorporated lipid bilayer, MDR1 was used as a model protein, and the effect of MDR1 protein amount was evaluated with a variety of concentration ranging from 0.7 to 5.0 μL. Dissipation analysis indicated that the protein amount conspicuously affected the lipid bilayer construction, and then, 1 μL of MDR1 amount provided optimum conditions for lipid layer formation. Another observation from QCM-D analysis was that membrane protein integration into the lipid bilayers reduced lipid bilayer fluidity possibly by restricting the mobility of phospholipids. This could be considered as an advantage since it would provide a more stable platform. Liquid-AFM analysis was also carried out to visualize MDR1-incorporated lipid bilayer system *in vitro*, and it was observed that overall roughness parameters (*i.e.*, roughness average) increased from 0.452 nm to 1.562 nm. Further, several jut-outs with ca. 1.2 - 2.8 nm in height were observed on the constructed layer. Theoretically, the dimensions for the exoplasmic and cytoplasmic regions of MDR1 protein in lipid bilayers were reported as ca. 2 nm and ca. 8.6 nm, respectively (Karasu, 2011). The dimension analysis demonstrated that

experimental and theoretical results for the exoplasmic section of the membrane protein were comparable, and thus it resulted in the integration of MDR1 into lipid bilayer platform. Additionally, antibody binding studies supported that MDR1 was successfully and efficiently inserted into the lipid bilayers without damaging its native structure.

In order to evaluate the applicability of constructed system in drug-membrane protein interaction studies, statin-based drugs were used. For doing this, three different statin molecules were selected but only water-soluble and polar one (*e.g.,* pravastatin) could be used to evaluate statin-MDR1 interactions. Lipophilic and non-polar statin molecules need organic solvent to be dissolved, and that interfere with the lipid bilayers' integrity therefore, only water-soluble drugs could be investigated on the constructed model membrane system. When two different pravastatin concentrations (0.01 and 0.05 mg/mL) were tested, it was observed that optical thickness parameter increased with the increased concentration. Although statin-based drugs are not exactly specific targets of MDR1 proteins, and such nonspecific ligand-membrane protein interactions can be monitored in real-time using the tethered lipid bilayer platform without any damage on membrane protein structure and function. The platform also provides such an important advantage to discover nonspecific ligand-membrane protein interactions, and open a novel and significant perspective to *in vivo* experiments, which require labor-intensive sample preparations, expensive infrastructures and skilled personnel.

In conclusion, a tethered lipid bilayer platform was successfully constructed using a spacer molecule, which generated an adequate reservoir section to accommodate large extra- or intracellular domains of MDR1 protein. Further, the constructed platform allowed to directly investigate drug-membrane interactions *in vitro*. The constructed tethered lipid bilayer platform presented an alternative method to discover membrane protein characteristics and drug-membrane protein interactions without any damaging the native structure of the protein, and thus, propose an alternative to address the challenges in membrane protein research for transmembrane proteins. Additionally, the constructed platform holds a great potential to be integrated with microfluidics, lab-on-a-chip systems and biosensor platforms, and presents a versatile platform to study with various membrane proteins and drugs *in vitro*.

REFERENCES

Adhikary, Gautam, Chandra, Sucheta, Sikdar, Rita, & Sen, Parimal C. (1995). The phase behaviour ofl-α-phosphatidylcholine in the presence of chlorpromazine under different experimental conditions. *Colloids and Surfaces B: Biointerfaces, 4*(6), 335-339. doi: 10.1016/0927-7765(95)01191-k

Alberts, B., Bray, D., Lewis, J., Raff, M., Roberts, K., Watson, J.D. (1989). *Molecular-biology of the cell (2nd Ed.).* New York: Garland Science.

Allen, C., Dos Santos, N., Gallagher, R., Chiu, G. N., Shu, Y., Li, W. M., . . . Bally, M. B. (2002). Controlling the physical behavior and biological performance of liposome formulations through use of surface grafted poly(ethylene glycol). *Biosci Rep, 22*(2), 225-250. doi:10.1023/A:1020186505848

Atanasov, V., Knorr, N., Duran, R. S., Ingebrandt, S., Offenhausser, A., Knoll, W., & Koper, I. (2005). Membrane on a chip: A functional tethered lipid bilayer membrane on silicon oxide surfaces. *Biophysical Journal, 89*(3), 1780-1788. doi: 10.1529/biophysj.105.061374

Backmann, N., Kappeler, N., Braun, T., Huber, F., Lang, H. P., Gerber, C., & Lim, R. Y. H. (2010). Sensing surface PEGylation with microcantilevers. *Beilstein Journal of Nanotechnology, 1*, 3-13. doi: 10.3762/bjnano.1.2

Bastiaanse, E. M. L., Hold, K. M., & VanderLaarse, A. (1997). The effect of membrane cholesterol content on ion transport processes in plasma membranes. *Cardiovascular Research, 33*(2), 272-283. doi: 10.1016/s0008-6363(96)00193-9

Bates, G. J., Fox, S. B., Han, C., Leek, R. D., Garcia, J. F., Harris, A. L., & Banham, A. H. (2006). Quantification of regulatory T cells enables the identification of high-risk breast cancer patients and those at risk of late relapse. *J Clin Oncol, 24*(34), 5373-5380. doi: 10.1200/JCO.2006.05.9584

Baumann, N., & Pham-Dinh, D. (2001). Biology of oligodendrocyte and myelin in the mammalian central nervous system. *Physiological Reviews, 81*(2), 871-927.

Bendas, G. (2010). Biosensor-based evaluation of liposomal binding behavior. *Methods Mol Biol, 606*, 519-529. doi: 10.1007/978-1-60761-447-0_35

Bendas, G. (2010). *Liposomes: Methods and Protocols, Vol 2: Biological Membrane Models*. Heidelberg: Springer.

Benz, R., & Janko, K. (1976). Voltage-Induced Capacitance Relaxation Of Lipid Bilayer Membranes - Effects of Membrane Composition. *Biochimica Et Biophysica Acta, 455*(3), 721-738. doi: 10.1016/0005-2736(76)90043-2

Berg, J. M, Tymoczko, J. L, & Stryer, L. (2002). *Biochemistry (5th Ed.). New York: W H Freeman*.

Binnig, G., Quate, C. F., & Gerber, C. H. (1986). Atomic Force Microscope. *Physical Review Letters, 56*(9), 930-933. doi: 10.1103/PhysRevLett.56.930

Borst, P., Evers, R., Kool, M., & Wijnholds, J. (2000). A Family of Drug Transporters: the Multidrug Resistance-Associated Proteins. *Journal of the National Cancer Institute, 92*(16), 1295-1302. doi: 10.1093/jnci/92.16.1295

Byun, K. M., Kim, S. J., & Kim, D. (2007). Grating-coupled transmission-type surface plasmon resonance sensors based on dielectric and metallic gratings. *Appl. Opt., 46*(23), 5703-5708. doi: 10.1364/AO.46.005703

Cafiso, D. S. (2005). *Protein-Lipid Interactions: From Membrane Domains to Cellular Networks*. Danvers, MA, USA: John Wiley & Sons, Inc.

Cappella, B., & Dietler, G. (1999). Force-distance curves by atomic force microscopy. *Surface Science Reports, 34*(1–3), 1-104. doi: 10.1016/s0167-5729(99)00003-5

Castellana, E. T., & Cremer, P. S. (2006). Solid supported lipid bilayers: From biophysical studies to sensor design. *Surface Science Reports, 61*(10), 429-444. doi: 10.1016/j.surfrep.2006.06.001

Chang, D. K., Lin, C. T., Wu, C. H., & Wu, H. C.. (2009). A Novel Peptide Enhances Therapeutic Efficacy of Liposomal Anti-Cancer Drugs in Mice Models of Human Lung Cancer. *PLoS ONE, 4*(1). doi: 10.1371/journal.pone.0004171

Chang, K. T., Tsai, M. J., Cheng, Y. T., Chen, J. J., Hsia, R. H., Lo, Y. S., . . . Weng, C. F. (2009). Comparative atomic force and scanning electron microscopy: An investigation of structural differentiation of hepatic stellate cells. *Journal of Structural Biology, 167*(3), 200-208. doi: 10.1016/j.jsb.2009.06.005

Cho, N. J., Frank, C. W., Kasemo, B., & Hook, F. (2010). Quartz crystal microbalance with dissipation monitoring of supported lipid bilayers on various substrates. *Nat Protoc, 5*(6), 1096-1106. doi: 10.1038/nprot.2010.65

Christians, U., Jacobsen, W., & Floren, L. C. (1998). Metabolism and drug interactions of 3-hydroxy-3-methylglutaryl coenzyme A reductase inhibitors in transplant patients: Are the statins mechanistically similar? *Pharmacology & Therapeutics, 80*(1), 1-34. doi: 10.1016/s0163-7258(98)00016-3

Cooper, R. A. (1978). Influence of increased membrane cholesterol on membrane fluidity and cell-function in human red blood-cells. *Journal of Supramolecular Structure, 8*(4), 413-430. doi: 10.1002/jss.400080404

Coster, H. G. L., & Laver, D. R. (1986). The effect of temperature on lipid normal-alkane interactions in lipid bilayers. *Biochimica Et Biophysica Acta, 857*(1), 95-104. doi: 10.1016/0005-2736(86)90102-1

Curie, J., & Curie, P. (1880). Développement, par pression, de l'électricité polaire dans les cristaux hémièdres à faces inclinées. *Comptes Rendus de l'Académie des Sciences, 91*, 294-295.

Curiel, T. J., Coukos, G., Zou, L. H., Alvarez, X., Cheng, P., Mottram, P., . . . Zou, W. P. (2004). Specific recruitment of regulatory T cells in ovarian carcinoma fosters immune privilege and predicts reduced survival. *Nature Medicine, 10*(9), 942-949. doi: 10.1038/nm1093

Deng, Z., Lulevich, V., Liu, F., & Liu, G.. (2010). Applications of Atomic Force Microscopy in Biophysical Chemistry of Cells. *The Journal of Physical Chemistry B, 114*(18), 5971-5982. doi: 10.1021/jp9114546

Diao, P., Guo, M., & Tong, R. T. (2001). Characterization of defects in the formation process of self-assembled thiol monolayers by electrochemical impedance spectroscopy. *Journal of Electroanalytical Chemistry, 495*(2), 98-105. doi: 10.1016/s0022-0728(00)00424-1

Dietschy, J. M., & Wilson, J. D. (1970). Regulation of cholesterol metabolism. *N Engl J Med, 282*(21), 1179-1183. doi: 10.1056/NEJM197005212822105

Dixon, M. C. (2008). Quartz crystal microbalance with dissipation monitoring: enabling real-time characterization of biological materials and their interactions. *J Biomol Tech, 19*(3), 151-158.

Dostálek, J., Čtyroký, J., Homola, J., Brynda, E., Skalský, M., Nekvindová, P., . . . Schröfel, J. (2001). Surface plasmon resonance biosensor based on integrated optical waveguide. *Sensors and Actuators B: Chemical, 76*(1–3), 8-12. doi: 10.1016/s0925-4005(01)00559-7

Fenter, P., Eberhardt, A., & Eisenberger, P. (1994). Self-assembly of n-alkyl thiols as disulfides on Au(111). *Science, 266*(5188), 1216-1218. doi: 10.1126/science.266.5188.1216

F**ettiplace, R., Andrews, D. M., & Haydon, D. A.** (1971). The thickness, composition and structure of some lipid bilayers and natural membranes. *Journal of Membrane Biology, 5*(3), 277-296. doi: 10.1007/bf01870555

Ford, I., Murray, H., Packard, C. J., Shepherd, J., Macfarlane, P. W., & Cobbe, S. M. (2007). Long-Term Follow-up of the West of Scotland Coronary Prevention Study. *New England Journal of Medicine, 357*(15), 1477-1486. doi: doi:10.1056/NEJMoa065994

Fujiki, Y., Hubbard, A. L., Fowler, S., & Lazarow, P. B. (1982). Isolation of intracellular membranes by means of sodium-carbonate treatment - application to endoplasmic-reticulum. *Journal of Cell Biology, 93*(1), 97-102. doi: 10.1083/jcb.93.1.97

Gabizon, A., & Papahadjopoulos, D. (1988). Liposome formulations with prolonged circulation time in blood and enhanced uptake by tumors. *Proc Natl Acad Sci U S A, 85*(18), 6949-6953. doi: 10.1073/pnas.85.18.6949

Giess, F., Friedrich, M. G., Heberle, J., Naumann, R. L., & Knoll, W. (2004). The protein-tethered lipid bilayer: A novel mimic of the biological membrane. *Biophysical Journal, 87*(5), 3213-3220. doi: 10.1529/biophysj.104.046169

Golomb, Beatrice A., & Evans, Marcella A. (2008). Statin Adverse Effects A Review of the Literature and Evidence for a Mitochondrial Mechanism. *American Journal of Cardiovascular Drugs, 8*(6), 373-418. doi: 10.2165/0129784-200808060-00004

Gomez-Hens, A., & Fernandez-Romero, J. M. (2006). Analytical methods for the control of liposomal delivery systems. *Trac-Trends in Analytical Chemistry, 25*(2), 167-178. doi: 10.1016/j.trac.2005.07.006

Gordon, D., MartinEauclaire, M. F., Cestele, S., Kopeyan, C., Carlier, E., BenKhalifa, R., . . . Rochat, H. (1996). Scorpion toxins affecting sodium current inactivation bind to distinct homologous receptor sites on rat brain and insect sodium channels. *Journal of Biological Chemistry, 271*(14), 8034-8045. doi: 10.1074/jbc.271.14.8034

Gottesman, M. M., & Pastan, I. (1993). Biochemistry of multidrug-resistance mediated by the multidrug transporter. *Annual Review of Biochemistry, 62*, 385-427. doi: 10.1146/annurev.biochem.62.1.385

Graneli, A., Rydstrom, J., Kasemo, B., & Hook, F. (2003). Formation of supported lipid bilayer membranes on SiO2 from proteoliposomes containing transmembrane proteins. *Langmuir, 19*(3), 842-850. doi: 10.1021/la026231w

Groves, J. T., Ulman, N., & Boxer, S. G. (1997). Micropatterning fluid lipid bilayers on solid supports. *Science, 275*(5300), 651-653. doi: 10.1126/science.275.5300.651

Hale, A. H., Ruebush, M. J., Lyles, D. S., & Harris, D. T. (1980). Antigen-liposome modification of target-cells as a method to alter their susceptibility to lysis by cyto-toxic lymphocytes-T. *Proceedings of the National Academy of Sciences of the United States of America-Biological Sciences, 77*(10), 6105-6108. doi: 10.1073/pnas.77.10.6105

Hansen, P. L., Cohen, J. A., Podgornik, R., & Parsegian, V. A. (2003). Osmotic properties of poly(ethylene glycols): quantitative features of brush and bulk scaling laws. *Biophys J, 84*(1), 350-355. doi: 10.1016/S0006-3495(03)74855-3

Henneberry, A. L., Lagace, T. A., Ridgway, N. D., & McMaster, C. R. (2001). Phosphatidylcholine synthesis influences the diacylglycerol homeostasis required for Sec14p-dependent Golgi function and cell growth. *Molecular Biology of the Cell, 12*(3), 511-520.

Hien, T. T., Kim, H. G., Han, E. H., Kang, K. W., & Jeong, H. G. (2010). Molecular mechanism of suppression of MDR1 by puerarin from Pueraria lobata via NF-kappaB pathway and cAMP-responsive element transcriptional activity-dependent up-regulation of AMP-activated protein kinase in breast cancer MCF-7/adr cells. *Mol Nutr Food Res, 54*(7), 918-928. doi: 10.1002/mnfr.200900146

Hinterdorfer, P., & Dufrene, Y. F. (2006). Detection and localization of single molecular recognition events using atomic force microscopy. *Nature Methods, 3*(5), 347-355. doi: 10.1038/nmeth871

Hoa, X. D., Kirk, A. G., & Tabrizian, M. (2007). Towards integrated and sensitive surface plasmon resonance biosensors: A review of recent progress. *Biosensors and Bioelectronics, 23*(2), 151-160. doi: 10.1016/j.bios.2007.07.001

Hobara, D., Uno, Y., & Kakiuchi, T. (2001). Immobilization of horseradish peroxidase on nanometre-scale domains of binary self-assembled monolayers formed from dithiobis-N-succinimidyl propionate and 1-tetradecanethiol on Au(111). *Physical Chemistry Chemical Physics, 3*(16), 3437-3441. doi: 10.1039/b101807h

Homola, J., Koudela, I., & Yee, S. S. (1999). Surface plasmon resonance sensors based on diffraction gratings and prism couplers: sensitivity comparison. *Sensors and Actuators B: Chemical, 54*(1–2), 16-24. doi: 10.1016/s0925-4005(98)00322-0

Hopfner, M., Rothe, U., & Bendas, G. (2008). Biosensor-based evaluation of liposomal behavior in the target binding process. *J Liposome Res, 18*(1), 71-82. doi: 10.1080/08982100801894000

Hrdina, P. D. (1996). Basic neurochemistry: Molecular, cellular and medical aspects - Siegel,GJ. *Journal of Psychiatry & Neuroscience, 21*(5), 352-353.

Hsu, I., Spinler, S. A., & Johnson, N. E. (1995). Comparative-evaluation of the safety and efficacy of HMG-CoA reductase inhibitor monotherapy in the treatment of primary hypercholesterolemia. *Annals of Pharmacotherapy, 29*(7-8), 743-759.

Huffer, S., Clark, M. E., Ning, J. C., Blanch, H. W., & Clark, D. S. (2011). Role of alcohols in growth, lipid composition, and membrane fluidity of yeasts, bacteria, and archaea. *Applied and Environmental Microbiology, 77*(18), 6400-6408. doi: 10.1128/aem.00694-11

Iacovache, I., van der Goot, F. G., & Pernot, L.. (2008). Pore formation: An ancient yet complex form of attack. *Biochimica Et Biophysica Acta-Biomembranes, 1778*(7-8), 1611-1623. doi: 10.1016/j.bbamem.2008.01.026

Ide, T., Aoki, T., Takeuchi, Y., & Yanagida, T. (2006). Lysenin forms a voltage-dependent channel in artificial lipid bilayer membranes. *Biochemical and Biophysical Research Communications, 346*(1), 288-292. doi: 10.1016/j.bbrc.2006.05.115

Janshoff, A., & Kunneke, S. (2000). Micropatterned solid-supported membranes formed by micromolding in capillaries. *European Biophysics Journal with Biophysics Letters, 29*(7), 549-554. doi: 10.1007/s002490000104

Janshoff, A., Galla, H. J., & Steinem, C. (2000). Piezoelectric Mass-Sensing Devices as Biosensors—An Alternative to Optical Biosensors? *Angewandte Chemie International Edition, 39*(22), 4004-4032. doi: 10.1002/1521-3773(20001117)39:22<4004::aid-anie4004>3.0.co;2-2

Jebrail, M., Schmidt, R., DeWolf, C. E., & Tsoukanova, V. (2008). Effect of aliphatic chain length on stability of poly(ethylene glycol)-grafted phospholipid monolayers at the air/water interface. *Colloids and Surfaces A: Physicochemical and Engineering Aspects, 321*(1–3), 168-174. doi: 10.1016/j.colsurfa.2008.02.049

Jesorka, A., & Orwar, O. (2008). Liposomes: Technologies and Analytical Applications *Annual Review of Analytical Chemistry* (Vol. 1, pp. 801-832). doi: 10.1146/annurev.anchem.1.031207.112747

Jokerst, J. V., Lobovkina, T., Zare, R. N., & Gambhir, S. S. (2011). Nanoparticle PEGylation for imaging and therapy. *Nanomedicine (Lond), 6*(4), 715-728. doi: 10.2217/nnm.11.19

Karasu, D. (2011). *Bir membran proteini olan P-glikoproteinin statin bazlı kolesterol düşürücü ilaçlarla etkileşiminin moleküler modelleme yoluyla incelenmesi* (Master Thesis), Istanbul Technical University, Turkey.

Karp, G. (2009). *Cell and Molecular Biology: Concepts and Experiments*. Danvers, MA, USA: John Wiley & Sons, Inc.

Keller, C. A., & Kasemo, B. (1998). Surface specific kinetics of lipid vesicle adsorption measured with a quartz crystal microbalance. *Biophys J, 75*(3), 1397-1402. doi: 10.1016/S0006-3495(98)74057-3

Kenworthy, A. K., Hristova, K., Needham, D., & McIntosh, T. J. (1995). Range and magnitude of the steric pressure between bilayers containing phospholipids with covalently attached poly(ethylene glycol). *Biophys J, 68*(5), 1921-1936. doi: 10.1016/S0006-3495(95)80369-3

Khan, T. R., Grandin, H. M., Mashaghi, A., Textor, M., Reimhult, E., & Reviakine, I. (2008). Lipid redistribution in phosphatidylserine-containing vesicles adsorbing on titania. *Biointerphases, 3*(2), FA90. doi: 10.1116/1.2912098

Kobayashi, N., Hiraoka, N., Yamagami, W., Ojima, H., Kanai, Y., Kosuge, T., . . . Hirohashi, S. (2007). FOXP3(+) regulatory T cells affect the development and progression of hepatocarcinogenesis. *Clinical Cancer Research, 13*(3), 902-911. doi: 10.1158/1078-0432.ccr-06-2363

Koehn, J., Fountoulakis, M., & Krapfenbauer, K. (2008). Multiple drug resistance associated with function of ABC-transporters in diabetes mellitus: molecular mechanism and clinical relevance. *Infect Disord Drug Targets, 8*(2), 109-118. doi: 10.2174/187152608784746510

Kopec, K. K., Bozyczko-Coyne, D., & Williams, M. (2005). Target identification and validation in drug discovery: the role of proteomics. *Biochemical Pharmacology, 69*(8), 1133-1139. doi: 10.1016/j.bcp.2005.01.004

Kretschmann, E., & Raether, H. (1968). Radiative decay of non radiative surface plasmons excited by light. *Zeitschrift Fur Naturforschung Part a-Astrophysik Physik Und Physikalische Chemie, A 23*(12), 2135

Lang, H., Duschl, C., & Vogel, H. (1994). A New class of thiolipids for the attachment of lipid bilayers on gold surfaces. *Langmuir, 10*(1), 197-210. doi: 10.1021/la00013a029

Lin, J., Szymanski, J., Searson, P. C., & Hristova, K. (2010). Effect of a polymer cushion on the electrical properties and stability of surface-supported lipid bilayers. *Langmuir, 26*(5), 3544-3548. doi: 10.1021/la903232b

Lingler, S., Rubinstein, I., Knoll, W., & Offenhausser, A. (1997). Fusion of small unilamellar lipid vesicles to alkanethiol and thiolipid self-assembled monolayers on gold. *Langmuir, 13*(26), 7085-7091. doi: 10.1021/la970600k

Liu, Yang, Jaiswal, Archana, Poggi, Mark A., & Wilson, W. David. (2011). *Chemosensors*. Danvers, MA, USA: John Wiley & Sons, Inc.

Lodish, Harvey, Berk, Arnold, Matsudaira, Paul, Kaiser, Chris A., Krieger, Monty, Scott, Matthew P., . . . Darnell, James. (2004). *Molecular Cell Biology (5th Ed.). New York: W. H. Freema*n.

Lodish, H. (2008). *Molecular Cell Biology (6th Ed.).* New York: W. H. Freeman.

Lofas, Stefan, Choulier, Laurence, Zeder-Lutz, Gabrielle, Baltzinger, Mireille, & Altschuh, Daniele. (2011). *Biophysical Approaches Determining Ligand Binding to Biomolecular Targets: Detection, Measurement and Modelling*.RSC Publishing.

Lucklum, R., & Hauptmann, P. (2000). The quartz crystal microbalance: mass sensitivity, viscoelasticity and acoustic amplification. *Sensors and Actuators B: Chemical, 70*(1–3), 30-36. doi: 10.1016/s0925-4005(00)00550-5

Lundquist, A., Hansen, S. B., Nordstrom, H., Danielson, U. H., & Edwards, K. (2010). Biotinylated lipid bilayer disks as model membranes for biosensor analyses. *Analytical Biochemistry, 405*(2), 153-159. doi: 10.1016/j.ab.2010.06.030

Lv, D., Huang, Y., Tang, Y., & Wang, H. (2012). Relationship between subsurface damage and surface roughness of glass BK7 in rotary ultrasonic machining and conventional grinding processes. *The International Journal of Advanced Manufacturing Technology*, 1-10. doi: 10.1007/s00170-012-4509-1

Maestrelli, F., González-Rodríguez, M. L., Rabasco, A. M., & Mura, P. (2006). Effect of preparation technique on the properties of liposomes encapsulating ketoprofen–cyclodextrin complexes aimed for transdermal delivery. *International Journal of Pharmaceutics, 312*(1–2), 53-60. doi: 10.1016/j.ijpharm.2005.12.047

Marx, K. A. (2003). Quartz crystal microbalance: a useful tool for studying thin polymer films and complex biomolecular systems at the solution-surface interface. *Biomacromolecules, 4*(5), 1099-1120. doi: 10.1021/bm020116i

Mausner-Fainberg, K., Luboshits, G., Mor, A., Maysel-Auslender, S., Rubinstein, A., Keren, G., & George, J.. (2008). The effect of HMG-CoA reductase inhibitors on naturally occurring CD4+CD25+ T cells. *Atherosclerosis, 197*(2), 829-839. doi: 10.1016/j.atherosclerosis.2007.07.031

McConnell, H. M., Watts, T. H., Weis, R. M., & Brian, A. A. (1986). Supported planar membranes in studies of cell-cell recognition in the immune-system. *Biochimica Et Biophysica Acta, 864*(1), 95-106. doi: 10.1016/0304-4157(86)90016-x

McMullen, T. P. W., Lewis, Rnah, & McElhaney, R. N. (2004). Cholesterol-phospholipid interactions, the liquid-ordered phase and lipid rafts in model and biological membranes. *Current Opinion in Colloid & Interface Science, 8*(6), 459-468. doi: 10.1016/j.cocis.2004.01.007

Merzlyakov, M., Li, E., Gitsov, I., & Hristova, K. (2006). Surface-supported bilayers with transmembrane proteins: role of the polymer cushion revisited. *Langmuir, 22*(24), 10145-10151. doi: 10.1021/la061976d

Mouritsen, O. G. (2005). *Life-as a Matter of Fat: The Emerging Science of Lipidomics*. Heidelberg: Springer.

Mozafari, M. R., Johnson, C., Hatziantoniou, S., & Demetzos, C. (2008). Nanoliposomes and Their Applications in Food Nanotechnology. *Journal of Liposome Research, 18*(4), 309-327. doi: 10.1080/08982100802465941

Mueller, P., Rudin, D. O., Tien, H. T., & Wescott, W. C. (1962). Reconstitution of cell membrane structure in vitro and its transformation into an excitable system. *Nature, 194*(4832), 979-&. doi: 10.1038/194979a0

Munro, J. C., & Frank, C. W. (2004). In situ formation and characterization of poly(ethylene glycol)-supported lipid bilayers on gold surfaces. *Langmuir, 20*(24), 10567-10575. doi: 10.1021/la048378o

Nataliya M. S., Liu, X., Brazdova, B., Franz, A. H., Samoshin, V. V., & Guo, X. (2011). Fliposomes: pH-Sensitive Liposomes Containing a trans-2-morpholinocyclohexanol-Based Lipid That Performs a Conformational Flip and Triggers an Instant Cargo Release in Acidic Medium. *Pharmaceutics, 3*(3), 379-405. doi: 10.3390/pharmaceutics3030379

Naumann, C. A., Prucker, O., Lehmann, T., Ruhe, J., Knoll, W., & Frank, C. W. (2002). The polymer-supported phospholipid bilayer: Tethering as a new approach to substrate-membrane stabilization. *Biomacromolecules, 3*(1), 27-35. doi: 10.1021/bm0100211

Naumann, R., Jonczyk, A., Kopp, R., Van Esch, J., Ringsdorf, H., Knoll, W., & Graber, P. (1995). Incorporation of membrane-proteins in solid-supported lipid layers. *Angewandte Chemie-International Edition, 34*(18), 2056-2058. doi: 10.1002/anie.199520561

Nelson, D. L., & Cox, M. M. (2004). *Lehninger Principles of Biochemistry (4th Ed.).* New York: W. H. Freeman.

Osborn, T. D., & Yager, P. (1995). Formation of planar solvent-free phospholipid-bilayers by langmuir-blodgett transfer of monolayers to micromachined apertures in silicon. *Langmuir, 11*(1), 8-12. doi: 10.1021/la00001a003

Otto, A. (1968). Excitation of nonradiative surface plasma waves in silver by method of frustrated total reflection. *Zeitschrift Fur Physik, 216*(4), 398-&. doi: 10.1007/bf01391532

Pollard. T. D. (1990). *Molecular cell biology (2nd Ed.). New York: W. H. Freema*n.

Pucadyil, T. J., & Schmid, S. L. (2010). Supported Bilayers with Excess Membrane Reservoir: A Template for Reconstituting Membrane Budding and Fission. *Biophysical Journal, 99*(2), 517-525. doi: 10.1016/j.bpj.2010.04.036

Purrucker, O., Hillebrandt, H., Adlkofer, K., & Tanaka, M. (2001). Deposition of highly resistive lipid bilayer on silicon-silicon dioxide electrode and incorporation of gramicidin studied by ac impedance spectroscopy. *Electrochimica Acta, 47*(5), 791-798. doi: 10.1016/s0013-4686(01)00759-9

Raghunathan, M., Zubovski, Y., Venable, R. M., Pastor, R. W., Nagle, J. F., & Tristram-Nagle, S. (2012). Structure and Elasticity of Lipid Membranes with Genistein and Daidzein Bioflavinoids Using X-ray Scattering and MD Simulations. *Journal of Physical Chemistry B, 116*(13), 3918-3927. doi: 10.1021/jp211904j

Raguse, B., Braach-Maksvytis, V., Cornell, B. A., King, L. G., Osman, P. D. J., Pace, R. J., & Wieczorek, L. (1998). Tethered lipid bilayer membranes: Formation and ionic reservoir characterization. *Langmuir, 14*(3), 648-659. doi: 10.1021/la9711239

Reimhult, E., Hook, F., & Kasemo, B. (2002). Vesicle adsorption on SiO2 and TiO2: Dependence on vesicle size. *Journal of Chemical Physics, 117*(16), 7401-7404. doi: 10.1063/1.1513230

Reimhult, E., Hook, F., & Kasemo, B. (2003). Intact vesicle adsorption and supported biomembrane formation from vesicles in solution: Influence of surface chemistry, vesicle size, temperature, and osmotic pressure. *Langmuir, 19*(5), 1681-1691. doi: 10.1021/la0263920

Reimhult, E., Zach, M., Hook, F., & Kasemo, B. (2006). A multitechnique study of liposome adsorption on Au and lipid bilayer formation on SiO2. *Langmuir, 22*(7), 3313-3319. doi: 10.1021/la0519554

Richter, R. P., Him, J. L. K., & Brisson, A. (2003). Supported lipid membranes. *Materials Today, 6*(11), 32-37. doi: 10.1016/s1369-7021(03)01129-5

Ries, R. S., Choi, H., Blunck, R., Bezanilla, F., & Heath, J. R. (2004). Black lipid membranes: visualizing the structure, dynamics, and substrate dependence of membranes. *Journal of Physical Chemistry B, 108*(41), 16040-16049. doi: 10.1021/jp048098h

Romer, W., & Steinem, C. (2004). Impedance analysis and single-channel recordings on nano-black lipid membranes based on porous alumina. *Biophysical Journal, 86*(2), 955-965. doi: 10.1016/S0006-3495(04)74171-5

Sackmann, E. (1996). Supported membranes: scientific and practical applications. *Science, 271*(5245), 43-48. doi: 10.1126/science.271.5245.43

Sapsford, K. E. (2010). *Optical Guided-Wave Chemical and Biosensos I* . Heidelberg: Springer.

Sauerbrey, G. (1959). Verwendung von Schwingquarzen zur Wägung dünner Schichten und zur Mikrowägung. *Zeitschrift für Physik A Hadrons and Nuclei, 155*(2), 206-222. doi: 10.1007/bf01337937

Schmidt, C., Mayer, M., & Vogel, H. (2000). A chip-based biosensor for the functional analysis of single ion channels. *Angewandte Chemie-International Edition, 39*(17), 3137-3140. doi: 10.1002/1521-3773(20000901)39:17<3137::aid-anie3137>3.0.co;2-d

Schreiber, F. (2000). Structure and growth of self-assembling monolayers. *Progress in Surface Science, 65*(5-8), 151-256. doi: 10.1016/s0079-6816(00)00024-1

Serajuddin, Abu T. M., Ranadive, Sunanda A., & Mahoney, Eileen M. (1991). Relative lipophilicities, solubilities, and structure-pharmacological considerations of 3-hydroxy-3-methylglutaryl-coenzyme a (HMG-COA) reductase inhibitors pravastatin, lovastatin, mevastatin, and simvastatin. *Journal of Pharmaceutical Sciences, 80*(9), 830-834. doi: 10.1002/jps.2600800905

Sessa, G., & Weissman.G. (1968). Phospholipid spherules (liposomes) as a model for biological membranes. *Journal of Lipid Research, 9*(3), 310

Shahin, V., Ludwig, Y., Schafer, C., Nikova, D., & Oberleithner, H. (2005). Glucocorticoids remodel nuclear envelope structure and permeability. *Journal of Cell Science, 118*(13), 2881-2889. doi: 10.1242/jcs.02429

Shalaev, E. Y., & Steponkus, P. L. (1999). Phase diagram of 1,2-dioleoylphosphatidyl ethanolamine (DOPE): water system at subzero temperatures and at low water contents. *Biochimica Et Biophysica Acta-Biomembranes, 1419*(2), 229-247. doi: 10.1016/s0005-2736(99)00068-1

Singer, S. J., & Nicolson, G. L. (1972). Fluid mosaic model of structure of cell-membranes. *Science, 175*(4023), 720-&. doi: 10.1126/science.175.4023.720

Singh, Bipin K., & Hillier, Andrew C. (2006). Surface Plasmon Resonance Imaging of Biomolecular Interactions on a Grating-Based Sensor Array. *Anal Chem, 78*(6), 2009-2018. doi: 10.1021/ac0519209

Speers, A. E., & Wu, C. C. (2007). Proteomics of integral membrane proteins-theory and application. *Chemical Reviews, 107*(8), 3687-3714. doi: 10.1021/cr068286z

Stalgren, J. J., Claesson, P. M., & Warnheim, T. (2001). Adsorption of liposomes and emulsions studied with a quartz crystal microbalance. *Adv Colloid Interface Sci, 89-90*, 383-394. doi: 10.1016/S0001-8686(00)00052-X

Suzuki, A., Kondoh, J., Matsui, Y., Shiokawa, S., & Suzuki, K. (2005). Development of novel optical waveguide surface plasmon resonance (SPR) sensor with dual light emitting diodes. *Sensors and Actuators B: Chemical, 106*(1), 383-387. doi: 10.1016/j.snb.2004.08.021

Torchilin, V. P. (2006). Multifunctional nanocarriers. *Advanced Drug Delivery Reviews, 58*(14), 1532-1555. doi: 10.1016/j.addr.2006.09.009

Toyama, Shigeru, Doumae, Narumasa, Shoji, Atsumu, & Ikariyama, Yoshihito. (2000). Design and fabrication of a waveguide-coupled prism device for surface plasmon resonance sensor. *Sensors and Actuators B: Chemical, 65*(1–3), 32-34. doi: 10.1016/s0925-4005(99)00427-x

Url-1<*http://www.madsci.org/posts/archives/2006-12/1164999854.Bc.r.html*>, date retrieved 10.03.2013.

Url-2<*http://www.accessexcellence.org/RC/VL/GG/ecb/membrane_proteins.php*>, date retrieved 10.03.2013.

Url-3<*http://upload.wikimedia.org/wikipedia/commons/8/84/Black_lipid_membrane.svg*>, date retrieved 10.03.2013.

Url-4<*http://www.azom.com/article.aspx?ArticleID=3279*>, date retrieved 10.03.2013.

Url-5<*http://avantilipids.com/images/Extruder/TheAvantiMiniExtruder.gif*>, date retrieved 10.03.2013.

Url-6<*http://avantilipids.com/images/PrepOfLiposome/PrepOfLip_4.jpg*>, date retrieved 10.03.2013.

Url-7<*http://www.directindustry.com/prod/reichert-inc/surface-plasmon-resonance-spr-spectrometers-56405-595427.html*>, date retrieved 10.03.2013.

Url-8<*http://www.chemeng.ntnu.no/research/polymer/ugelstadlab/pic/ksvqcm.jpg*>, date retrieved 10.03.2013.

Url-9<*http://robbybing.en.ec21.com/offer_detail/Sell_quartz_crystal_microbalance--1253136.html?gubun=S*>, date retrieved 10.03.2013.

Url-10<*http://www.sigmaaldrich.com/medium/structureimages/45/mfcd00042045.png*>, date retrieved 10.03.2013.

Url-11<*http://avantilipids.com/images/structures/880128s.gif*>, date retrieved 10.03.2013.

Url-12<*http://upload.wikimedia.org/wikipedia/commons/d/d8/Pravastatin.svg*>, date retrieved 10.03.2013.

Url-13<*http://nanomagnetics-inst.com/product.html*>, date retrieved 10.03.2013.

Url-14<*http://www.caymanchem.com/pdfs/10010344.pdf*>, date retrieved 10.03.2013.

Vashist, S. K., & Vashis, P. (2011). Recent Advances in Quartz Crystal Microbalance-Based Sensors. *Journal of Sensors, 2011*. doi: 10.1155/2011/571405

Velasco-Garcia, M. N. (2009). Optical biosensors for probing at the cellular level: A review of recent progress and future prospects. *Seminars in Cell & Developmental Biology, 20*(1), 27-33. doi: 10.1016/j.semcdb.2009.01.013

Vockenroth, I. K., Ohm, Ch., Robertson, J. W. F., McGillivray, D. J., Loesche, M., & Koeper, I. (2008). Stable insulating tethered bilayer lipid membranes. *Biointerphases, 3*(2), FA68-FA73. doi: 10.1116/1.2912097

von Heijne, G. (2006). Membrane-protein topology. *Nat Rev Mol Cell Biol, 7*(12), 909-918. doi: 10.1038/nrm2063

Wagner, A., & Vorauer-Uhl, K. (2011). Liposome technology for industrial purposes. *Journal of drug delivery, 2011*, 591325-591325. doi: 10.1155/2011/591325

Wagner, M. L., & Tamm, L. K. (2000). Tethered polymer-supported planar lipid bilayers for reconstitution of integral membrane proteins: Silane-polyethyleneglycol-lipid as a cushion and covalent linker. *Biophysical Journal, 79*(3), 1400-1414. doi: 10.1016/S0006-3495(00)76392-2

Wang, E. J., Casciano, C. N., Clement, R. P., & Johnson, W. W. (2001). HMG-CoA reductase inhibitors (statins) characterized as direct inhibitors of P-glycoprotein. *Pharmaceutical Research, 18*(6), 800-806. doi: 10.1023/a:1011036428972

Wang, Q., Tan, G., Lawson, L. B., John, V. T., & Papadopoulos, K. D. (2010). Liposomes in Double-Emulsion Globules. *Langmuir, 26*(5), 3225-3231. doi: 10.1021/la9032157

Wang, R. G., Takeda, M., & Kido, M. (2002). Micro pure water wettability evaluation with an AC no-contact mode of atomic force microscope. *Materials Letters, 54*(2-3), 140-144. doi: 10.1016/s0167-577x(01)00552-3

Wang, W., Yang, Y., Wang, S., Nagaraj, V. J., Liu, Q., Wu, J., & Tao, N. (2012). Label-free measuring and mapping of binding kinetics of membrane proteins in single living cells. *Nature Chemistry, 4*(10), 846-853. doi: 10.1038/nchem.1434

Woods, C. M., & Lazarides, E. (1988). The erythroid membrane skeleton - expression and assembly during erythropoiesis. *Annual Review of Medicine, 39*, 107-122. doi: 10.1146/annurev.med.39.1.107

Ye, Q., Konradi, R., Textor, M., & Reimhult, E. (2009). Liposomes tethered to omega-functional PEG brushes and induced formation of PEG brush supported planar lipid bilayers. *Langmuir, 25*(23), 13534-13539. doi: 10.1021/la902039g

APPENDICES

APPENDIX A: Chemicals
APPENDIX B: Laboratory Equipments

APPENDIX A: Chemicals

Chemicals	Supplier
Phosphatydilcholine	Sigma-Aldrich
3,3′-Dithiodipropionic acid di(N-hydroxysuccinimide)	Sigma-Aldrich
Pravastatin	Sigma-Aldrich
P-glycoprotein	Sigma-Aldrich
Monoclonal anti-P-glycoprotein (anti-MDR1) clone F4	Sigma-Aldrich
Monoclonal anti-Pin-1 Mouse antibody	Sigma-Aldrich
Dimethylsulfoxide	Merck
Chloroform	Merck
1,2-distearoyl-sn-glycero-3-phosphoethanolamine-N-[amino (polyethylene glycol)-2000] (ammonium salt)	Avanti Polar Lipids

APPENDIX B: Laboratory Equipments

Laboratory Equipments	Supplier
Deep freezers and refrigerators	Arçelik, 1061 M Refrigerator
Ice machine	Scotsman, AF 10
Micropipettes	Eppendorf AG, 5000 µl, 2500 µl, 1000 µl, 100 µl, and 10 µl
Precision weigher	Precisa, XB220A
pH-meter	InoLab, 720
Pure water systems	Elga Labwater, USF Elga UHQ-PS-MK3
Shaker	Heidolph, Duomax 1030
Vortex apparatus	Heidolph, Reax Top
Round bottom flask (100 mL)	Sigma-Aldrich
Surface Plasmon Resonance System	Reichert SR7000 SPR system
Gold-coated BK7 slides	Reichert
Quartz Crystal Microbalance-Dissipation	KSV, QCM Z500
Gold-coated quartz crystals	KSV, Q-Sense
Liquid-Atomic Force Microscopy	NanoMagnetics Instruments
Au(111)-coated mica surfaces	SPI
Avanti Mini-Extruder System	Avanti Polar Lipids

CURRICULUM VITAE

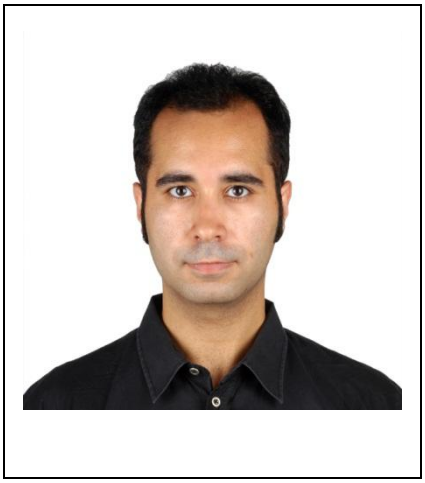

Name Surname: Fatih İNCİ

Place and Date of Birth: İstanbul, 30.06.1985

E-Mail: fthinci@yahoo.com

B.Sc.: İstanbul University, Faculty of Science, Department of Molecular Biology & Genetics, İstanbul/TURKEY

Professional Experience and Rewards:

- European Science Foundation – European Molecular Biology Organization (ESF-EMBO) Scientific Travel Grant (2011)
- Istanbul Technical University Scientific Travel Grants (2010 - 2011)
- TUBITAK (Turkey Scientific and Technological Research Society) Ph.D. Scholarship (2007-2012)

PUBLICATIONS/PRESENTATIONS ON THE THESIS

- Inci, F., Turken, B., Celik, U., Ozer, O., and Kok, F.N., 2012: Construction and Characterization of P-Glycoprotein Incorporated Tethered Lipid Bilayers. (in preparation).
- Inci, F., Turken, B., Celik, U., Ozer, O., and Kok, F.N., 2012. Integration of P-Glycoprotein into Artificial Membranes and Its Interaction with Drugs. 22nd Biosensors Congress, Cancun, Mexico.
- Inci, F., Turken, B., Celik, U., Ozer, O., and Kok, F.N., 2012. Construction of an in vitro Drug-Protein Interaction Platform Using Artificial Lipid Bilayers. 24th European Conference on Biomaterials (ESB), Dublin, Ireland.
- Inci, F., and Kok, F.N., 2011. Characterization of Tethered Bilayer Lipid Membranes by Quartz Crystal Microbalance-Dissipation (QCM-D). ESF-EMBO Symposium, Biological Surfaces and Interfaces, Sant Feliu de Guíxols, Spain.

▪ Turken, B., Inci, F., and Kok, F.N., 2011. The Effect of Liposome Phospholipid Content on the Formation of Tethered Bilayer Lipid Membranes. 36th FEBS Congress, Biochemistry for Tomorrows Medicine, Torino, Italy.

▪ Parlatan, U., Inci, F., Seninak, S., Kok, F.N., and Basar, G., 2011. Investigation of Effects of Transmembrane Protein Presence on Liposomes by Raman Tweezers. 28th International Physics Congress, Turkish Physical Society, Bodrum, Turkey.

▪ Seninak, S., Parlatan, U., Inci, F., Kok, F.N., and Basar, G., 2011. Investigation Modifications in Physicochemical Structures of Liposomes Due to Transmembrane Proteins by Raman Spectroscopy." Paper presented at the 28th International Physics Congress, Turkish Physical Society, Bodrum,Turkey.

▪ Inci, F., and Kok, F.N., 2010. Integration of P-Glycoprotein, a Membrane Protein, to Artificial Lipid Membranes. 6th Nanoscience and Nanotechnology Conference (NanoTR VI), Izmir, Turkey.

▪ Inci, F., and Kok, F.N., 2010. Construction of Artificial Lipid Membranes for Membrane Protein Research. Workshop on Current Trends in Molecular Nanosciences, Ankara, Turkey.

▪ Inci, F., and Kok, F.N., 2010. Construction of a Tethered Lipid Bilayer for Membrane Protein Research. 35th Federation of European Biochemical Societies Congress (FEBS), Gothenburg, Sweden.

▪ Inci, F., and Kok, F.N., 2010: Artificial Lipid Bilayers and Applications. Bogazici University Molecular Biology and Genetics (MBG) Weekend Seminars V, Istanbul, Turkey.

▪ Inci, F., Turken, B., and Kok, F.N., 2010. A New Tethered Lipid Bilayer System for Membrane Protein Research. 3rd International NanoBio Conferance, Zürich, Switzerland.